THE DE HAAS VAN ALPHEN EFFECT

IN A ZINC ALLOY

HAVING A RESISTANCE MINIMUM

by

W. Burnett Muir

Submitted in partial fulfillment
of the requirements for the degree of
Doctor of Philosophy

Faculty of Pure and Applied Science
University of Ottawa
Ottawa, Canada

1962

ABSTRACT

The de Haas van Alphen effect has been measured using a torque method at magnetic fields up to 8 kilo-oersteds and temperatures between 4.2° K and 1.6° K for both pure zinc and a zinc manganese alloy exhibiting a resistance minimum. Experimentally it is shown that there is no change in the period of the oscillations although the field and temperature dependence of the amplitude of the oscillations are found to be anomalous. A consideration of the influence of the conduction electron relaxation time on the de Haas van Alphen effect shows that the observed behaviour may be explained if the relaxation time is allowed to approach zero in a small energy interval, Δ , about the Fermi energy. Using the phenomenological theory of the resistance minimum, due to Korringa and Gerritsen, and the value of Δ obtained from the de Haas van Alphen Effect experiments the resistance as a function of temperature was calculated and found to agree within experimental error with the measured values.

ACKNOWLEDGEMENTS

I would like to express my appreciation to Dr. F. T. Hedgcock for suggesting the problem and for his advice throughout the course of the research. I would also like to thank Prof. J. M. Robson, chairman of the physics department, for making the facilities of the department available and the technical staff of the department for their help in the construction of the apparatus. I would like to thank: Dr. J. S. Dugdale, Dr. A. V. Gold, Dr. F. Wienberg, Prof. C. Pisot, Dr. R. B. Dingle, Dr. M. Bailyn, and Mr. R. O. Kornelsen for many helpful discussions; Dr. C. M. Mitchell for help in the orientation of the single crystals, Dr. F. R. Hunt for the design of the magnet current regulator, and Mr. E. E. Wallingford for the calibration of two carbon thermometers.

I would also like to thank Mr. C. G. McLachlan for his generous support and my wife, Marilyn, for typing the manuscript and forebearance throughout the entire course of the research.

Contracts

The author wishes to acknowledge the financial support, under contracts to Dr. F. T. Hedgcock, of the National Research Council, The Defence Research Board and the Aeronautical Systems Division of the United States Airforce.

Contents

List of Figures

Chapter IV

Chapter V

Appendix I

Appendix II

List of Tables

Chapter III

Chapter IV

STATEMENT OF ORIGINALITY

The author believes that, to the best of his knowledge, this is the first time the resistance, thermo e.m.f., and de Haas van Alphen Effect have been measured on an alloy showing a resistance minimum. It is also the first time that the effect of an energy dependent relaxation time on the de Haas van Alphen effect has been investigated.

CHAPTER I

1.1 INTRODUCTION

In normal metals and alloys the electrical resistance decreases with decreasing temperature and eventually becomes constant at temperatures sufficiently low that the scattering of the conduction electrons is chiefly due to crystal imperfections and impurities. In 1930 Meissner and Voigt observed that in certain metals the electrical resistivity fell to a small value with decreasing temperature and then rose by a few percent as the temperature was further lowered. This effect was studied more closely by deHaas and van den Berg (1934) who found that the temperatures at which the minimum occurred increased with increasing residual resistance ratio. This established that the minimum in electrical resistance was due to the presence of crystal imperfections and/or impurities. MacDonald and Pearson (1955) have shown that along with the resistance minimum there also occurs an anomalous thermo e.m.f. Large negative values of the thermo e.m.f. are observed at temperatures somewhat higher than the temperature at which the resistance minimum occurs in these alloys. The experimental position as of 1960 is summarized by van den Berg (1960) who points out that the anomalies in the transport properties are now believed to be due to the presence of certain transition element impurities and in fact the ability to produce a resistive anomaly seems to depend on the existance of a localized magnetic moment introduced by the impurity.

Recent extensions of the Schmitt (1956) theory of the resistance minimum by Kasuya (1959), Bailyn (1961), and de Vroomen (1959), to

explain "giant" thermoelectric powers in dilute alloys at low temperatures predict an effective relaxation time which is sharply energy dependent near the Fermi energy.[1] Domenicali (1960), in an extension of some early work of Korringa and Gerritsen (1953), has shown that such a relaxation time will explain the resistance and thermoelectric power of these alloys over a wide temperature range.

Since the amplitude of the de Haas van Alphen Effect is related to the relaxation time of the conduction electrons a study of this effect in an alloy which exhibited a resistance minimum was made in order to obtain further information about the relaxation time in these alloys.

The experimental study was made on a zinc manganese alloy since it was known to exhibit a resistance minimum, (Muto et. al. 1959), and a large amplitude de Haas van Alphen Effect. (Verkin and Dmitrenko 1958)

1.2 Discussion of the Theory of the de Haas van Alphen Effect for Zinc

The present experiments on the de Haas van Alphen effect consist of measurements on the field dependence of the torque exerted on a single crystal sample in a homogeneous magnetic field. The torque, C, about an axis can be derived from the free energy, F, of the electron system since

$$C = - \partial F / \partial \psi \qquad 1.1$$

---

[1] For a discussion of these effects and the present situation the reader is referred to D.K.C. MacDonald's "Thermoelectricity, and Introduction to Principles", John Wiley and Sons, New York, 1962, and also to MacDonald, D.K.D. and Guenault, A.M., Phil. Mag. 6, 1201, 1961.

where ψ is an angle specifying rotation in a plane normal to the prescribed axis. (See Figure 1a) The large amplitude long period de Haas van Alphen oscillations observed in pure zinc arise from pieces of Fermi surface which are ellipsoidal in shape (Verkin and Dmitrenko 1958, Harrison, 1960) and are situated as shown in Figure 1b. Since the surfaces are ellipsoidal it is possible to use the expression for the free energy of the conduction electrons derived by Dingle (1952). He showed that the part of the free energy that depends periodically on the magnetic field is given by:

$$F_p = \frac{2\pi(2m^*)^{3/2} kTV(\beta^* H)^{3/2}}{\sqrt{2}\, h^3} \sum_{r=1}^{\infty} \left[\frac{(-1)^r \cos(2\pi r E_o/\beta^* H - \pi/4)}{r^{3/2} \sinh(2\pi^2 r kT/\beta^* H)} \cos r\pi(m^*/m)\, e^{-rh/\tau\beta^* H} \right] \qquad 1.2$$

where

$\beta^* = eh/m^* c$ is an effective double Bohr magneton

V is the volume of the crystal

T is the absolute temperature

E_o is the Fermi energy measured from the bottom of the ellipsoid

τ is the electron relaxation time

m^* is the cyclotron effective mass

This expression can be simplified for zinc since it has been shown experimentally (Dhillon and Shoenberg 1955), that harmonics are absent. Also the effective mass is of the order of 0.01 of the free electron mass and hence $\cos \pi m^*/m$ is unity. Combining equations 1.1 and 1.2

FIGURE I

a) The orientation of the zinc crystal in the magnetic field.

b) The Fermi surface of zinc (after Fawcett 1961). The surfaces marked K are associated with the long period de Haas van Alphen Effect.

.c field.

he surfaces

hen Effect.

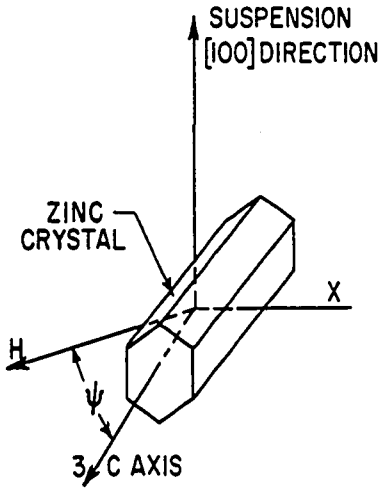

(a)

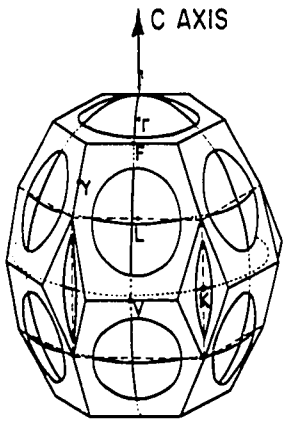

(b)

and noting that $E_o/\beta^*H \gg 1$ the torque on the sample is given by

$$C = BH^{1/2}T \frac{\sin(2\pi E_o/\beta^*H - \pi/4)}{\sinh(2\pi^2 kT/\beta^*H)} e^{-2\pi^2 k\chi/\beta^*H} \qquad 1.3$$

where

$$B = \frac{E_o k V}{\pi^3}\left(\frac{e\hbar}{c}\right)^{1/2}\frac{\partial m^*}{\partial \psi} \qquad 1.4$$

and $\chi = \hbar/\pi k\tau$

The quantity χ has the dimensions of temperature and is called the collision or Dingle temperature. From equation 1.3 it can be seen that the period, P, of the oscillations can be written

$$P = \beta^*/E_o = \beta/E_o(m^*/m) \qquad 1.5$$

where $\beta = e\hbar/mc$ is a double Bohr magneton.

The effective mass of the electrons can be determined from the ratio of the amplitude $|C_1|$ of the oscillations at temperature T_1 to the amplitude $|C_2|$ at temperature T_2. Assuming that the temperature is sufficiently low that the relaxation time is constant then the ratio of the amplitudes, from equation 1.3, is given by

$$\frac{|C_1|}{|C_2|} = \frac{T_1 \sinh(2\pi^2 kT_2/\beta)(m^*/mH)}{T_2 \sinh(2\pi^2 kT_1/\beta)(m^*/mH)} = W \qquad 1.6$$

where m^*/m is the only unknown quantity. Equation 1.6 can be solved by graphical methods for m^*/m. From the value of m^*/m and the corresponding

period the value of the Fermi energy, E_0 , can be calculated from equation 1.5.

Once the effective mass has been determined the collision temperature χ can be evaluated from the field dependence of the amplitude of the oscillations. Excluding the periodic term equation 1.3 may be written:

$$\alpha = \xi - \chi H^{-1} \qquad 1.7$$

where

$$\alpha = \frac{\beta \ln.\left[(|C|/H^{1/2}T)\sinh(2\pi^2 kT/\beta H)(m^*/m)\right]}{2\pi^2 k(m^*/m)} \qquad 1.8$$

and

$$\xi = (\beta \ln. B)/2\pi^2 k(m^*/m)$$

whence if α is plotted as a function of H^{-1} a straight line should result whose slope is $-\chi$.

Since the relaxation time is related to χ, (equation 1.4) then any anomalous behaviour in the relaxation time should be reflected in the graph of α as a function of H^{-1}. Figure 18 of CHAPTER IV shows the results of plotting α as a function of H^{-1} for the zinc manganese alloy which exhibits a resistance minimum. From the figure it can be seen that, contrary to the expected behaviour (equation 1.7) the intercept of the lines at infinite field, ($H^{-1} = 0$), is temperature dependent. In CHAPTER V it is shown that this behaviour is consistent with an energy dependent relaxation time similar to that discussed in section 1.1 in connection with the resistance and thermoelectric power anomalies.

CHAPTER II

Experimental Methods and Apparatus

2.1 Resistance Measurements

The relative resistance, as a function of temperature, was obtained by the current and potential lead method, ie by measuring the potential difference between two points on the specimen as a function of temperature, while passing a known current through it.

A galvanometer amplifier of the type described by Preston (1946) with the modifications due to MacDonald (1947) was used to measure the potential difference between the potential leads. The same galvanometer amplifier was used to monitor the specimen current by including a suitable (2.26×10^{-2} ohm) standard resistor in series with the current leads. The potential difference appearing across this resistor was periodically measured with the galvanometer amplifier throughout a set of resistance measurements. The circuit of the galvanometer amplifier is given in Figure 1a. From Figure 1a and following MacDonald (1947) we can see, if the amplification in the photo cells is high enough so that the input current i_i can be neglected compared to the output current i_o, that the input voltage is given by:

$$e_i = i_o R_f \qquad 2.1$$

where R_f is the value of the f eedback resistor being used. If the sensitivity of the secondary galvanometer is K_2, then the deflection D of the secondary galvanometer due to the output current is given by:

$$K_2 D = i_o \qquad 2.2$$

FIGURE I

a) The schematic diagram of galvanometer amplifier.

b) The circuit diagram of the resistance measuring apparatus.

Potentiol
Reverse

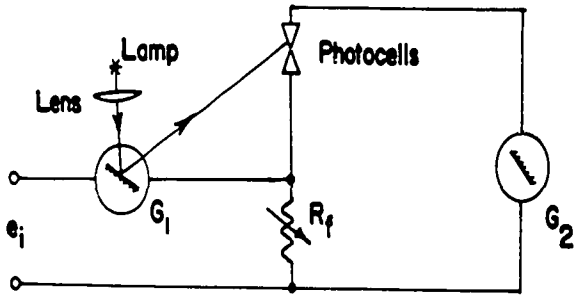
Lamp
Photocells
Lens
G_1
R_f
G_2
e_i

(a)

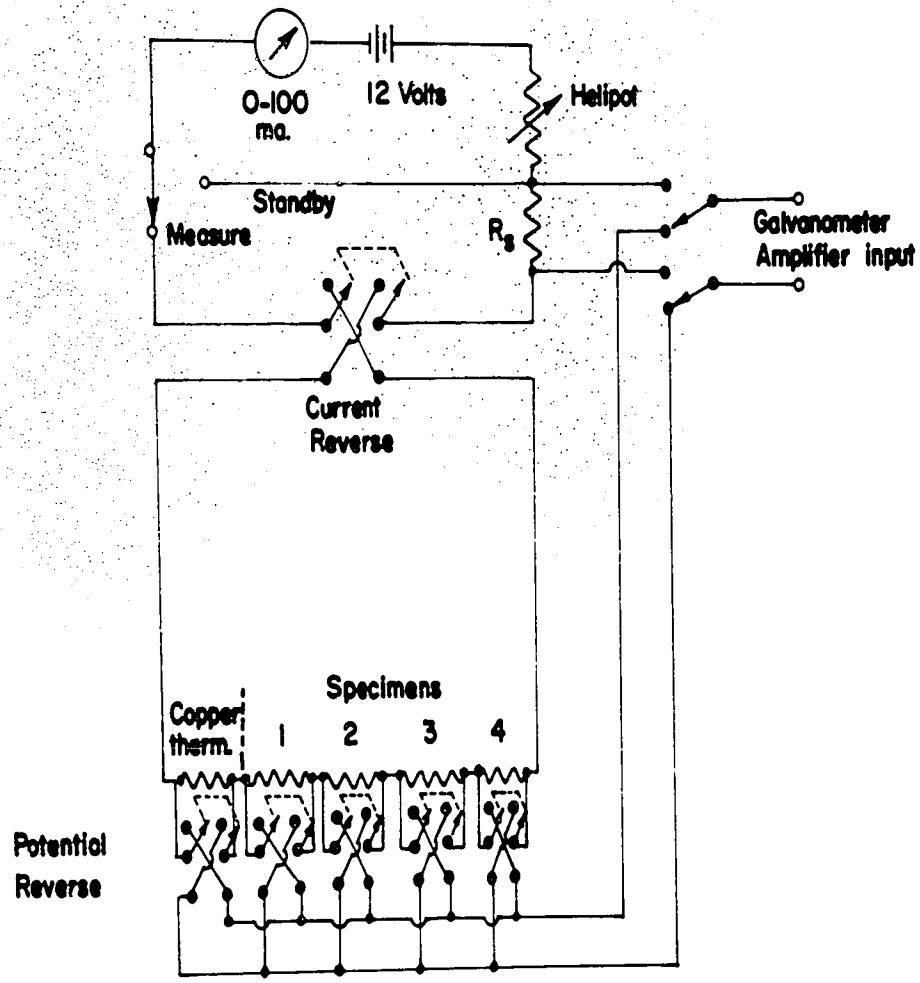
0-100 ma.
12 Volts
Helipot
Standby
Measure
R_s
Galvanometer Amplifier input
Current Reverse
Specimens
Copper therm.
1
2
3
4
Potential Reverse

(b)

whence, combining 2.1 and 2.2:

$$e_i = K_2 R_f D \qquad 2.3$$

Since the resistance of a sample is measured relative to its resistance at 273° K then, using 2.3, it can be seen that if R_T is the resistance of the specimen at any temperature T and i_T is the corresponding current flowing through the sample then:

$$e_i = i_T R_T = K_2 D_T R_{fT} \qquad 2.4$$

But i_T is determined using the same galvanometer amplifier and a standard resistor R_s and hence:

$$i_T R_s = K_2 D_i' R_{fi} \qquad 2.5$$

where D_i' is the deflection obtained when measuring the potential difference across the standard resistor, R_s, and R_{fi} is the value of feed-back resistor R_f used. Then the resistance at any given temperature is R_T where:

$$R_T = \frac{K_2 D_T R_{fT}}{i_T} = \frac{D_T R_{fT} R_s}{D_{iT} R_{fi}}$$

Now, during any series measurements i_T is kept constant and R_{fi} is not changed. Then the relative resistance of the sample is:

$$\frac{R_T}{R_{273}} = \frac{D_T R_{fT} D_{i273}}{D_{273} R_{f273} D_{iT}} \qquad 2.6$$

which allows for any slight fluctuations in i_T. To make resistivity measurements an absolute value of the resistance of the sample at 273° K must be obtained. The resistance of the current sampling resistor can easily be measured using one of the standard techniques.

Thus, by comparing the resistance of the current sampling resistor to the resistance of the specimen, the resistance of the specimen can be found. Combining equations 2.4 and 2.5, the resistance of the specimen in terms of that of the current sampling resistor is:

$$R_T = R_S D_T R_{fT} / D_i R_{fi} \qquad 2.7$$

Using equation 2.7 for the resistance, R_T, of the specimen the resistivity, ρ can be obtained if the distance, L_e, between the potential leads and the cross-sectional area, A, are known, since:

$$\rho = RA/L_e .$$

"A" can be determined by weighing the specimen, since:

$$A = W/L d$$

where W, L and d are the weight, length and density of the sample respectively. The resistivity of the sample is then given by:

$$\rho = R_T W/d L L_e \qquad 2.8$$

To eliminate any thermo e.m.f.'s which might be generated in the potential leads from the specimen, provision was made for reversing the current through the sample. If e_o is the observed voltage at the galvanometer amplifier, e_c the correct voltage due to current flowing through the specimen and e_s the spurious voltage due to thermo e.m.f.'s then:

$$e_o = e_c + e_s$$

Upon reversing the current:

$$-e_o' = -e_c + e_s$$

Subtracting we obtain:

$$e_o + e_o' = 2e_c$$

or

$$e_c = (e_o + e_o')/2 \qquad 2.9$$

FIGURE 2

The Resistance Cryostat

1. Cartesian manostat to control the vapour pressure above the helium bath.
2. Vacuum tight feed through seal for the electrical leads.
3. Copper experimental chamber.
4. Carbon resistance thermometer consisting of a 47 ohm 1/2 watt Allen Bradley resistor.
5. Resistance specimens.
6. Pressure contact block.
7. Charcoal contained in a perforated copper can.
8. Boil-off heater.
9. Connection for the vapour pressure gauge.
10. H elium transfer hole.
11. Discharge tube to indicate the pressure of the exchange gas.
12. Connection to cryostat vacuum system.
13. Connection to helium pumping system.
14. Copper resistance thermometer mounted on reverse side of the pressure contact block 6.

above the helium

leads.

ım 1/2 watt

ıange gas.

de of the

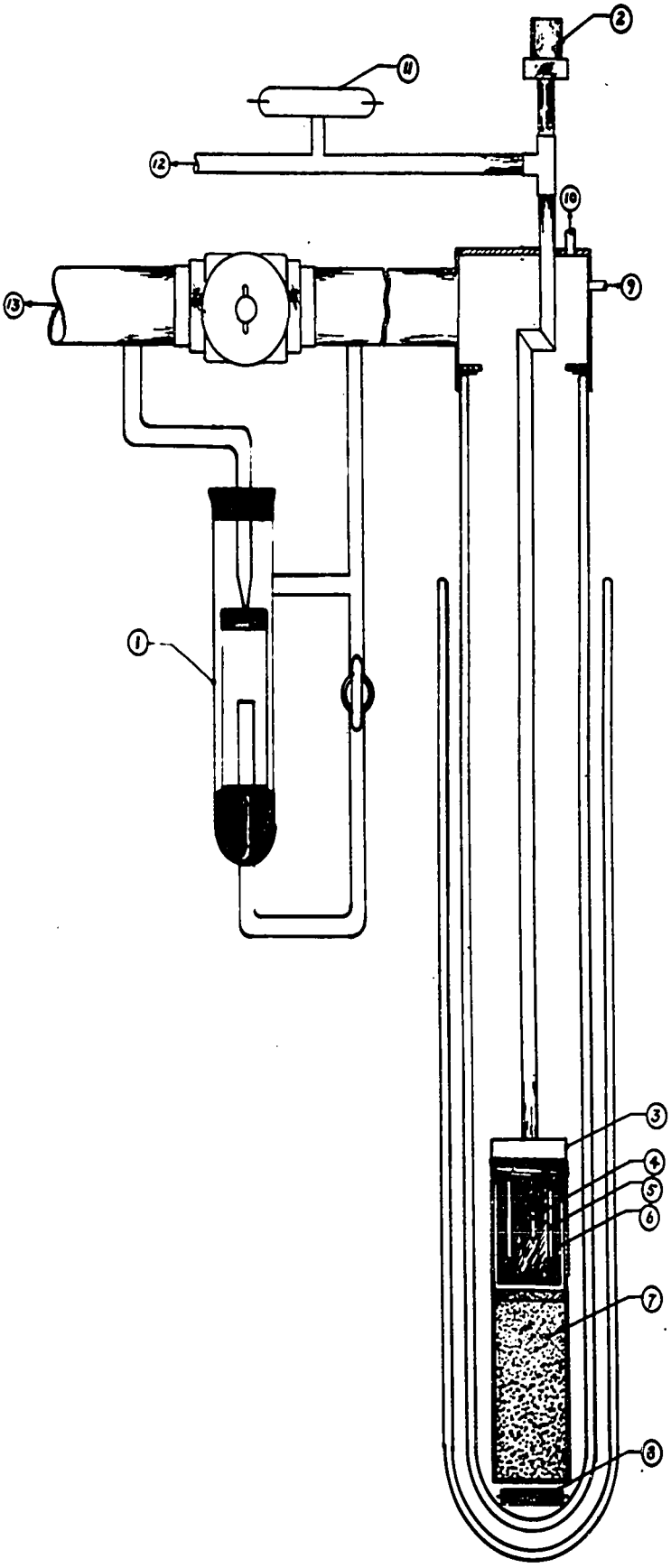

A complete circuit diagram of the resistance measuring apparatus is given in FIGURE 1b.

The resistance measurements were made in a helium desorption cryostat similar to that of Rose*Innes and Broom (1956). A diagram of the cryostat is shown in FIGURE 2. After pumping out the experimental chamber about 5 cm. of helium exchange gas was admitted to insure good thermal contact between the chamber, specimens and thermometers. The cryostat was then filled with liquid helium and the temperature reduced in steps to its lowest value of 1.8° K by pumping on the helium bath. The vapor pressure over the helium bath was measured and the temperature determined from the tables of Clement Logan and Gaffney (1955). The remaining helium was then boiled off and the cryostat temperature would drift slowly towards the nitrogen point due to the large effective thermal capacity of the helium vapor absorbed by the charcoal.

In the temperature range 4.2° K to 25° K the temperature was measured with a carbon resistance thermometer which was calibrated using the method of Clement and Quinell (1952). In the temperature range 25° K to 80° K the temperature was measured with a copper resistance thermometer, The temperature was determined from the $Z_3 = (R_T/R_{273} - R_{4.2}/R_{273}) / (1 - R_{4.2}/R_{273})$, function for copper which has been tabulated as a function of temperature by White (1959). Calibration curves for the thermometers are given in APPENDIX I.

2.2 Thermo E.M.F. Measurements

The apparatus used to measure the thermo e.m.f. of the zinc manganese alloys relative to pure zinc is similar to that used by MacDonald and Pearson (1953) and is shown in FIGURE 3.

FIGURE 3

The thermal e.m. f. cryostat

1. Hot junction heater.
2. Copper resistance thermometer woulnd on the hot junction contact block.
3. Carbon resistance thermometer.
4. The zinc manganese lead of the thermocouple.
5. The zinc lead of the thermocouple.
6. Superconducting reversing switch magnet assembly.
7. Superconducting elements of the switch.
8. Boil-off heater.
9. Helium transfer hole.
10. Thermocouple mounting block.
11. Copper shield tube.

n contact

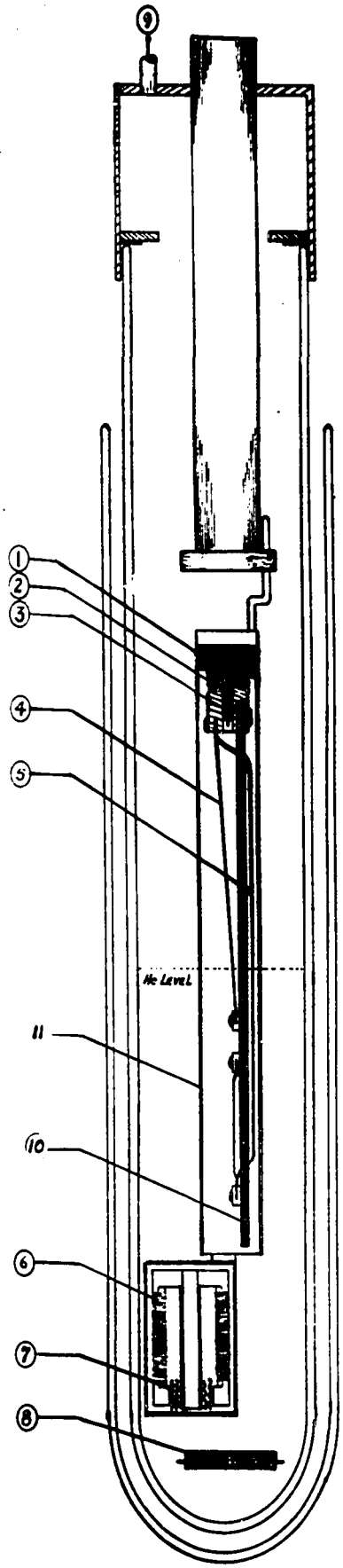

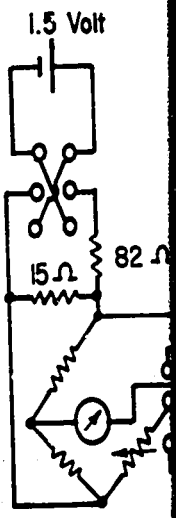

FIGURE 4

a) The circuit diagram of the thermo E.M.F. apparatus.

b) The superconducting reversing switch in the forward position.

c) The superconducting reversing switch in the reverse position.

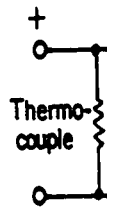

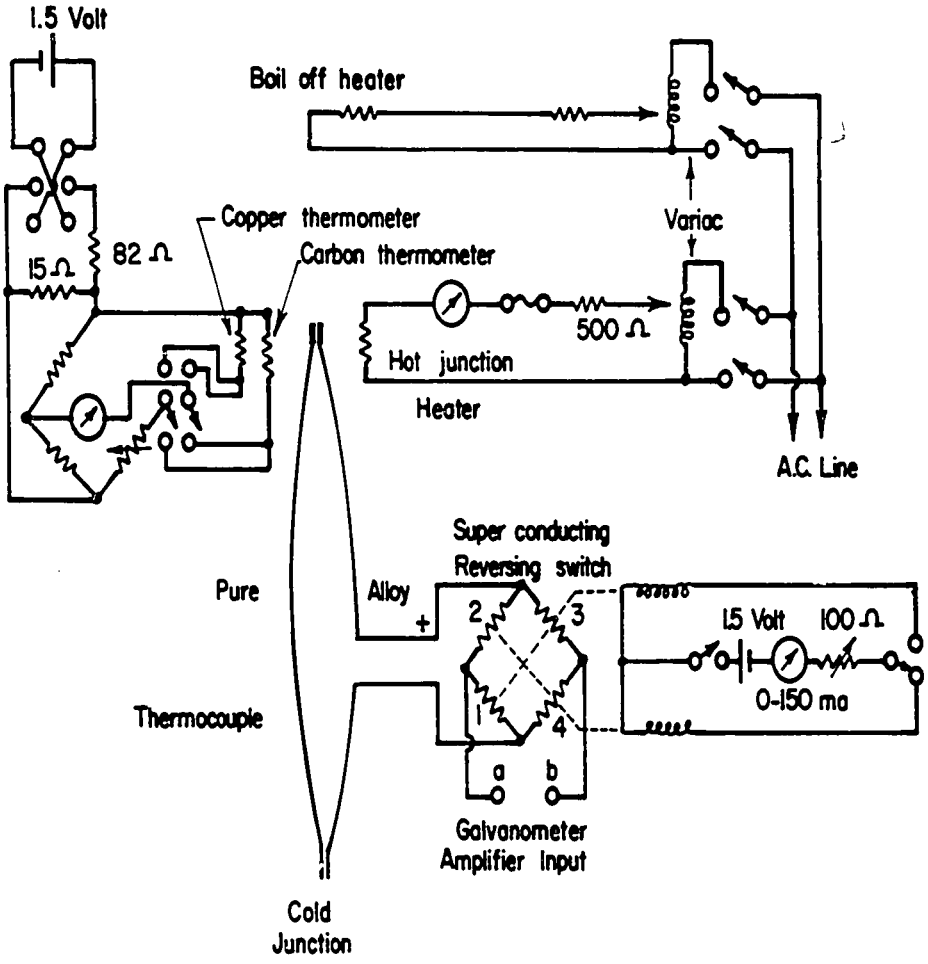
1.5 Volt
Boil off heater
Copper thermometer
Carbon thermometer
Variac
82 Ω
15 Ω
500 Ω
Hot junction
Heater
A.C. Line
Super conducting
Reversing switch
Pure
Alloy
+
2
3
1.5 Volt
100 Ω
0-150 ma
Thermocouple
1
4
a
b
Galvanometer
Amplifier Input
Cold
Junction

(a)

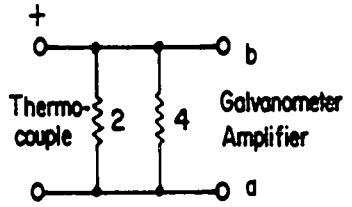
+
b
Thermo-
couple
2
4
Galvanometer
Amplifier
a

(b)

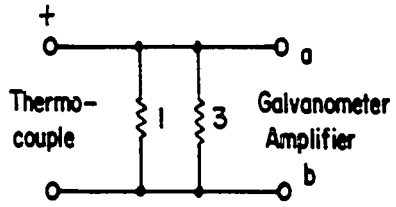
+
a
Thermo-
couple
1
3
Galvanometer
Amplifier
b

(c)

In operation the thermocouples are mounted on the specimen holder which is then inserted in the copper shield and clamped in position. The Dewars are attached and filled to about two inches below the hot junction. The boiloff heater is turned on and the hot junction cooled to the lowest desired temperature, (about 5° K). The thermo e.m.f. is measured for both directions of the superconducting reversing switch.[1] The temperature of the hot junction is then raised by first reducing the current flowing through the boiloff heater and then turning on and increasing the current flowing through the hot junction heater. In this manner it is possible to measure the thermo e.m.f. as a function of hot junction temperature from 5° K to 100° K. A complete circuit diagram of the apparatus is shown in FIGURE 4. The temperature of the hot junction is measured using copper and carbon resistance thermometers whose calibration is given in APPENDIX I.

2.3 The Torsion Balance

The torsion balance used for this research is similar to that of Croft, Donnahoe and Love (1955) and is shown in FIGURE 5. The balance consists of a modified Leeds and Northrup wall type galvanometer having the crystal, which is to be investigated, attached to the end of a long quartz rod which is fixed to the bottom of the

---

1. The superconducting reversing switch, (Templeton, 1955), allows the polarity of the thermocouple to be reversed in the helium bath, thus eliminating any stray thermo e.m.f.'s which might arise in the leads.

FIGURE 5

The Torsion Balance

1. and 2. Coil and mirror assembly which is suspended from the torsion head by a 0.002 inch diameter berylium copper wire. This wire serves as one lead to the coil.
3. Magnet assembly.
4. Berylium copper spiral which serves as the other lead to the coil.
5. Dash pot containing out gassed Dow Corning number 200 silicone oil into which dip the damping vanes attached to the suspension.
6. Brass bell jar.
7. Plexiglass window.
8. Crystal and crystal holder.
9. Lower suspension rod, 1/32 inch diameter quartz rod.
10. Ball and socket joint incorporated in the shielding tube to facilitate alignment of the balance.
11. Magnet.
12. Connection to balance evacuating system.
13. Connection to the helium pumping system.

the

re. This

o the coil.

ilicone oil

sion.

be to

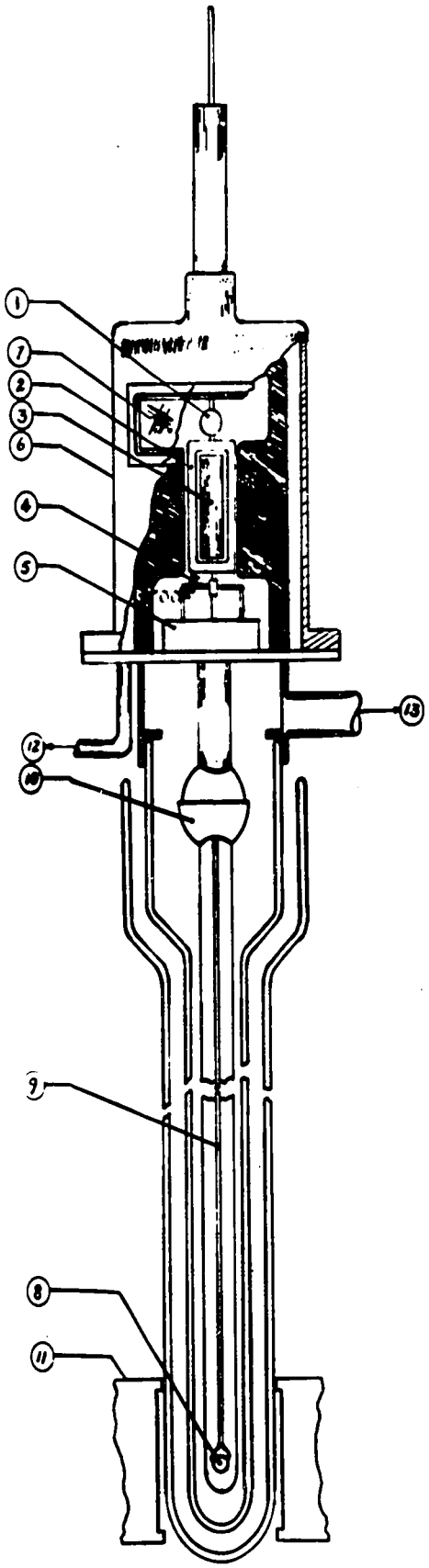

galvanometer coil. Counter torques sufficient to restore the crystal to its original position, after the application of a magnetic field, can be obtained by passing a current through the galvanometer coil.

In practice, the restoring torque is applied automatically by including the galvanometer in a feed-back loop. A block diagram of the system is shown in FIGURE 6. The signal developed by light reflected from the galvanometer mirror, falling on the phototube, is fed to a cathode-follower, then to the D.C. amplifier, stabilizing network, output current recorder and finally to the galvanometer coil in such a way as to oppose any change from the initial balanced condition. Referring to FIGURE 6, the sensitivity control is seen to consist of three General Radio decade resistors of 10,100 and 1,000 ohms, thus allowing a change in sensitivity by a factor of 1,000. The shunt resistor R_2 serves to set the overall sensitivity of the balance and is adjusted so that the maximum desired sensitivity is obtained with the sensitivity control at its maximum value. The 1,000 ohm resistor of the sensitivity control combined with R_1 and C_1 form a stabilizing network which serves to damp any oscillations arising due to phase shift in the feed-back loop. A detailed circuit diagram of the D.C. amplifier is given in FIGURE 7.

The circuit used for measuring the feed-back current is also shown in FIGURE 7. The voltage, generated across 2 of the 3 decade resistors which are in series with the galvanometer coil, is fed to a 10 millivolt Leeds and Northrup recording potentiometer. A zero suppression device makes it possible to increase the sensitivity and back off to new zero while still keeping the recorder on scale. To reduce any noise on the feed-back current, the signal is fed to the

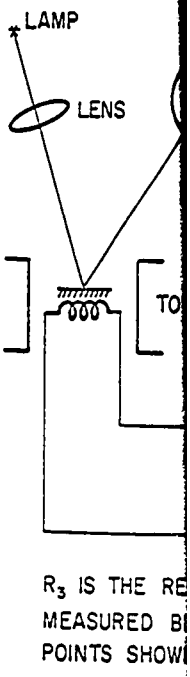

FIGURE 6

A block diagram of the complete torsion balance.

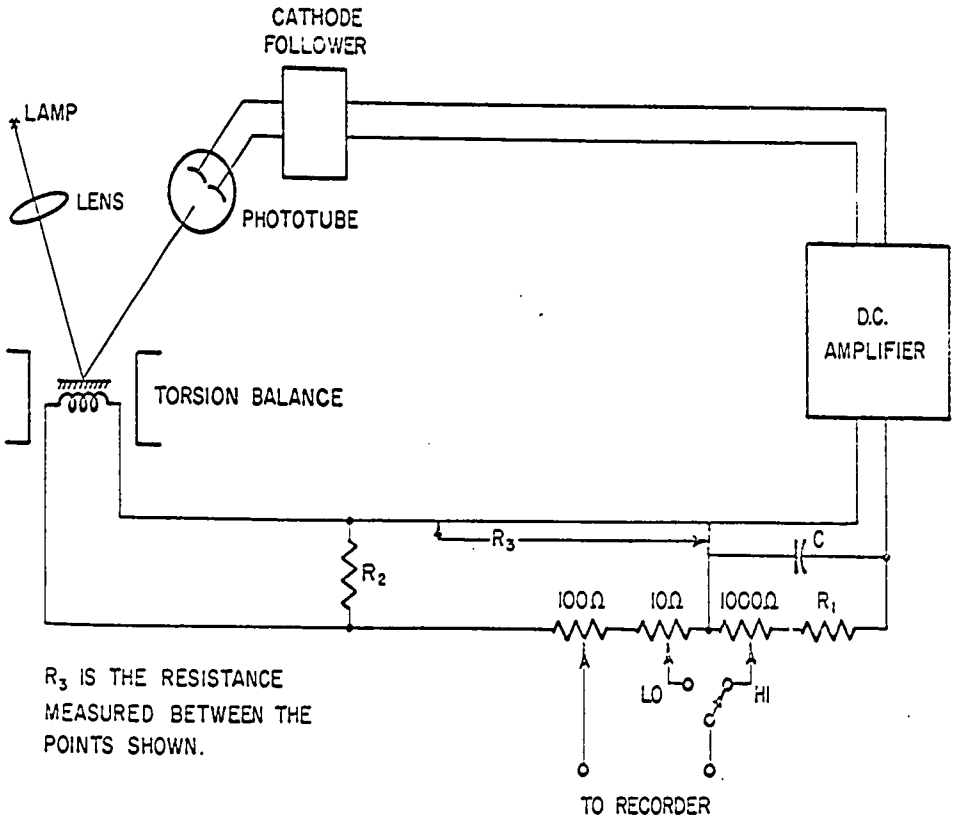

R_3 IS THE RESISTANCE MEASURED BETWEEN THE POINTS SHOWN.

FIGURE 7

The circuit diagram of the amplifier and zero suppression unit.

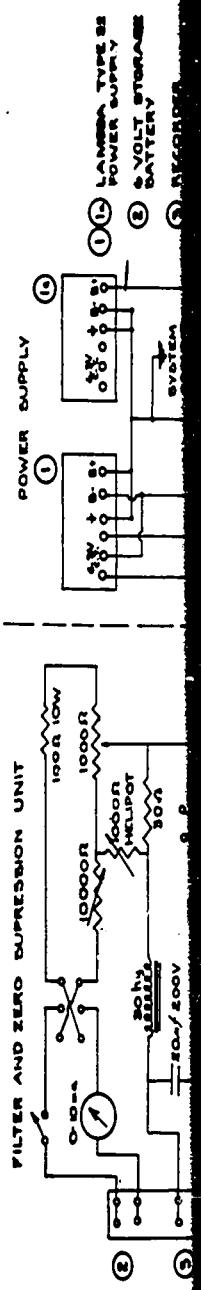

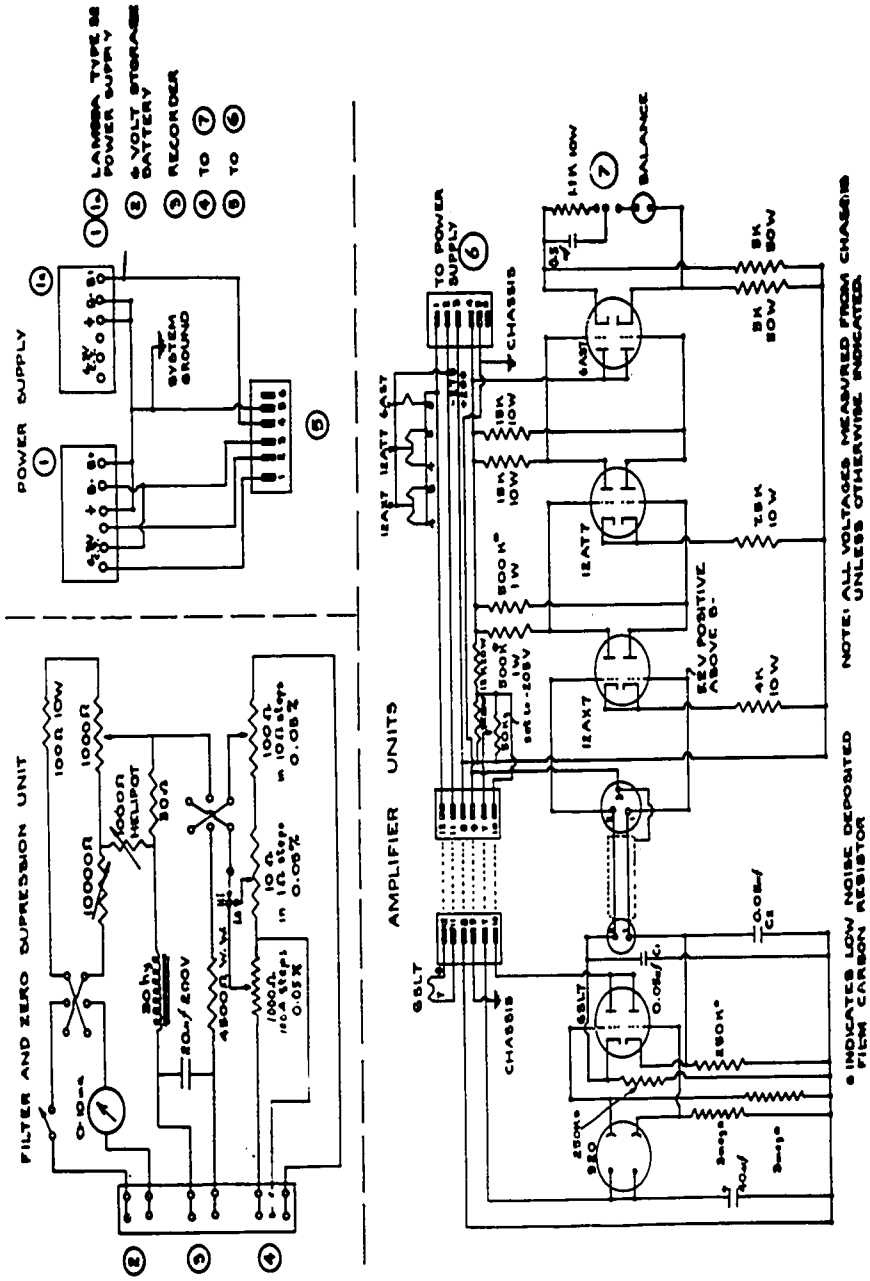
POWER SUPPLY
LAMBDA TYPE 28 POWER SUPPLY
6 VOLT STORAGE BATTERY
RECORDER
TO
TO
SYSTEM GROUND
FILTER AND ZERO SUPPRESSION UNIT
AMPLIFIER UNITS
TO POWER SUPPLY
CHASSIS
BALANCE
REV POSITIVE ABOVE 8-
NOTE: ALL VOLTAGES MEASURED FROM CHASSIS UNLESS OTHERWISE INDICATED.
INDICATES LOW NOISE DEPOSITED FILM CARBON RESISTOR

recorder through a low pass filter. A detailed description of the amplifier, including the method used to determine the values of the components of the stabilizing network, is given by Hedgcock and Muir (1960).

2.4 Specimen Orientation and Method of Measurement

Harrison (1960) has pointed out that the low field de Haas van Alphen effect in zinc is attributable to the needle-like portions of Fermi surface containing electrons which lie along the zone edges parallel to the C axis of the crystal. Accordingly the crystals used in the present experiments were mounted with their c axis in the plane of the magnetic field. Verkin and Dmitrenko (1955) in their study of the de Haas van Alphen effect in pure zinc made measurements with the [100] direction of the crystal either in the direction of the suspension or perpendicular to it. To facilitate the comparison of results, the present measurements were made with the [100] direction in the direction of the suspension.

The direction of the c axis was determined by cleaving the crystal using the method described in CHAPTER III. The zinc crystals cleave most easily along the basal plane which is prependicular to the c axis of the crystal. An arrow of arbitrary direction was then scratched in the basal plane of the crystal and the crystal mounted in an X-ray spectrometer. The orientation of the crystal relative to the arrow was then determined when Bragg reflection from the (110) planes occurred. The angle between the arrow and the [100] direction could

then easily be determined. The above orientation procedure was kindly done for me by Dr. C. M. Mitchell of the Department of Mines and Technical Surveys, Ottawa.

In order to attach the crystal to the suspension of the torsion balance it was mounted on a nylon sample holder which is shaped like a golf tee. To determine the correct position of the crystal on the sample holder the apparatus shown in FIGURE 8 was made. One of the cross hairs in the microscope was aligned parallel to the vee groove which holds the shank of the sample holder. The crystal was then mounted on the top of the goniometer with the cleaved face up. By placing a block of brass, extending over the g oniometer on top of the vee groove support the crystal could be oriented so that its basal plane was parallel with the vee groove by raising the goniometer until the cleaved face of the crystal was in contact with the brass block. After the rubber cement[2] holding the crystal to the top of the goniometer had set it was a simple matter to align the arrow with the cross hair in the microscope and hence with the vee groove. Knowing the angle between the arrow and 100 direction the crystal could be set so that the 100 direction lay along the direction of the vee groove and hence the axis of suspension. Once the above direction had been set a drop of rubber cement was put in the cup of the sample holder, its shank laid in the vee groove and the holder pressed gently against the crystal. When the cement had set the crystal was lifted

---

2. Best Test White Rubber Cement made by Union Rubber and Asbestos Company, Trenton, N.J., was found to have very good sticking properties at liquid helium temperatures.

FIGURE 8

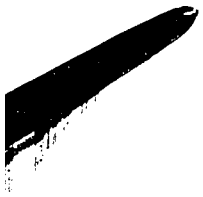

Vee - Groove

The crystal alignment apparatus.

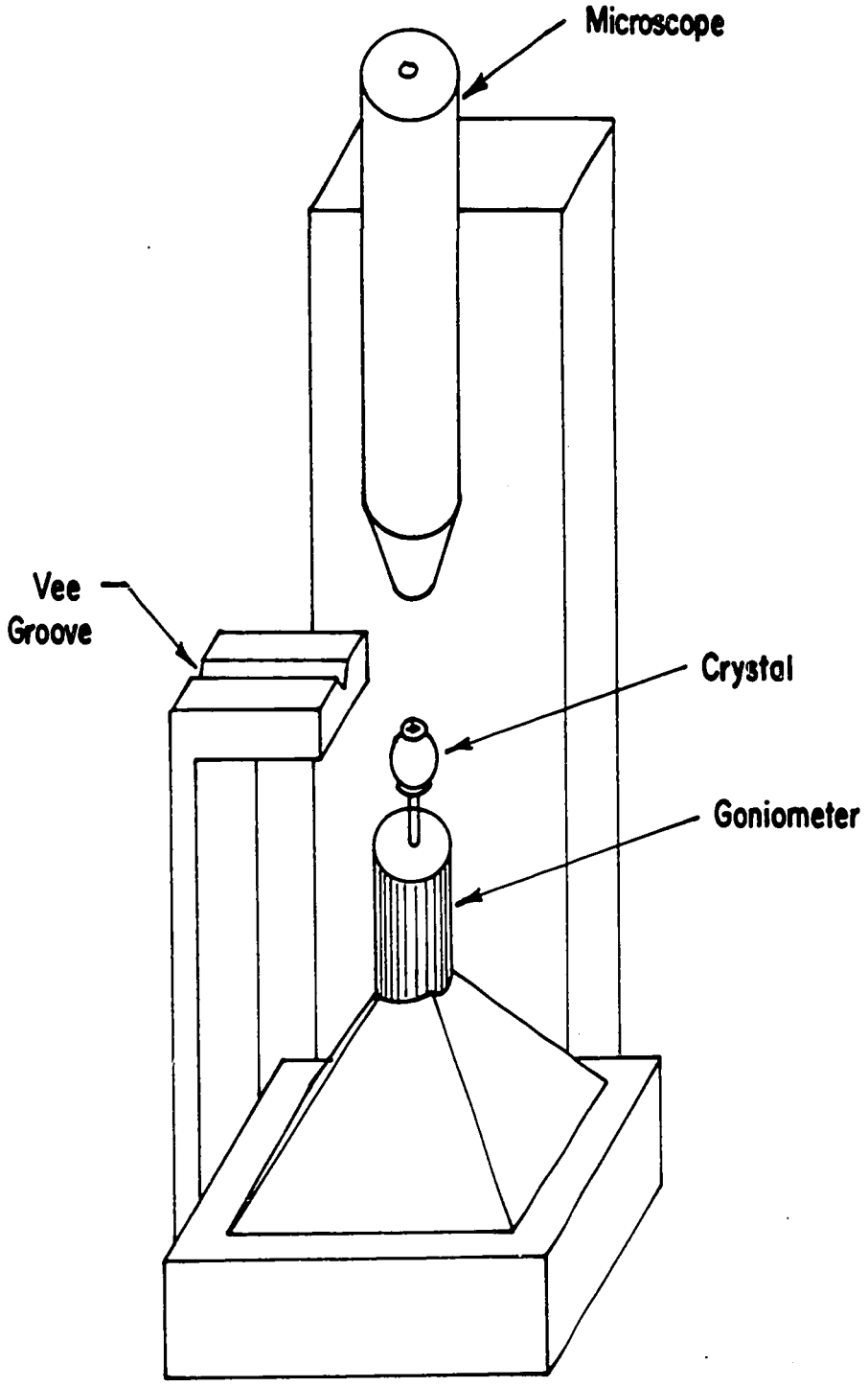
Microscope
Vee
Groove
Crystal
Goniometer

off the goniometer, the excess rubber cement rubbed off, and the crystal and crystal holder stuck on the end of the quartz suspension of the torsion balance using rubber cement. The accuracy with which the arrow could be located with respect to the pole of the 110 plane was about 0.5° and the overall accuracy of the orientation of the crystal should not have been worse than 1°.

After the crystal and crystal holder were mounted on the quartz suspension of the torsion balance the position of the c axis of the crystal relative to the angle scale, ϕ , on the magnet base was found approximately by observation and then two torque measurements at ten degree intervals on either side of the approximate c axis position were made. The torque as a function of angle has been plotted for a typical case in FIGURE 9 and according to equation 1. of APPENDIX II the torque vanishes when the c axis is in the direction of the field. The torque in FIGURE 9 is seen to vanish for an angle ϕ_o and hence by knowing this angle and the angle ϕ at which measurements are to be made the angle ψ between the field and the c axis can be determined from

$$\psi = \phi - \phi_o . \qquad 2.10$$

Shoenberg (1952) has pointed out that in some cases a more desirable method of finding ϕ_o is to determine the angle for which the amplitude of the de Haas van Alphen oscillations vanish since then any changes which might occur in the suspension during the cooling process would be taken into account. Shoenberg's method was used, FIGURE 10, as a check on the previously described method of finding ϕ_o.

FIGURE 9

The torque exerted on a crystal as a function of magnet orientation at room temperature for a typical case.

FIGURE 10

The amplitude of the de Haas van Alphen effect as a function of magnet orientation for the same case as FIGURE 4.

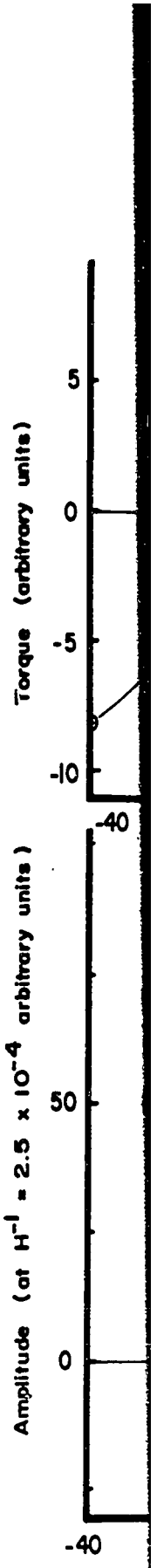

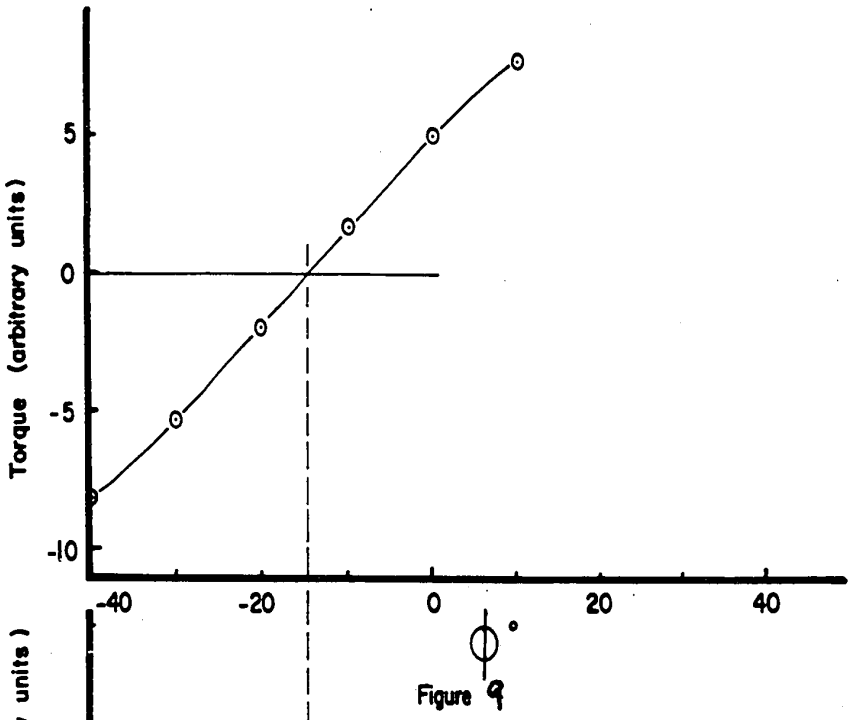

Figure 9

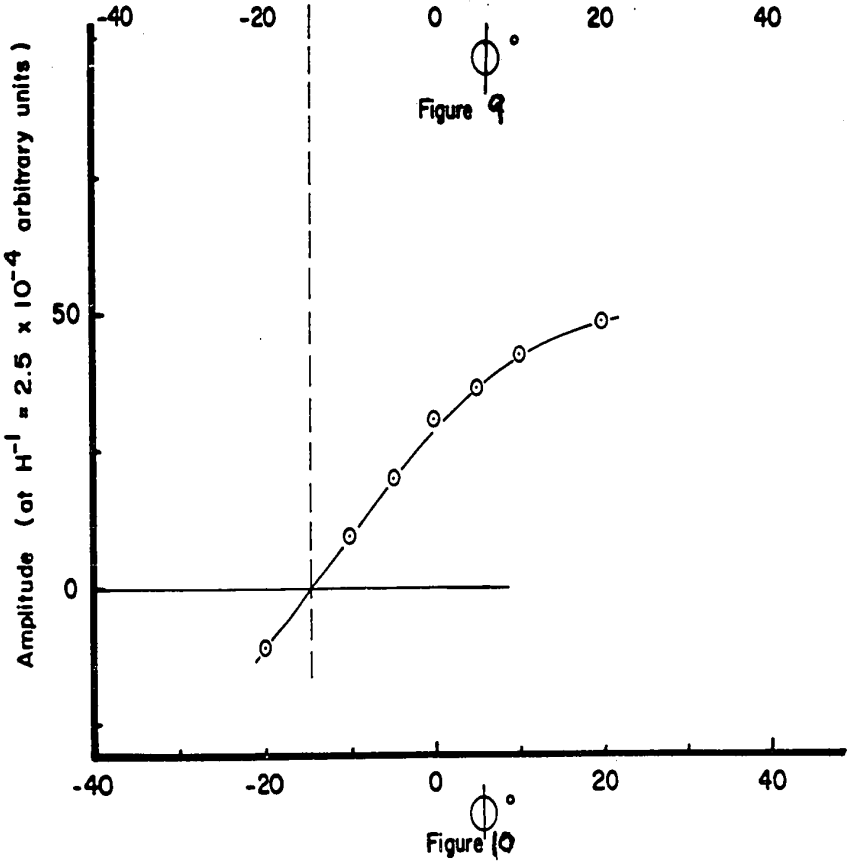

Figure 10

By comparing FIGURES 9 and 10 it is seen that no significant difference between the two methods was observed.[3] Since measuring the torque as a function of angle at room temperature is a simpler experiment this method was adopted.

With the magnet set so that $\psi = 45^{\circ}$ the torque on each crystal was measured as a function of field at room temperature. A plot of C/H^2 as a function of $1/H$ (Honda plot) was made to check for ferromagnetic impurities. Any crystals showing ferromagnetic impurities were rejected.

Once the oriented crystal was mounted, the balance aligned and ϕ_o determined the balance was evacuated and about one centimeter of helium heat exchange gas admitted. Helium was then transferred to the Dewar and the filled Dewar assembly lifted into position around the crystal. The magnet was rolled into position, rotated until the desired direction between the field and the c axis of the crystal was obtained, and cycled three or four times to insure that it was in cyclic condition. After a trial run or two to determine the correct setting of the sensitivity control, the field was increased to its highest value of about 5.3 kilo-oersteds and reduced from that value to a value of about 1.6 kilo-oersteds in 130 steps of approximately equal decrement in $1/H$. The torque was recorded for each of the above steps and in this way a detailed curve of torque as a function of reciprocal field could be drawn. To obtain the greatest possible accuracy a given set of measurements was often broken up

---

3. Donahoe and Nix (1954) also found this to be the case using a balance which had an almost identical method of suspending the crystal.

into two or three parts as shown typically in FIGURE 5, CHAPTER IV, and the sensitivity of the balance increased as the field became smaller and the amplitude of the oscillations reduced. It should be noted here that during the above operations the magnet was always kept cyclic and the measurements were made for only one direction of current flow through the magnet. After the de Haas van Alphen effect had been measured for all the desired angles between the field and the c axis at 4.2° K, the liquid helium in the inner Dewar was pumped down to a temperature of about 1.7° K and measurements of torque as a function of reciprocal field were made for each of the angles between the field and the c axis of the crystal that were used in the measurements at 4.2° K. The temperature of the helium bath was determined by measuring the vapour pressure of the helium using a bourdon guage, which was connected to the top of the cryostat. The temperature was determined from the table of Clement and Logan and Gaffney (1955).

2.5 The Magnet and Magnet Current Regulator

The magnet used for the present experiments was a Newport Instruments type A with 4-inch diameter shimmed pole tips. With a gap of 6 cm. the maximum available field was 5.5 kilo-oersteds at 5 amperes. The field homogeniety was measured using a Rawson type 720 flux meter both along the line of centers of the pole tips and perpendicular to the line of centers of the pole tips. The results of these measurements are shown in FIGURE 11.

Since the intervals of reciprocal field required for the de Haas van Alphen effect measurements lead to intervals of current

FIGURE 11

Field Homogeniety

a) The magnetic field measured along the line of centers from the center of the gap to the pole tip face.

b) The magnetic field measured perpendicular to the line of centers at the center of the gap away from the line of centers.

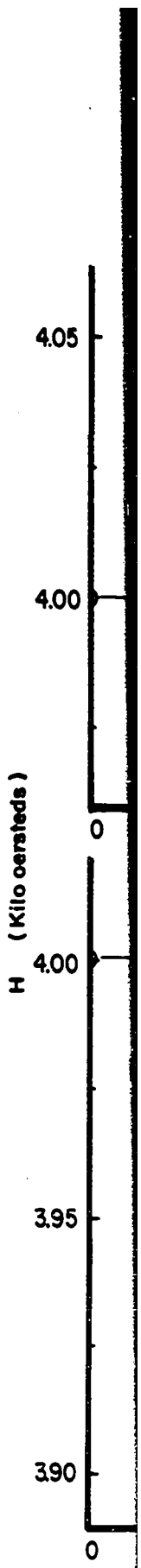

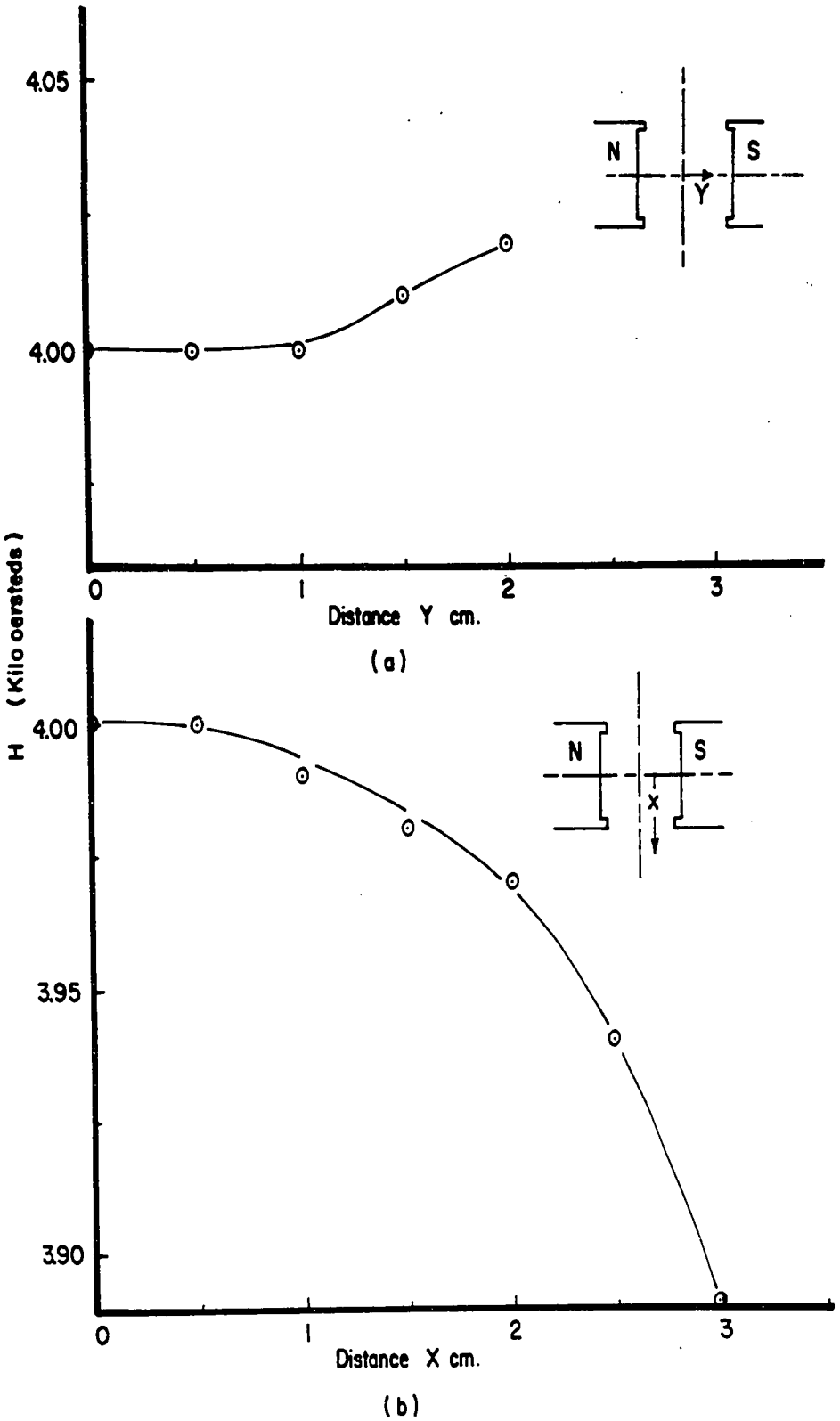
4.05
4.00
N
S
Y
0
1
2
3
Distance Y cm.
(a)
H (Kilo oersteds)
4.00
3.95
3.90
N
S
X
0
1
2
3
Distance X cm.
(b)

FIGURE 12

Reciprocal magnetic field as a function of potentiometer reading for a typical case.

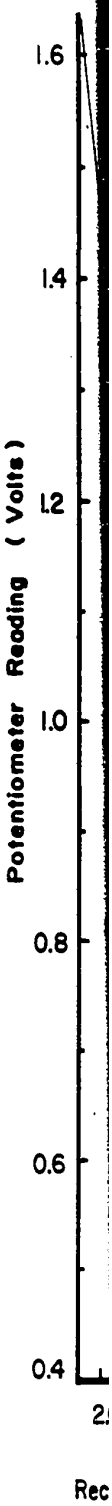

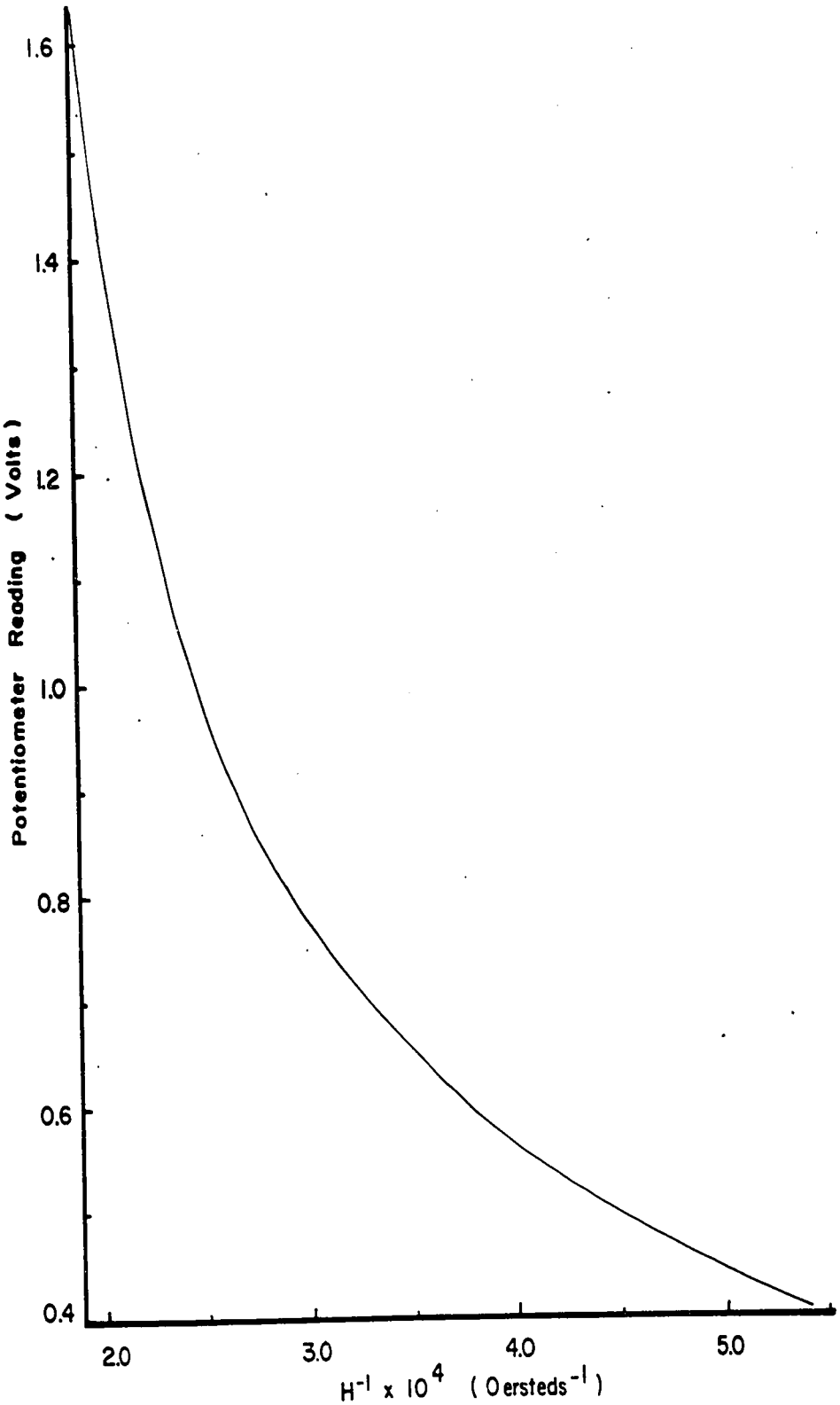

Reciprocal Field as a Function of Potentiometer Reading

which are too small to be accurately read on an ammeter a potentiometer was connected across a section of the current sensing resistor in the magnet current regulator, (FIGURE 13). The voltage appearing at the potentiometer terminals was then used as a measure of the current flowing through the magnet. The magnetic field corresponding to a given potentiometer reading was measured and the magnet calibrated. The magnet was calibrated in the above way after each series of de Haas van Alphen effect experiments in order to eliminate any errors which might arise due to a change in the pole tip spacing between runs. Field readings were taken for every value of current used in the experiment and a typical graph of reciprocal field as a function of potentiometer reading is shown in FIGURE 12.

In most magnetic work it is necessary to vary the magnetic field continuously without back tracking and also to hold it constant for a reasonable period of time. For the present research it was also desirable to have as little noise on the magnet current as possible because small fluctuations in magnetic field cause large eddy currents to be induced in the highly conducting zinc crystals which resulted in spurious torques or noise on the output of the servo balance. To meet the above requirements an electronic current regulator was designed by Dr. F. R. Hunt to control the current from a back of storage batteries. The circuit diagram of the current regulator is shown in FIGURE 13.

FIGURE 13

The circuit diagram of the magnet current regulator.

All resistors high stability deposited carbon types

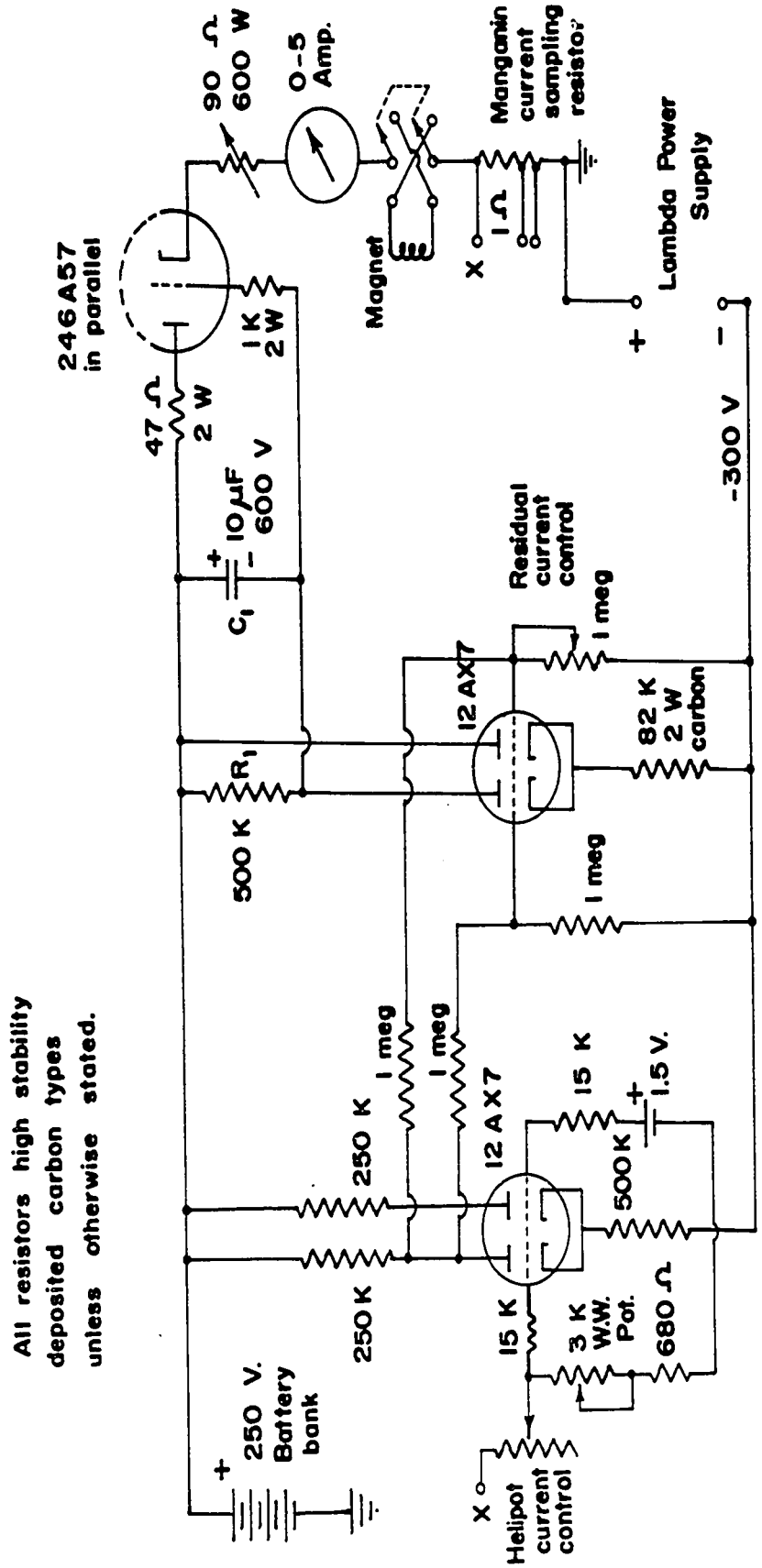
All resistors high stability deposited carbon types unless otherwise stated.
246A57 in parallel
90 Ω 600 W
0-5 Amp.
Manganin current sampling resistor
1 Ω
Magnet
X
Lambda Power Supply
+
-300 V
-
47 Ω 2 W
1 K 2 W
10 μF 600 V
C1
Residual current control
1 meg
12 AX7
82 K 2 W carbon
R1
500 K
1 meg
1 meg
1 meg
250 K
250 K
12 AX7
15 K
1.5 V.
500 K
250 V. Battery bank
15 K
3 K W.W. Pot.
680 Ω
X
Helipot current control

CHAPTER III

Alloy and Specimen Preparation

3.1 Alloy Preparation

For the present research it was desired to measure both the resistance and thermo e.m.f. of the zinc mananese alloys not only as a function of temperature but also as a function of manganese concentration. A series of alloys was accordingly prepared with manganese concentrations ranging from about 0.01% manganese by weight up to the solid solubility limit for manganese in zinc. FIGURE 1 shows the phase diagram of the zinc manganese system as given by Anderson (1948). From the phase diagram the solid solubility limit of manganese in zinc is seen to be 0.45 weight percent at 420° C. It was therefore decided to prepare a series of zinc alloys with the concentrations of manganese varying from 0.43 to 0.01 percent by weight. The alloys were prepared using 99.999 percent pure zinc supplied by the New Jersey Zinc Company with the specification shown in TABLE I.

TABLE I

New Jersey Zinc Company. Special Horsehead Zinc. Purity 99.999%			
Major Impurities:			
Pb	0.0002%	Fe	0.0003%
Cd	0.00005%	As	0.000006%
Cu	0.00005%	Sn	0.00005%

FIGURE I

The phase diagram for the zinc manganese system.

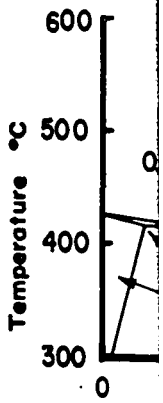

FIGURE 2

The resistance ratio ($R_{4.2}$ / R_{273} - $R_{4.2}$) of zinc manganese alloys as a function of manganese concentration.

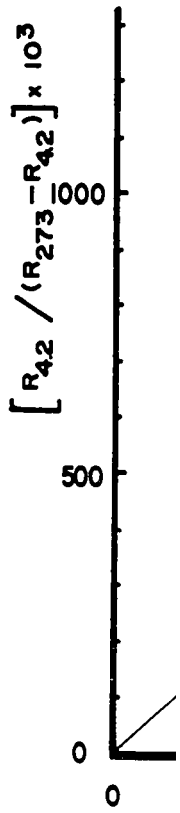

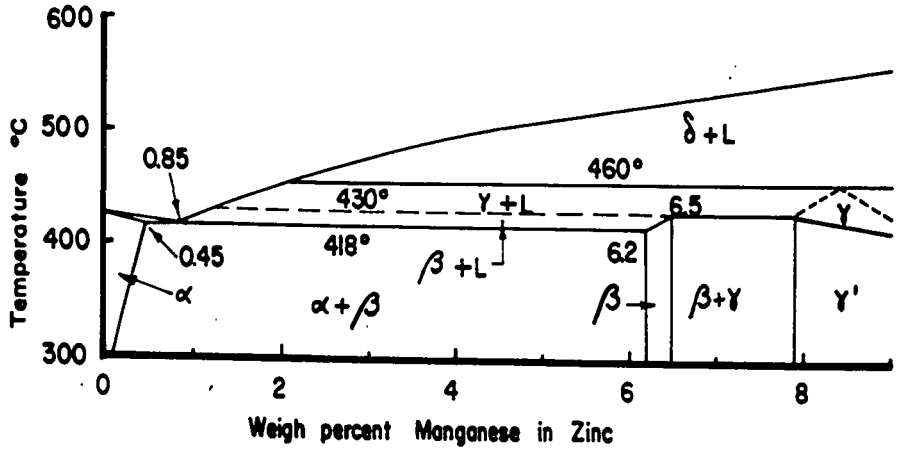
600
500
400
300
Temperature °C
0.85
δ+L
460°
430°
γ+L
6.5
γ
0.45
418°
β+L
6.2
α
α+β
β
β+γ
γ'
0
2
4
6
8
Weigh percent Manganese in Zinc

Fig. 1

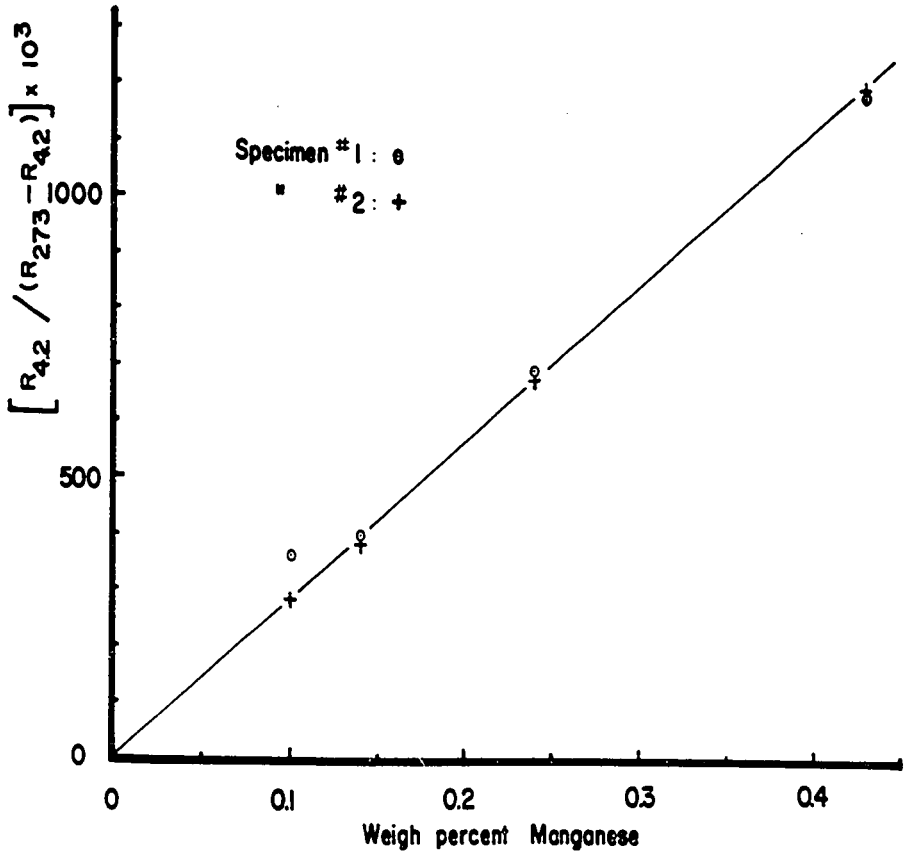
$[R_{42}/(R_{273}-R_{42})] \times 10^3$
Specimen #1 : o
" #2 : +
1000
500
0
0
0.1
0.2
0.3
0.4
Weigh percent Manganese

Fig. 2

The Manganese was supplied by A. D. Mackay Inc. and has the specification shown in TABLE II.

TABLE II

Manganese Specification	Purity 99.99 percent
Impurity	Quantity parts per million
Mg	30
Si	2
Fe	4
Cu	less than 1

To prepare the alloy, a small ingot of zinc weighing about 20 grams was cut from the stock and a hole bored out of its centre about 1/2 inch deep and 1/4 inch in diameter. The zinc was then cleaned using an etchant which consists of 50 percent concentrated hydrochloric acid by volume in distilled water. The zinc was then weighed carefully. An appropriate amount of manganese was cleaned using dilute nitric acid in the following way: The bottom of a small, 100 cc. beaker was covered by about 1/8 inch of distilled water and concentrated nitric acid was added drop by drop, while swirling the beaker, until the desired reaction rate was achieved. When the manganese appeared bright and shiny it was judged clean and was then rinsed thoroughly with distilled water. The manganese was dried by rinsing it in ethyl alcohol and then in ether. After pouring off the ether, the sample air-dried almost instantly. The manganese was then powdered in an agate mortar and the manganese

powder poured into the hole in the zinc ingot. The zinc ingot containing the manganese powder was weighed and the concentration of manganese calculated. The ingot was sealed into an evacuated quartz tube and heated to a temperature of 700° C in an electric furnace. The melt was maintained at 700° C for two hours and during that time was shaken vigorously every 15 minutes. It was removed from the furnace and quenched in ice water to insure that all the manganese present remained in solution. The quartz tube was broken open and the alloy cleaned by etching in the hydorchloric acid solution, rinsed with distilled water and dried with a clean paper towel. In an attempt to increase the homogeniety of the alloy it was sealed in an evacuated pyrex tube, annealed for 48 hours at 400° C and quenched in ice water. The ingot was then cleaned, rinsed and dried and two pieces cut from it that could be rolled out into specimens suitable for resistance measurements. The results obtained from the measurement of the resistance ratio, $R_{4.2} / (R_{273} - R_{4.2})$, as a function of manganese concentration for four carefully prepared alloys is given in TABLE III and is plotted in FIGURE 2. The concentration of manganese in the other alloys used in the experiments was obtained from the graph of FIGURE 2 after measuring the resistance ratio of the specimen concerned.

3.2 Resistance Specimen Preparation

Specimens suitable for resistance and resistivity measurements were prepared from the alloys shown in TABLE III. The specimens were prepared by cutting a slice about 1/16 of an inch thick from the ingot. The slice was then cleaned using the hydrochloric acid etch,

rinsed, dried, and rolled into a thin strip. The strip was sliced to make a specimen of uniform crossectional area using the punch designed by Wallingford (1961). After the specimen was cut, it was cleaned by etching in the hydrochloric acid solution, rinsed, dried and sealed in an evacuated pyrex tube. The specimen was given a strain-relieving aneal for about 24 hours at 400° C. It was then quenched in ice water to assure that all the manganese stayed in solid solution, removed from the pyrex tub, etched, rinsed, and dried. TABLE III gives the resistance ratio, $(R_{4.2} / (R_{273} - R_{4.2})$, the concentration of manganese as deduced using FIGURE 2, and the resistivity of all the resistance specimens.

3.3 The Thermo e.m.f. Specimens

A slice about 1/8 inch thick was cut from the ingot and rolled into a strip about 16 inches long which was then trimmed to a width of about 1/8 of an inch using scissors. This narrow strip was treated in the same way as the resistance specimens to obtain the final thermo e.m.f. specimen. A piece suitable for resistance ratio measurements was cut from each end as a check on the homogeniety of the specimen. The values obtained are tabulated in TABLE III along with the concentrations of manganese as read from FIGURE 2.

3.4 Zinc and Zinc Manganese Single Crystals

Both pure and alloy spherical, single crystals were successfully grown by the method to be described. The spherical shape was adopted so that the crystal could easily be positioned on the sample

holder, with the desired crystallographic orientation relative to the suspension of the balance, (CHAPTER II, Section 3). Since the amplitude of the de Haas van Alphen effect oscillations decreases rapidly with increasing impurity concentration, due to the scattering of the conduction electrons by the impurity ions, single crystals were grown using only alloys containing relatively low manganese concentrations.

The 5/16 inch diameter crystals were grown in the graphite mould shown in FIGURE 3 in the following way: Sufficient metal to fill the mould and leave about 1/2 inch of metal in the sprue was put in the chamber at the top of the mould. The mould was then heated rapidly in a hot furnace and the molten metal jarred into the lower section of the mould. The mould was removed from the furnace and allowed to cool quickly in air. It was separated and the polycrystalline ingot in the shape of the desired crystal was removed, cleaned by etching in hydrochloric acid, rinsed and dried. The clean ingot was then re-inserted in the mould, which had been wiped clean, and the mould and ingot positioned in the furnace as shown in FIGURE 4. The temperature of the furnace was raised until the thermocouple in the mould indicated that the temperature at the bottom of the crystal was about 15° C above the melting point. The current flowing through the furnace was then reduced sufficiently so that over a period of about two hours the crystal would solidify slowly from the bottom up due to the thermal gradient at the end of the furnace. By adjusting the position of the mould in the furnace, and the amount by which the current was reduced, conditions could be found so that about 80% of the growing operations were successful. After cooling the crystal

FIGURE 3

The graphite mould used to grow the spherical single crystals.

FIGURE 4

The position in the furnace of the graphite mould containing the crystal is shown.

Vermiculite —

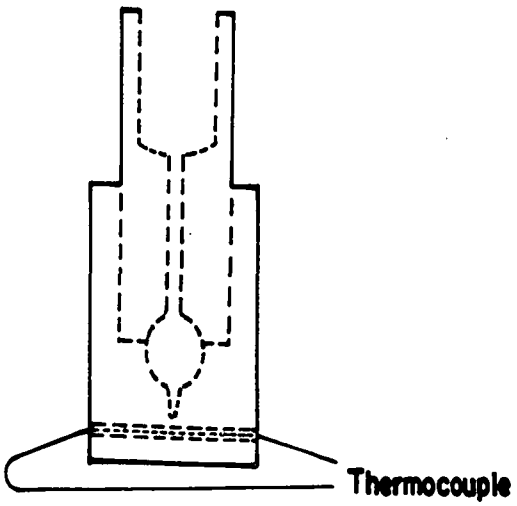
Thermocouple

Fig. 3

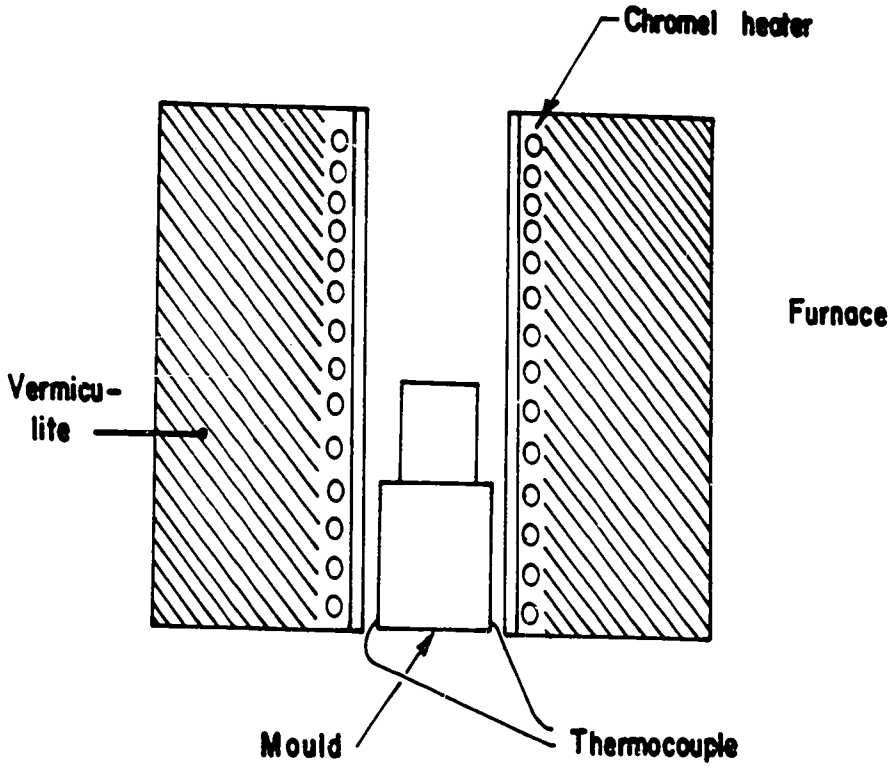
Chromel heater
Furnace
Vermicu-
lite
Mould
Thermocouple

Fig. 4

to room temperature, it was etched using fifty-percent hydrochloric acid. The grain structure, if any, was then clearly visible and polycrystalline specimens or single crystals with strays could easily be picked out and rejected.

The crystals were then cleaved to expose the basal plane and to determine the direction of the c axis which is perpendicular to the basal plane. This was accomplished without unduly distorting the crystal by cooling it in liquid nitrogen and then cleaving on the cylindrical portion of the crystal that was formed in the sprue of the mould, in such a way that the cleavage extended into the main spherical body of the crystal removing a small portion of it. The remainder of the cylinder and the conical tail of the crystal were then cut off using a jeweller's saw. The crystal was etched to remove any traces o f iron which might remain. The pieces cut from the crystal were made into specimens suitable for resistance ratio measurements. TABLE III shows the results of these measurements. From TABLE III it is seen that the difference in resistance ratio and hence in manganese concentration between each end of the crystal is reasonably small.

TABLE III

SAMPLE	Resistance Ratio $R_{4.2} / (R_{273} - R_{4.2}) \times 10^3$		Conc. Mn Wt. % * indicates alloys used for calibration	Resistivity ohm - cm. x 10^6
	end 1	end 2		
RESISTANCE	1.2		Pure Zn	5.5
	14.7		0.006	5.0
	171		0.06	5.7
	362	282	0.10*	6.7
	396	380	0.14*	6.9
	692	677	0.24*	8.1
	1190	1200	0.43*	12.0
THERMO e.m.f.	40.6	42.8	0.015	
	174	1.81	0.063	
	334	300	0.11	
	676	583	0.22	
	1060	1060	0.37	
Crystals	23.5	24.1	0.008	
	82.3	85.7	0.025	

CHAPTER IV

RESULTS

4.1 Resistance and Thermo e.m.f.

The results of the resistance measurements are shown in FIGURE I. Inset "C" shows the resistance of the zinc manganese single crystal used in the de Haas van Alphen effect experiments. Inset "a" shows the low temperature resistance of the most concentrated alloy containing 0.42 wt. % manganese. No evidence of a resistance maximum was found, the resistance of the alloy being constant between 2.0° K and 5.0° K. The temperature at which the minimum occurs and the depth of the minimum, D defined by $D \equiv (R_{2.0} - R_{min}) / R_{min}$, are plotted as a function of manganese concentration and shown in inset "b". These results are similar to those for other alloys showing a resistance minimum.[1, 2] The results of measuring the thermo e.m.f. of a series of zinc manganese alloys, relative to pure zinc, as a function of temperature are also shown in FIGURE I. They agree qualitatively, at least, with other thermo e.m.f. measurements on alloys showing a resistance minimum.[3]

4.2 The de Haas van Alphen Effect

The de Haas van Alphen effect was investigated by measuring the torque on a crystal of zinc having its [100] direction parallel

---

1) Hedgcock, Muir and Wallingford (1961).
2) Gerritsen (1959).
3) MacDonald and Pearson (1953).

The resistance and the thermo e.m.f., relative to pure zinc, of a series of dilute zinc manganese alloys.

a) The resistance of the most concentrated alloy, showing no evidence of a maximum down to 2° K.

b) The depth and temperature of the minimum as a function of manganese concentration.

c) The resistance of the zinc manganese crystal used in the de Haas van Alphen effect measurements.

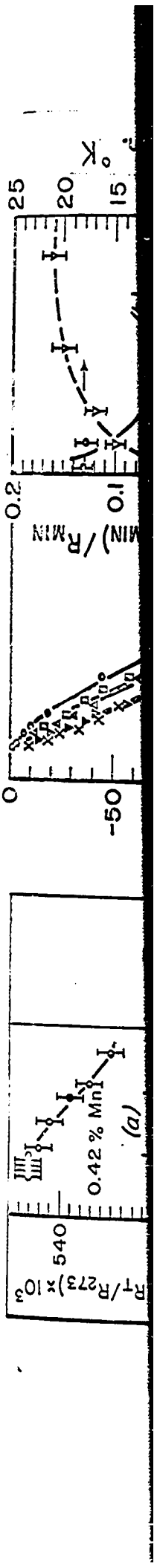

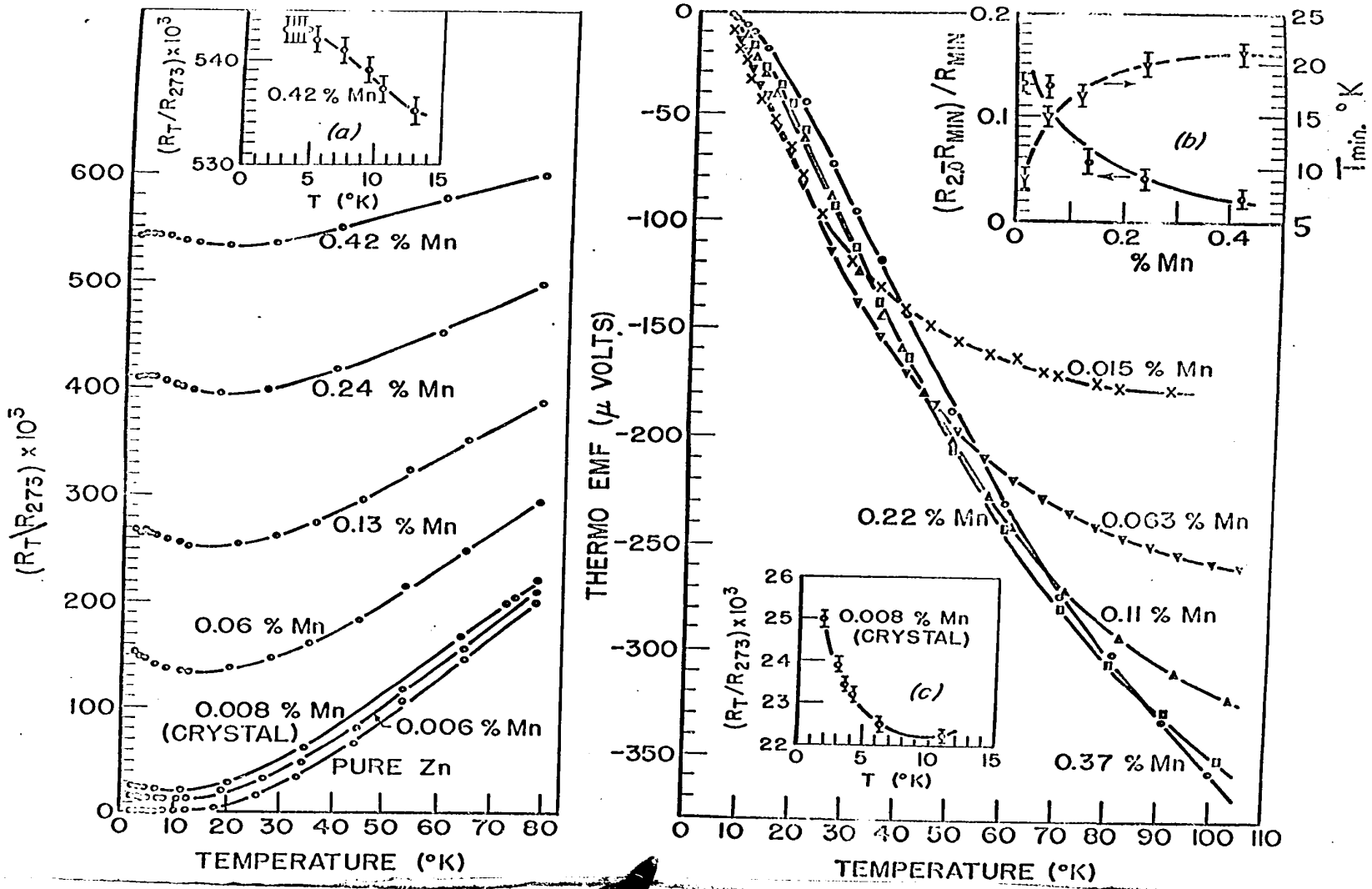

e de Haas

of manganese

no evidence

o

to the suspension of the torsion balance for various orientations of the "c" axis of the crystal relative to the magnetic field. The results for pure zinc are shown in FIGURES 2 to 5 and those for the 0.008 wt. % zinc manganese alloy in FIGURES 6 to 12. It is seen that a relatively large steady state torque was observed at 1.7° K for the zinc manganese alloy. This effect is studied more closely in a more concentrated alloy in APPENDIX III.

4.3 Analysis of the de Haas van Alphen Effect Measurements

The period of the oscillations is given by the slope of the line obtained by plotting the values of H^{-1}, obtained at the extreme values of the torque, against half integers as shown in FIGURE 13 for pure zinc and in FIGURE 14 for the 0.008 wt. % zinc manganese alloy. As can be seen in FIGURE 15 the square of the period, P, is a linear function of $\cos^2\psi$ which is to be expected for an ellipsoidal Fermi surface[4]. Included in FIGURE 15 is the data obtained by Verkin and Dmitrenko (1958) for pure zinc. All the results are seen to be identical within the indicated 1.5% experimental error in the period.

The effective mass of the electrons is determined by plotting W (see equation 1.6 of CHAPTER I) as a function of m^*/mH for various values of T_1 as shown in FIGURE 16.[5] Using the experimental values of $|C_1|/|C_2|$ and T_1 corresponding values of m^*/mH are read from the graph and m^*/m calculated. The values obtained for the effective mass of the electrons in pure zinc are plotted as a function of

---

4) Shoenberg (1959).
5) T_2 remains fixed at 4.2° K.

FIGURES 2 through 5

The torque exerted on a single crystal of pure zinc for various orientations as a function of magnetic field and temperature.

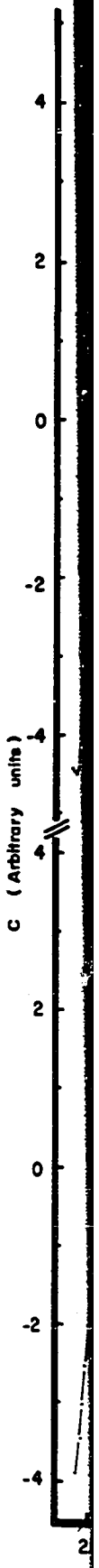

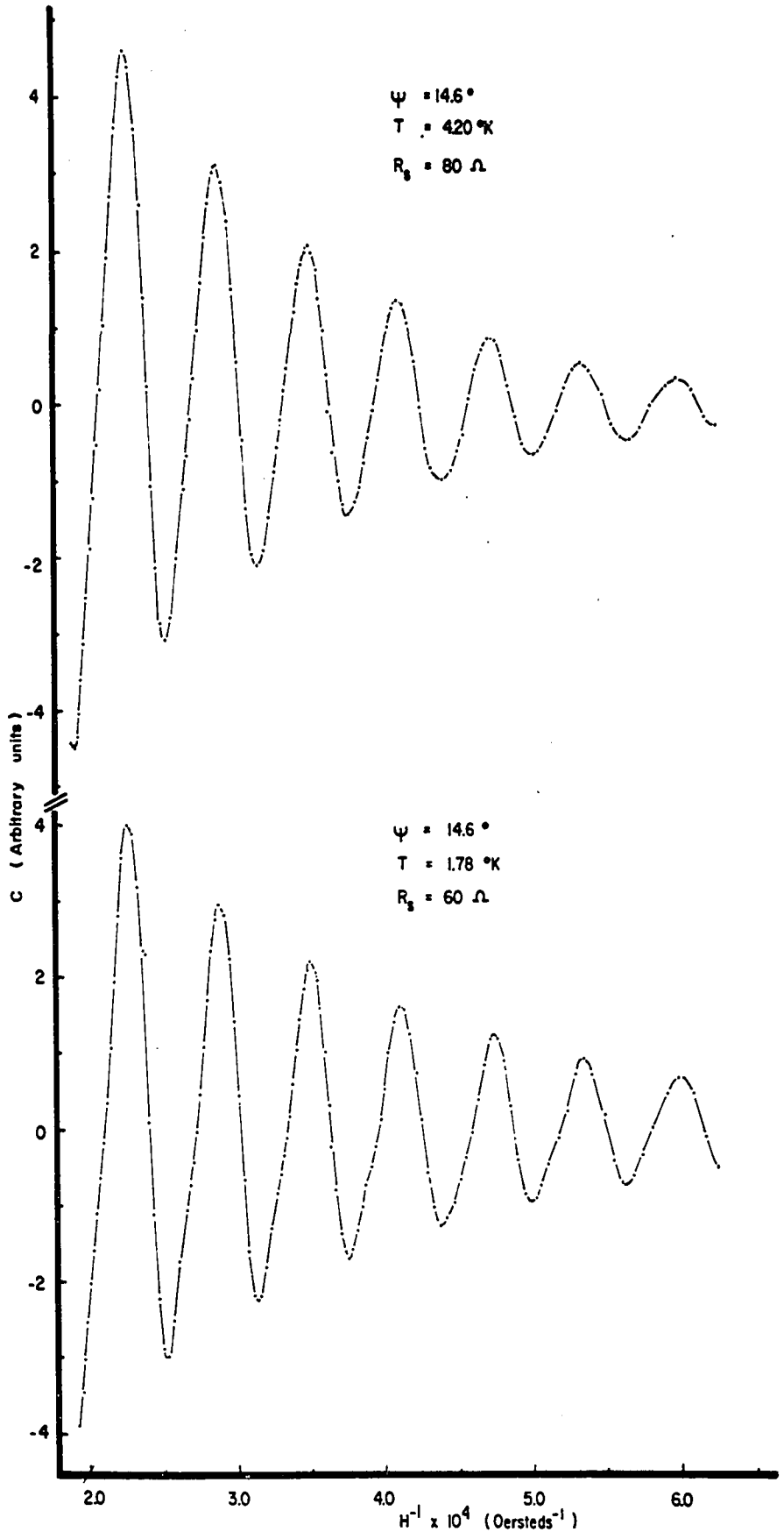
ψ = 14.6°
T = 4.20°K
R_s = 80 Ω
ψ = 14.6°
T = 1.78°K
R_s = 60 Ω
C (Arbitrary units)
4
2
0
-2
-4
2.0
3.0
4.0
5.0
6.0
$H^{-1} \times 10^4$ (Oersteds^{-1})

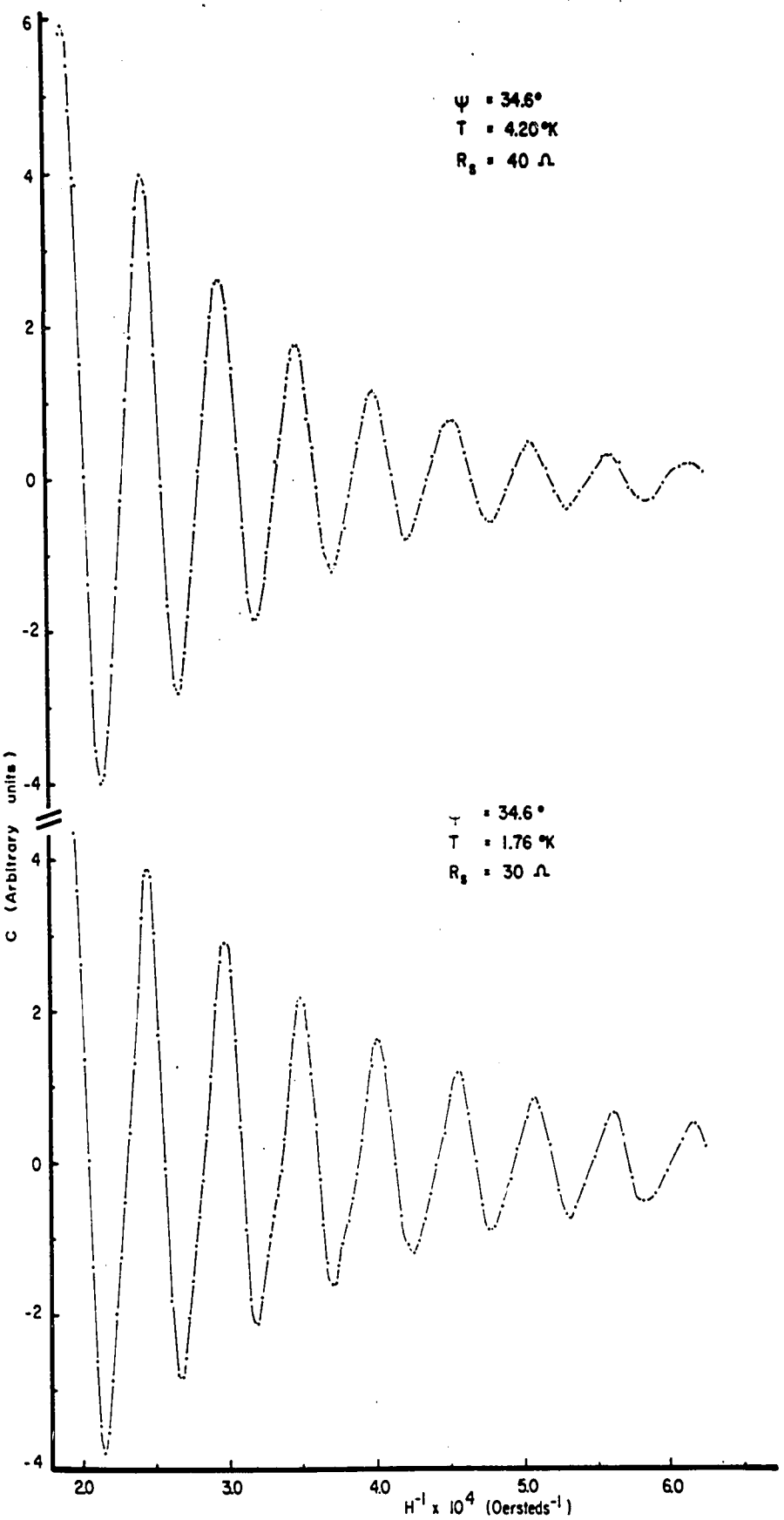
ψ = 34.6°
T = 4.20°K
R_s = 40 Ω
ψ = 34.6°
T = 1.76 °K
R_s = 30 Ω
C (Arbitrary units)
6
4
2
0
-2
-4
4
2
0
-2
-4
2.0
3.0
4.0
5.0
6.0
$H^{-1} \times 10^4$ (Oersteds^{-1})

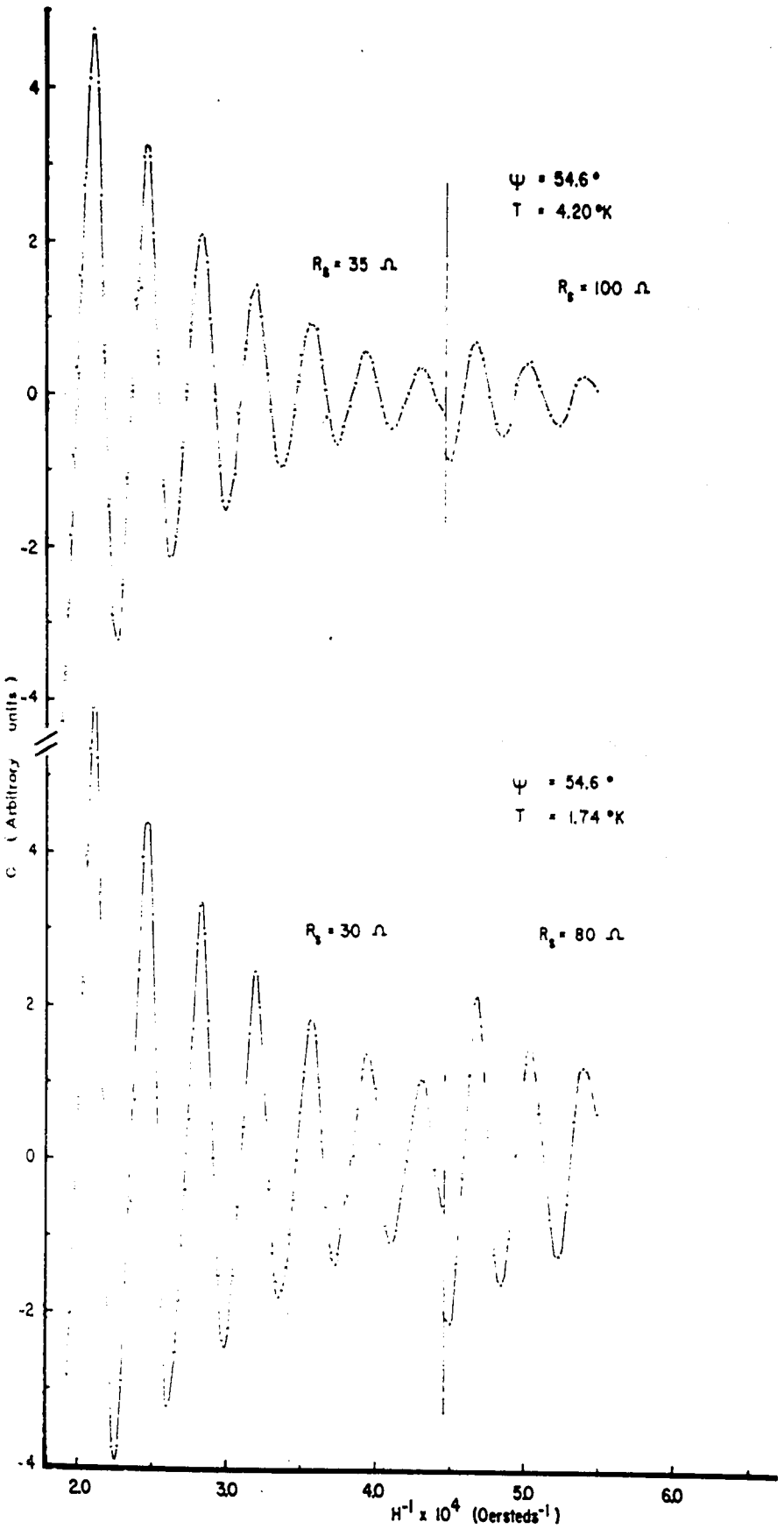
Ψ = 54.6°
T = 4.20°K
R_s = 35 Ω
R_s = 100 Ω
Ψ = 54.6°
T = 1.74°K
R_s = 30 Ω
R_s = 80 Ω
G (Arbitrary units)
4
2
0
-2
-4
2.0
3.0
4.0
5.0
6.0
H^-1 x 10^4 (Oersteds^-1)

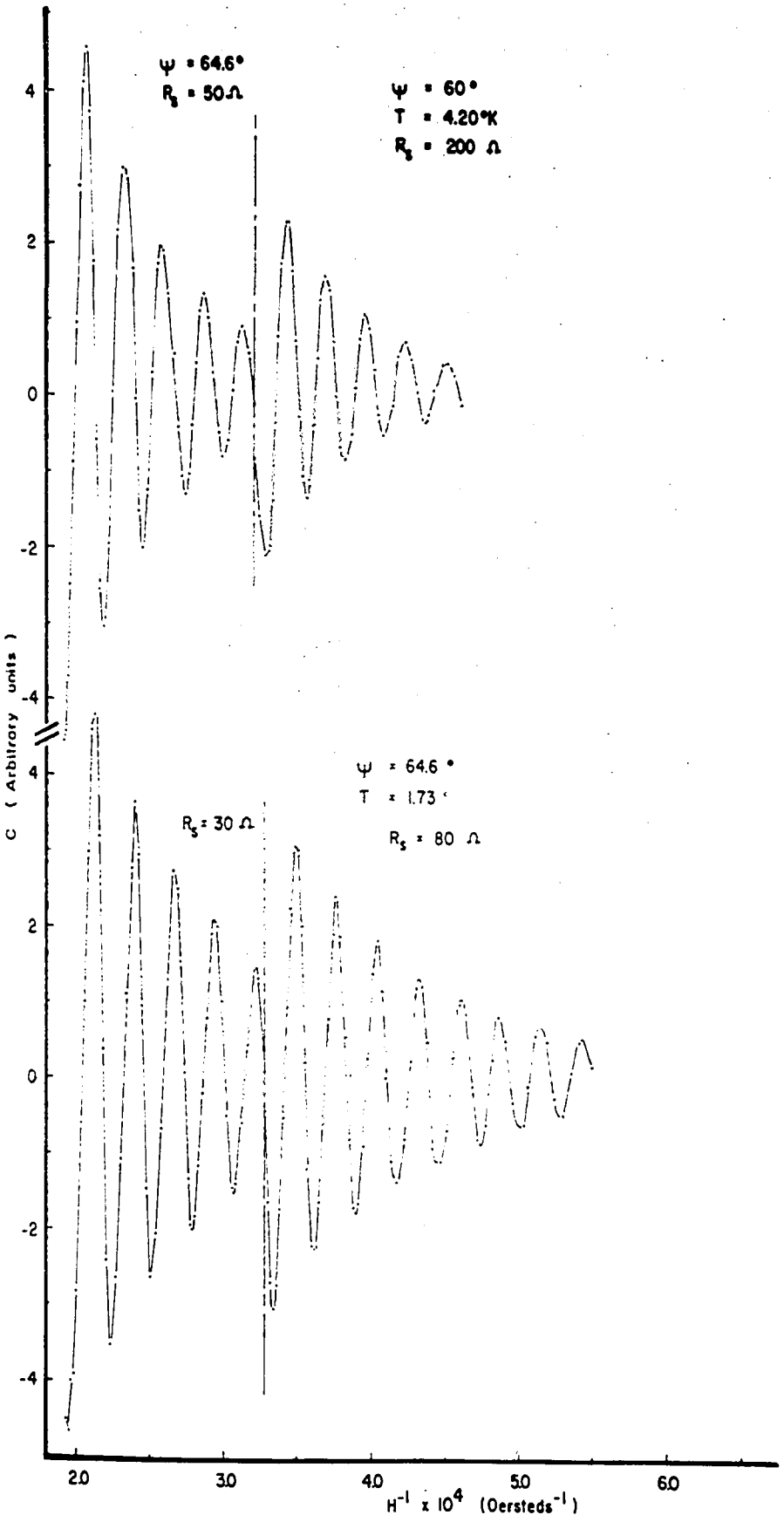
Ψ = 64.6°
R_s = 50 Ω
Ψ = 60°
T = 4.20°K
R_s = 200 Ω
Ψ = 64.6°
T = 1.73°K
R_s = 30 Ω
R_s = 80 Ω
C (Arbitrary units)
4
2
0
-2
-4
2.0
3.0
4.0
5.0
6.0
H^-1 x 10^4 (Oersteds^-1)

FIGURES 6 through 12

The torque exerted on a 0.008% zinc manganese crystal, for varoius orientations, as a function of magnetic field and temperature. The vertical assymmetry observed in the low temperature data is due to the steady magnetic anisotropy of the crystal which is discussed in more detail in APPENDIX II.

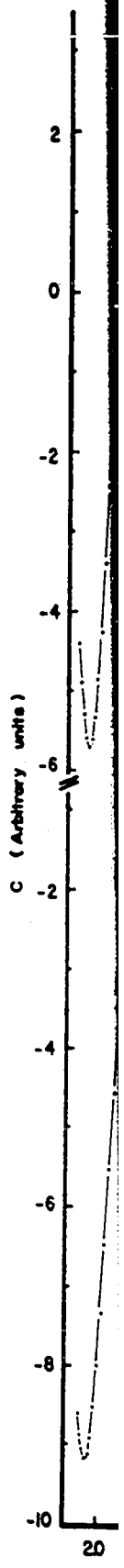

is

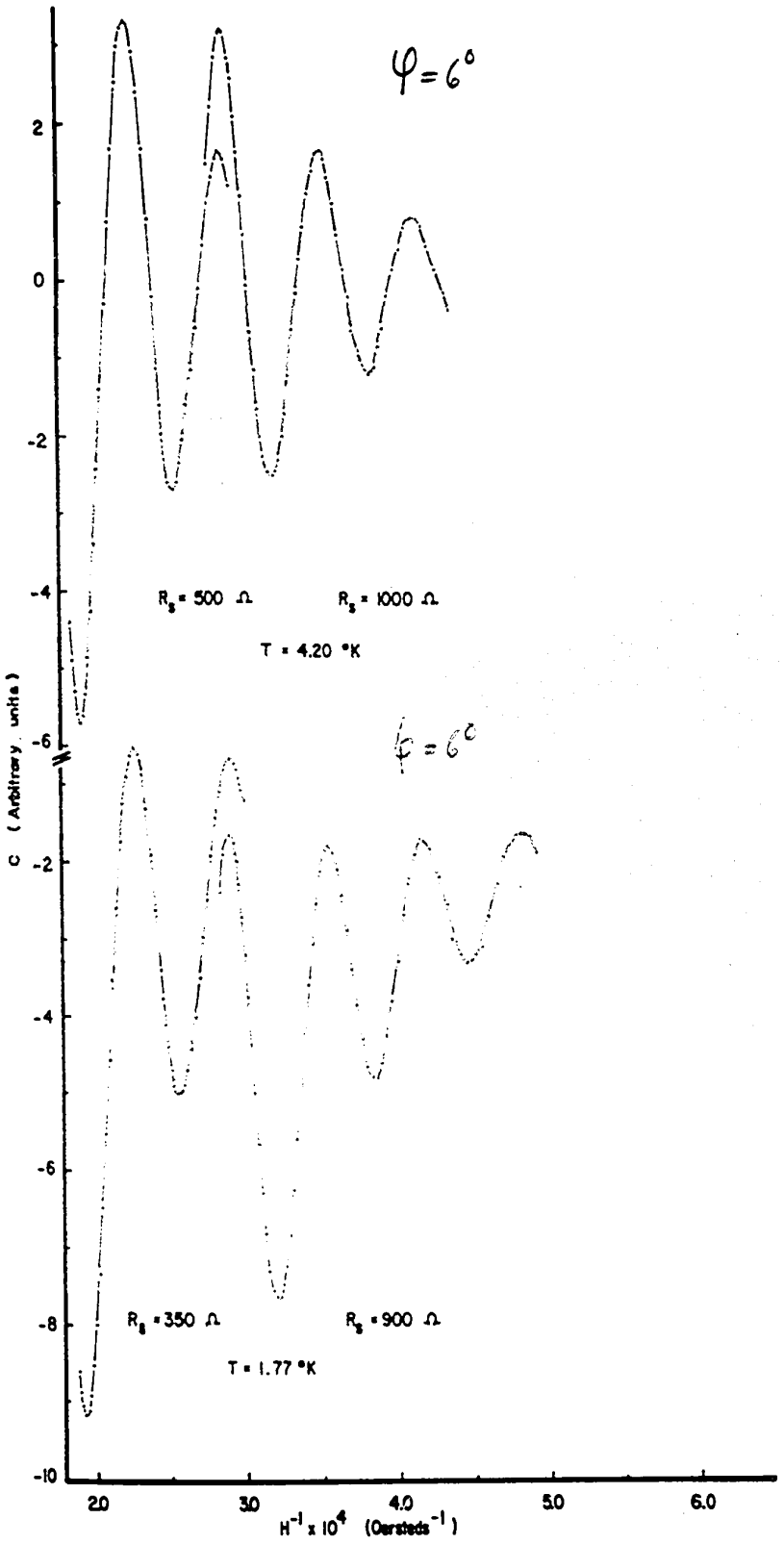
φ = 6°
2
0
-2
-4
-6
R_s = 500 Ω
R_s = 1000 Ω
T = 4.20 °K
φ = 6°
-2
-4
-6
-8
-10
R_s = 350 Ω
R_s = 900 Ω
T = 1.77 °K
σ (Arbitrary units)
2.0
3.0
4.0
5.0
6.0
H^-1 x 10^4 (Oersteds^-1)

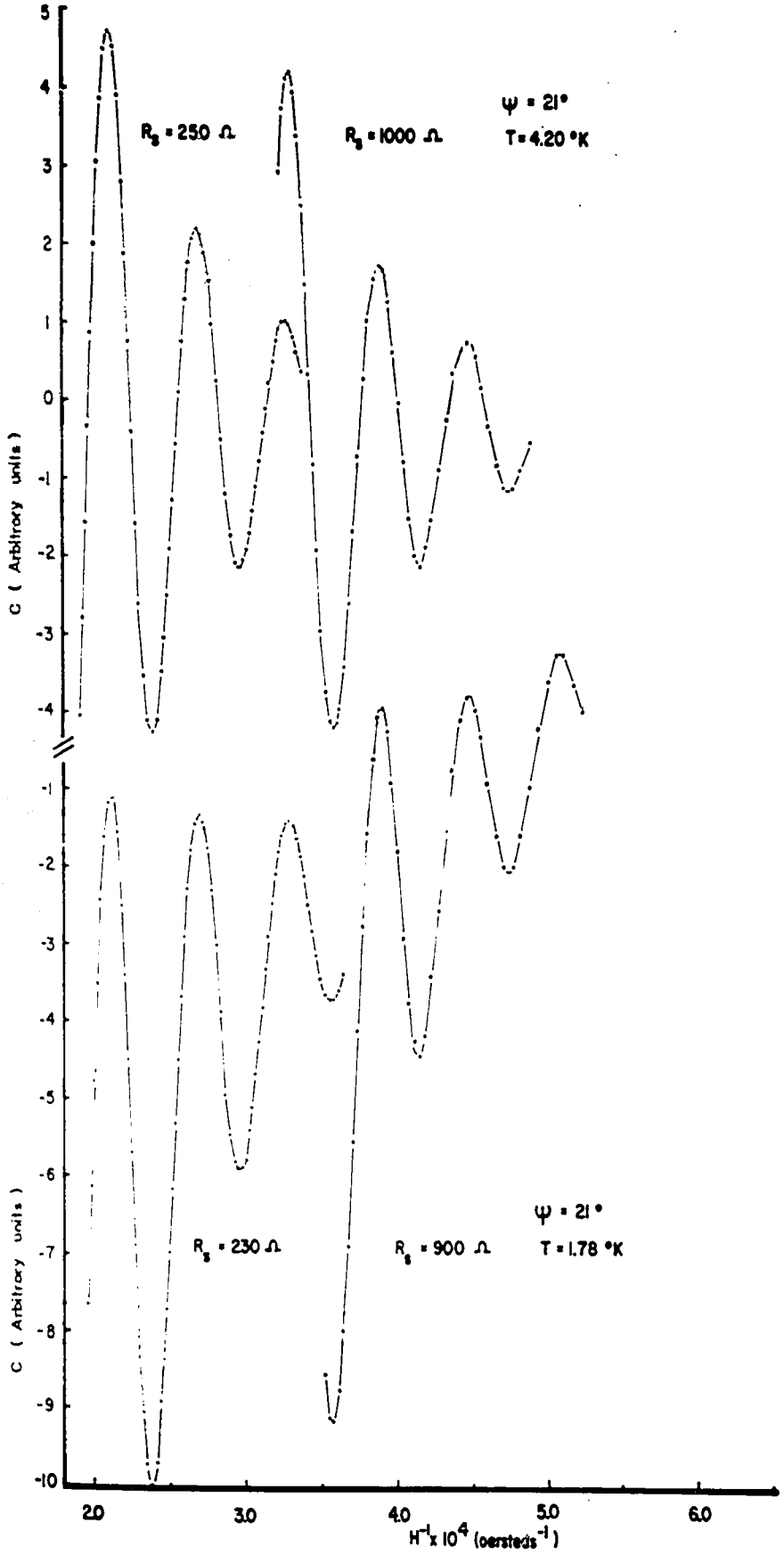
R_s = 250 Ω
R_s = 1000 Ω
ψ = 21°
T = 4.20 °K
C (Arbitrary units)
R_s = 230 Ω
R_s = 900 Ω
ψ = 21°
T = 1.78 °K
C (Arbitrary units)
$H^{-1} \times 10^{-4}$ (oersteds^{-1})

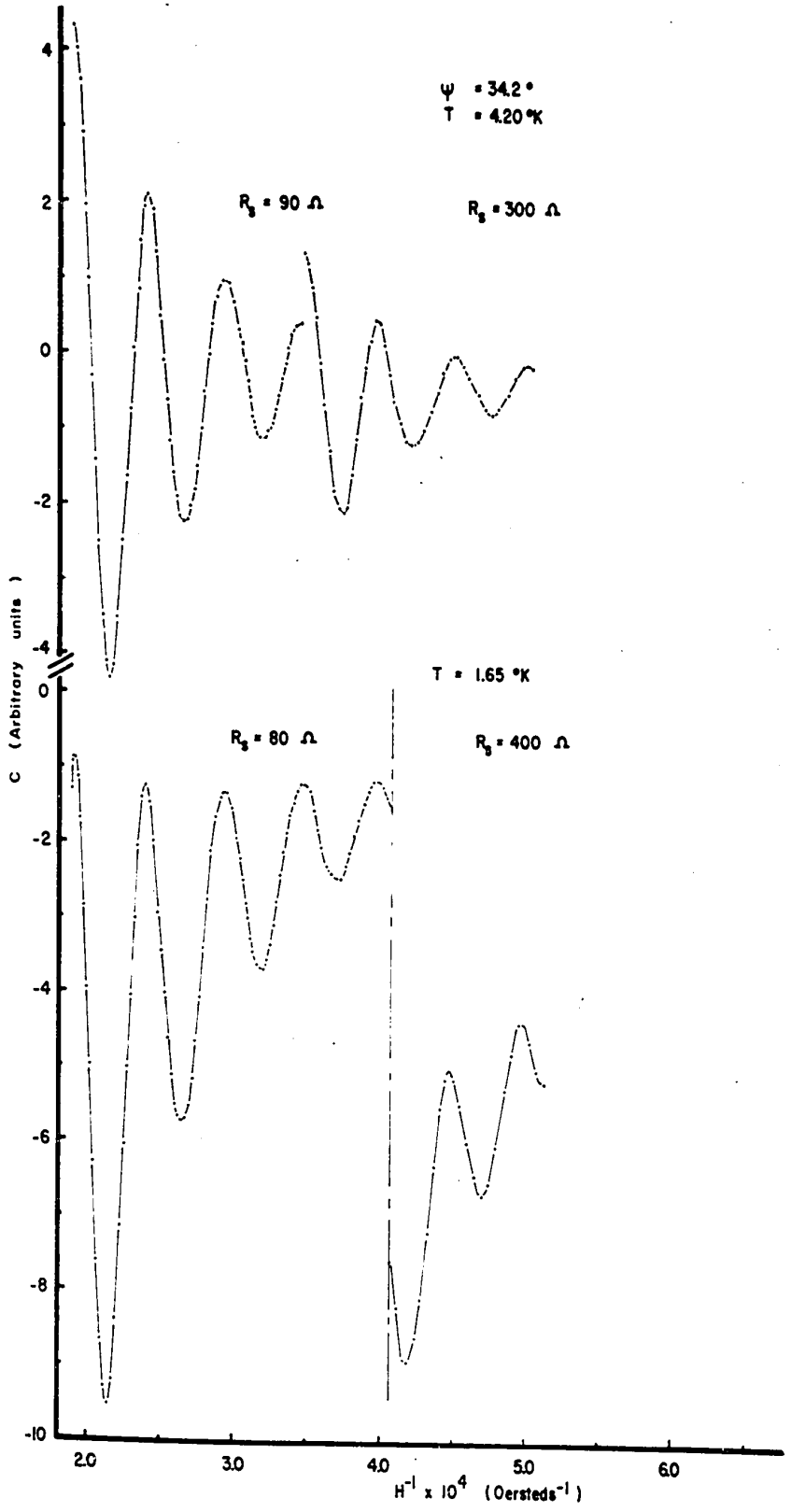
ψ = 34.2°
T = 4.20°K
R_s = 90 Ω
R_s = 300 Ω
T = 1.65 °K
R_s = 80 Ω
R_s = 400 Ω
C (Arbitrary units)
4
2
0
-2
-4
0
-2
-4
-6
-8
-10
2.0
3.0
4.0
5.0
6.0
H^-1 x 10^4 (Oersteds^-1)

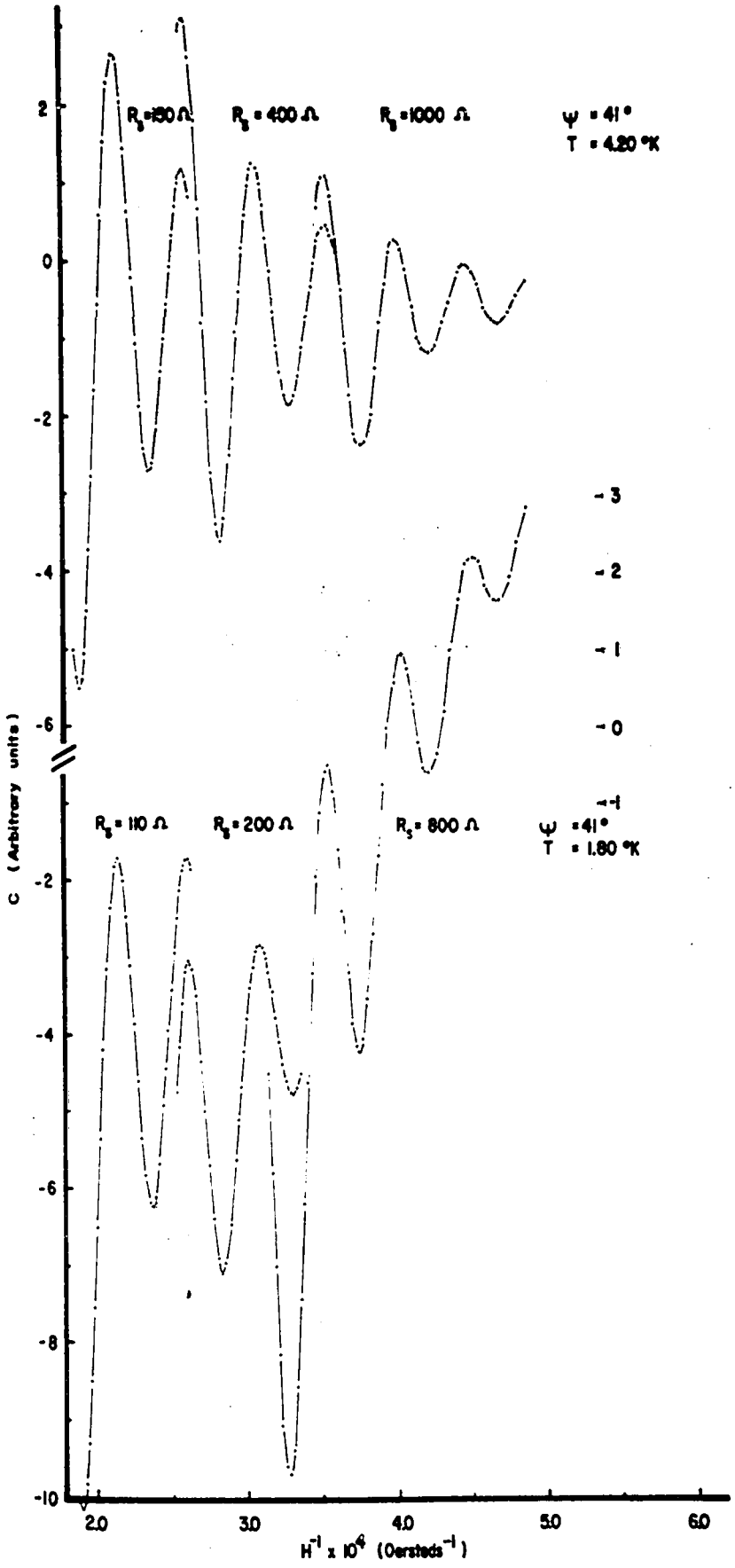
R_s = 130 Ω
R_s = 400 Ω
R_s = 1000 Ω
ψ = 41°
T = 4.20 °K
- 3
- 2
- 1
- 0
- 1
R_s = 110 Ω
R_s = 200 Ω
R_s = 800 Ω
ψ = 41°
T = 1.80 °K
C (Arbitrary units)
2
0
-2
-4
-6
-2
-4
-6
-8
-10
2.0
3.0
4.0
5.0
6.0
$H^{-1} \times 10^6$ (Oersteds^{-1})

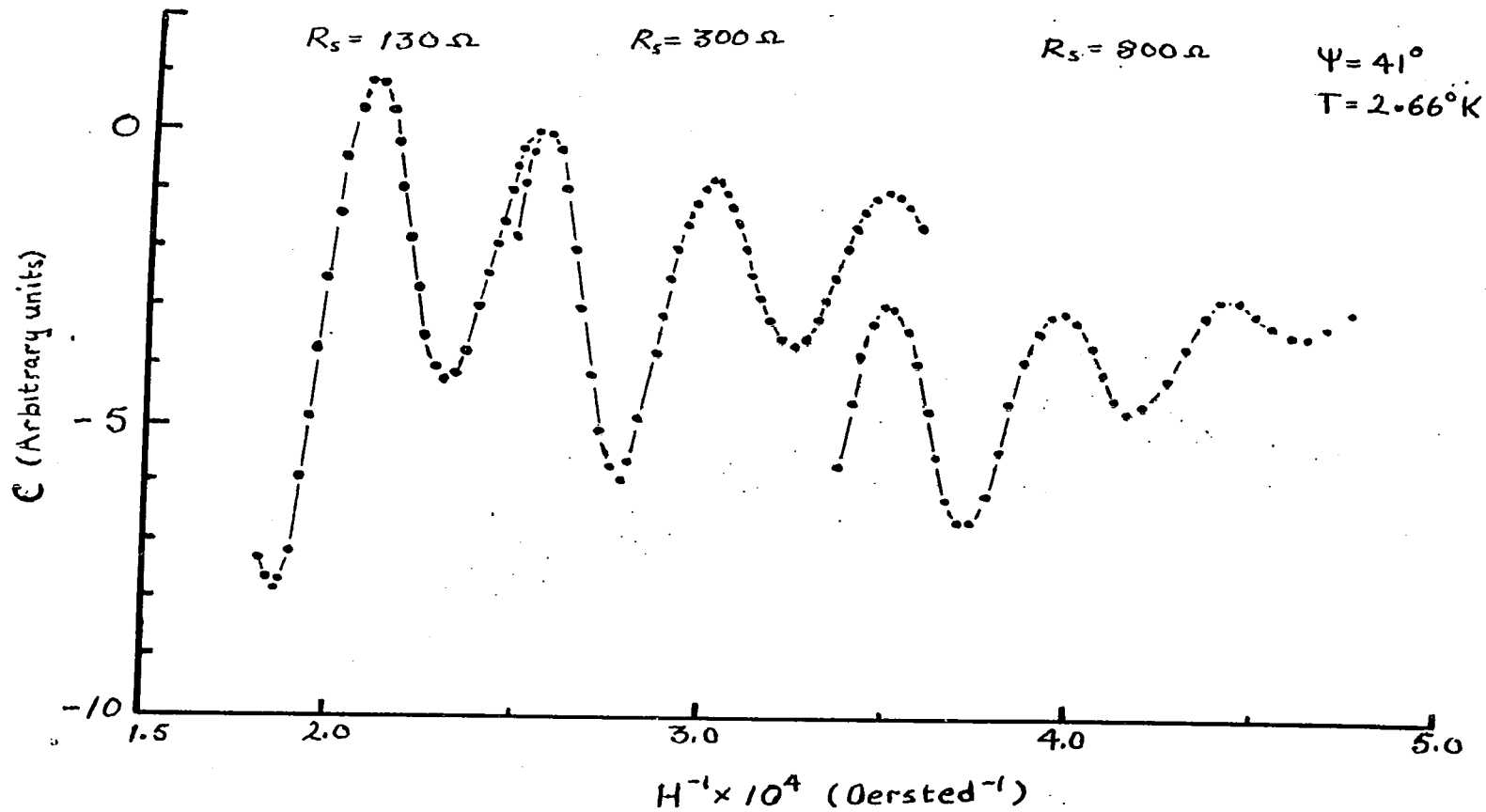
R_s = 130 Ω
R_s = 300 Ω
R_s = 800 Ω
Ψ = 41°
T = 2.66°K
0
-5
-10
ε (Arbitrary units)
1.5
2.0
3.0
4.0
5.0
$H^{-1} \times 10^4$ (Oersted^{-1})

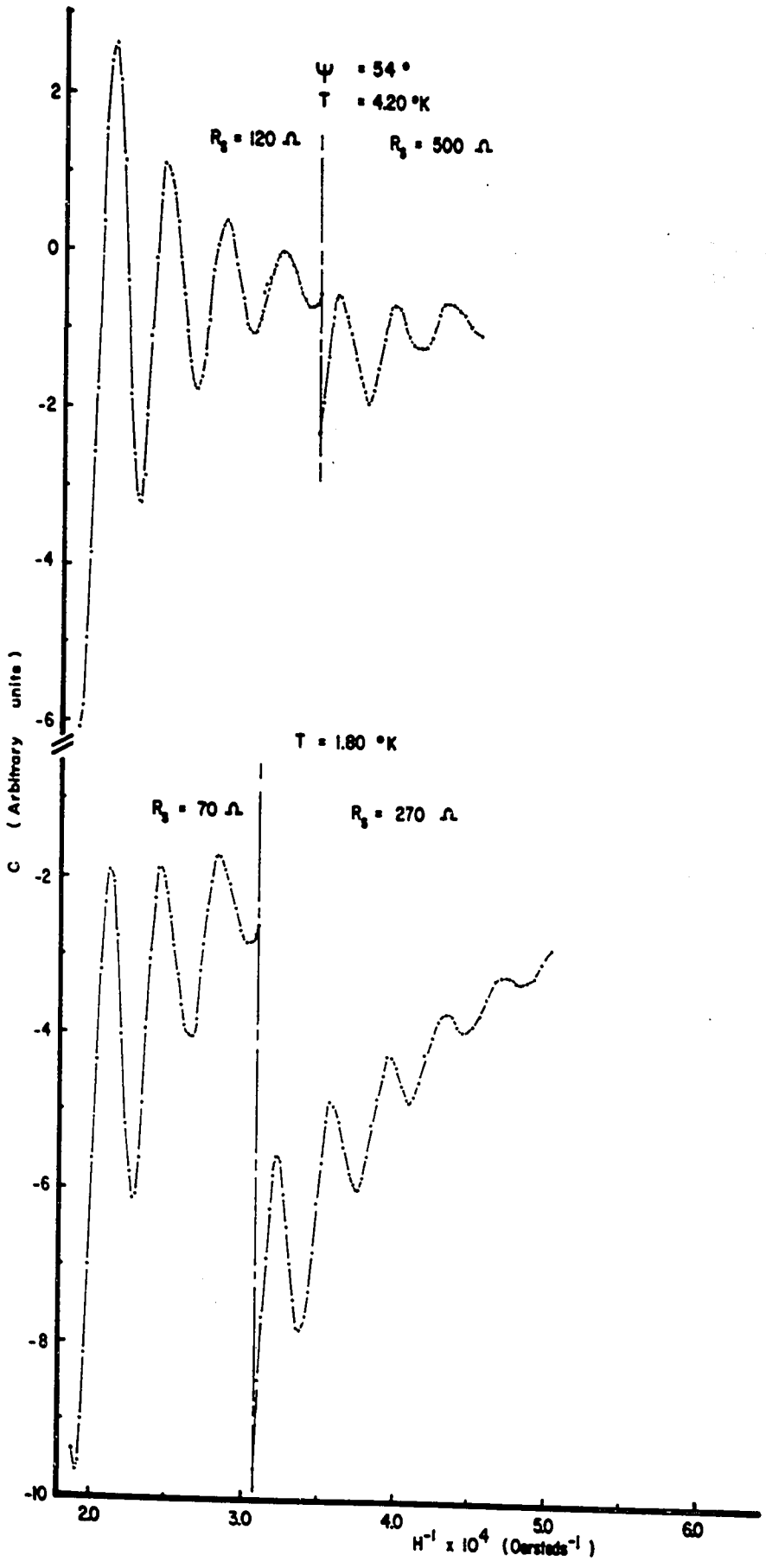
Ψ = 54°
T = 4.20 °K
R_s = 120 Ω
R_s = 500 Ω
T = 1.80 °K
R_s = 70 Ω
R_s = 270 Ω
C (Arbitrary units)
2
0
-2
-4
-6
-2
-4
-6
-8
-10
2.0
3.0
4.0
5.0
6.0
H^-1 x 10^4 (Oersteds^-1)

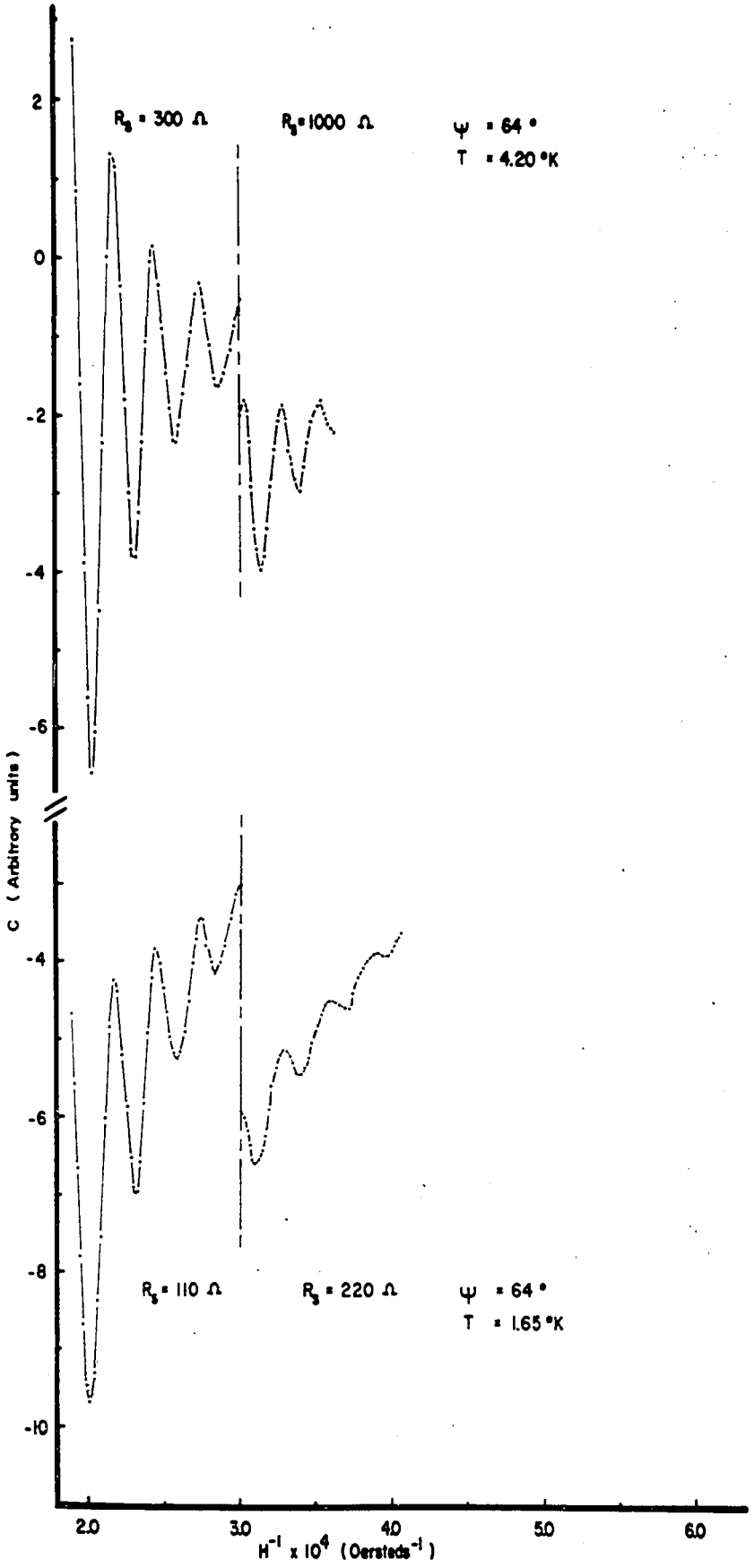
2
0
-2
-4
-6
-4
-6
-8
-10
C (Arbitrary units)
R_s = 300 Ω
R_s = 1000 Ω
ψ = 64 °
T = 4.20 °K
R_s = 110 Ω
R_s = 220 Ω
ψ = 64 °
T = 1.65 °K
2.0
3.0
4.0
5.0
6.0
$H^{-1} \times 10^4$ (Oersteds^{-1})

FIGURE 13

Values of 1/H at the peaks plotted against half integers for pure zinc at 4.2° K and 1.8° K.

● 4.2° K

▼ 1.8° K

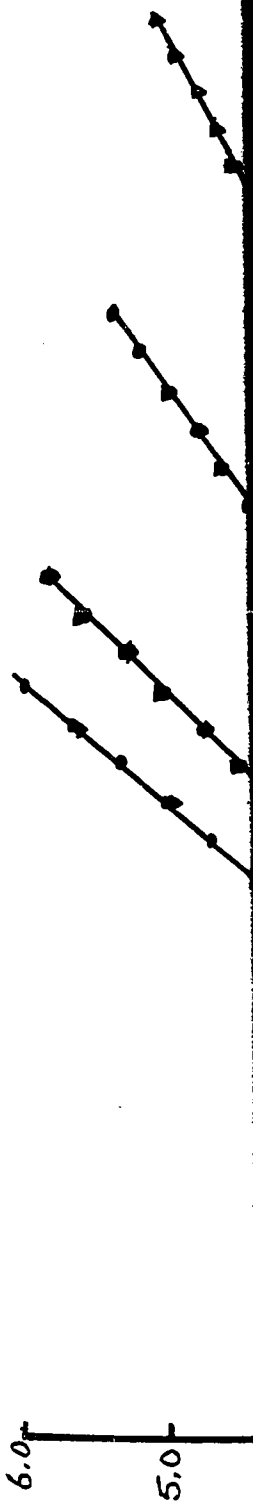

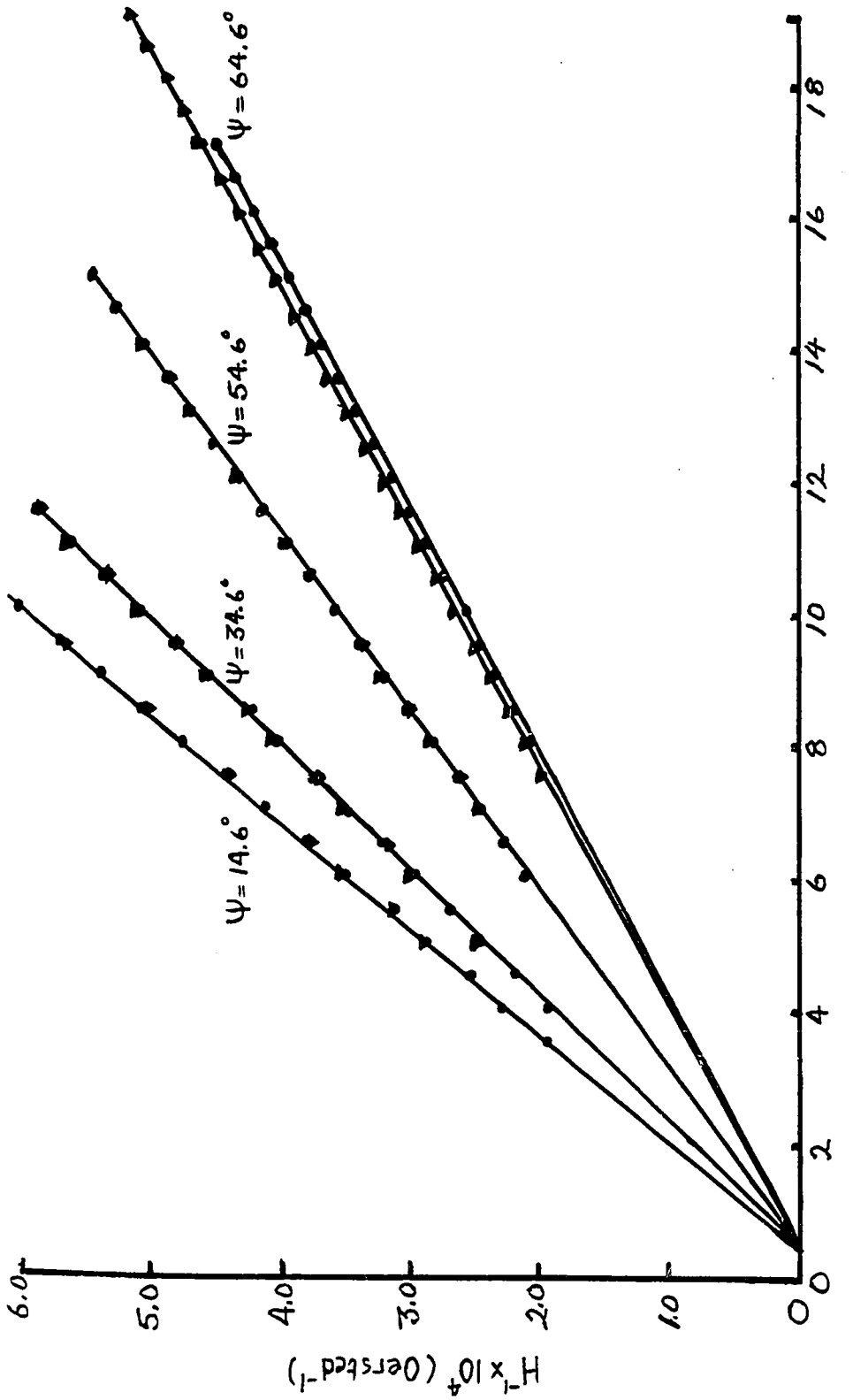
$H^{-1} \times 10^4$ (Oersted^{-1})
6.0
5.0
4.0
3.0
2.0
1.0
0
0
2
4
6
8
10
12
14
16
18
Integers
$\psi = 64.6°$
$\psi = 54.6°$
$\psi = 34.6°$
$\psi = 14.6°$

FIGURE 14

Values of 1/H at the peaks plotted against half integers for the 0.008% zinc manganese alloy at 4.2° K and 1.8° K.

- ● 4.2°K
- ▼ 1.8°K

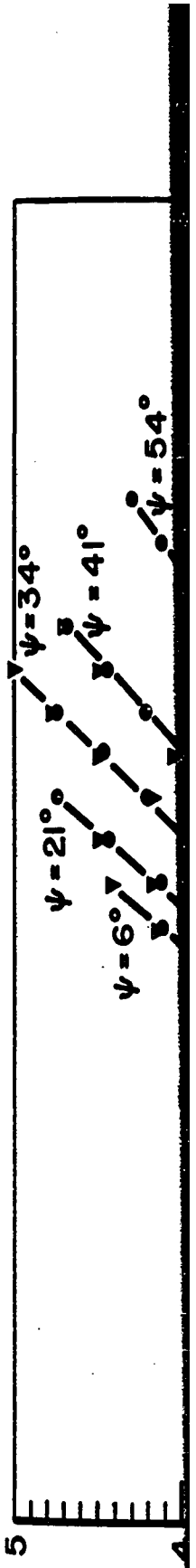

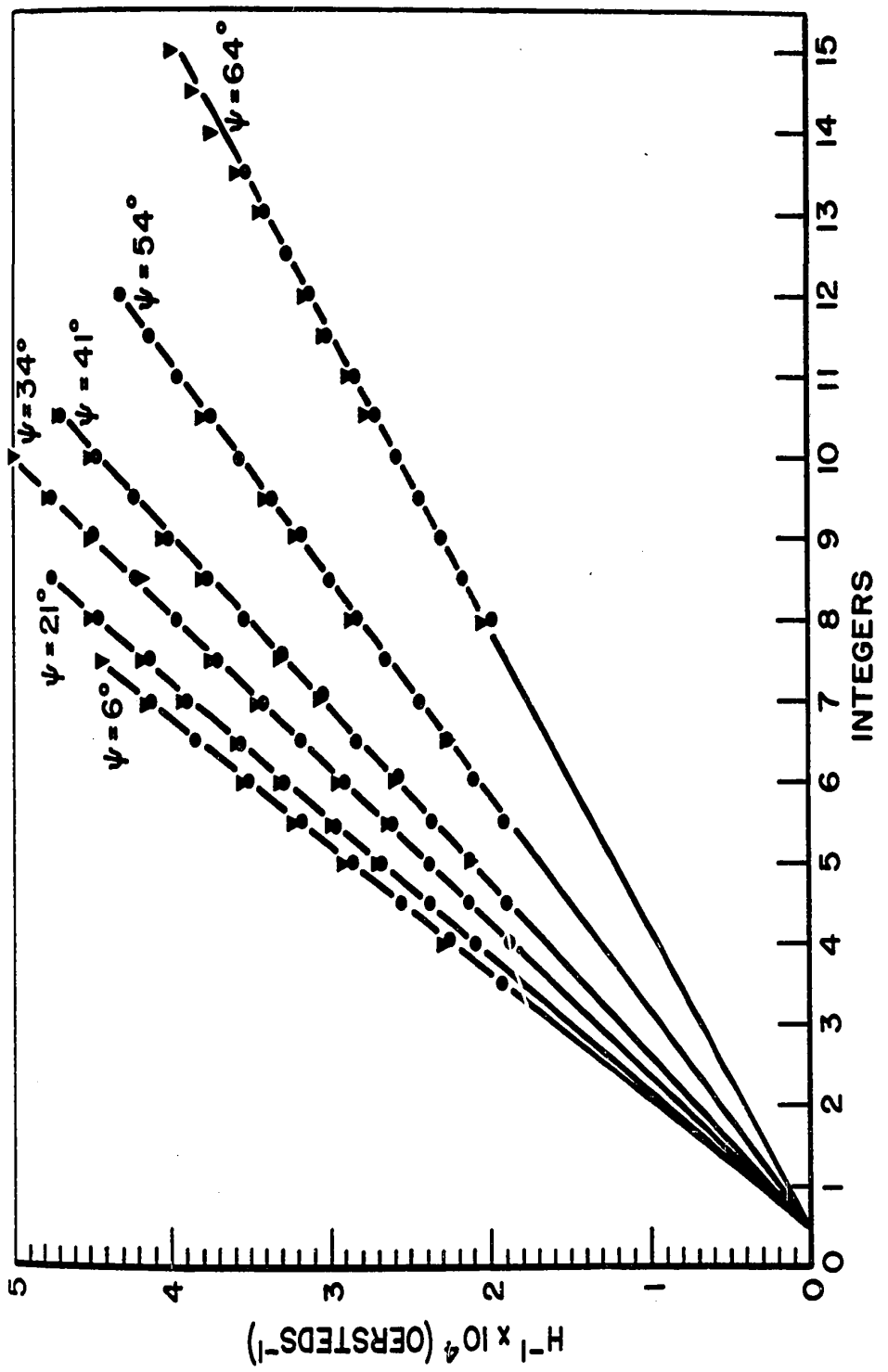
ψ=64°
ψ=54°
ψ=41°
ψ=34°
ψ=21°
ψ=6°
INTEGERS
H⁻¹ x 10⁴ (OERSTEDS⁻¹)

FIGURE 15

P^2 as a function of $\cos^2\psi$

The dotted lines indicate an experimental error in the periods of 1.5%.

- Data obtained by Verkin and Dmitrenko for pure zinc.
- ▼ Present data for pure zinc.
- × Data for a 0.008 wt. % zinc manganese alloy.

The inset shows m^*/m as a function of orientation for pure zinc.

Indicates the value obtained by Dhillon and Shoenberg, (195).

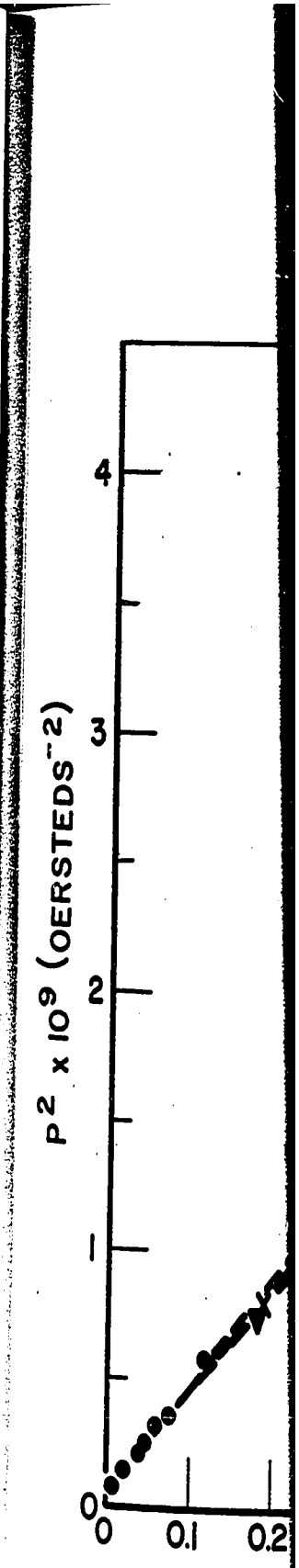

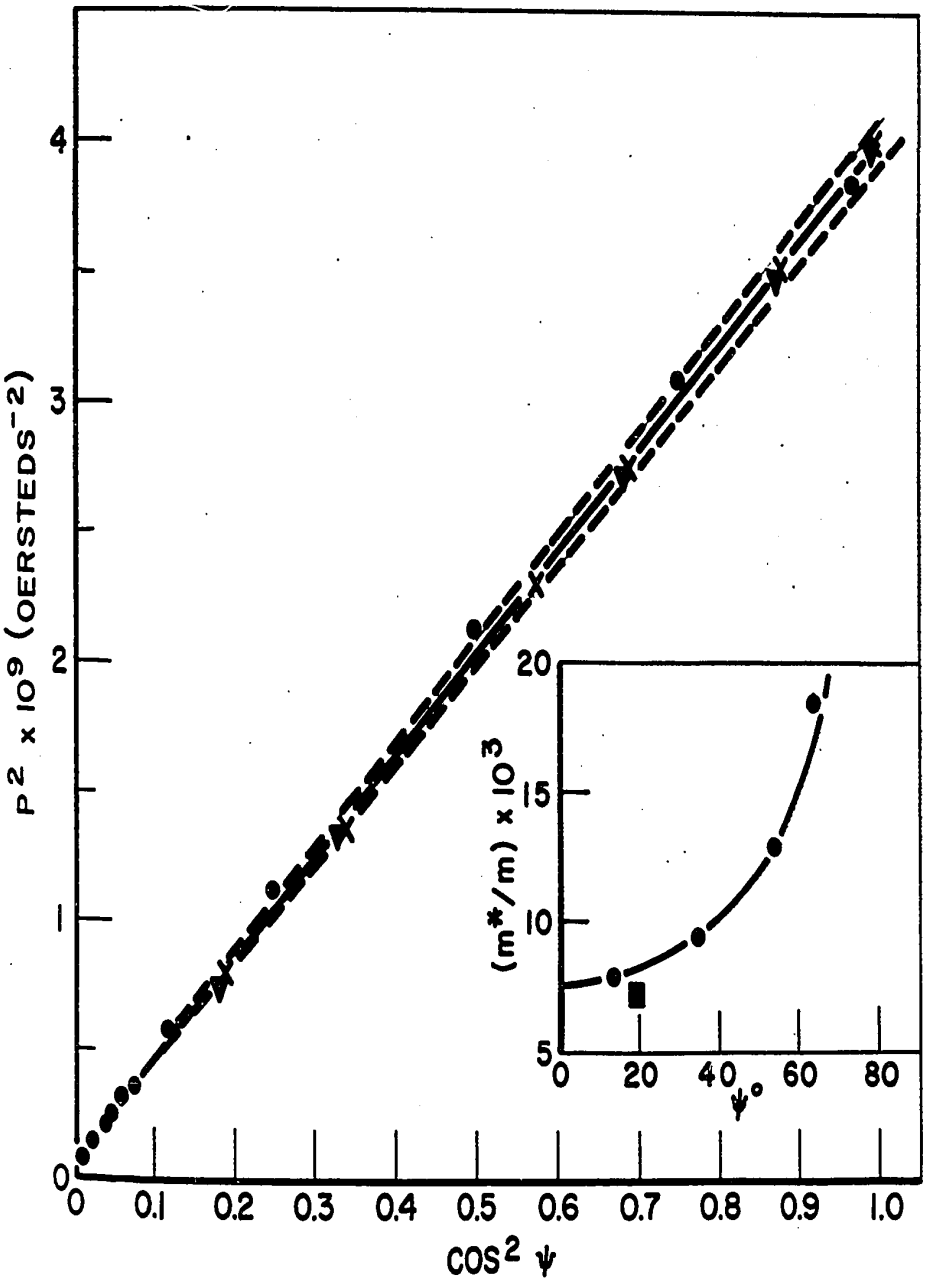
$P^2 \times 10^9$ (OERSTEDS^{-2})
0
1
2
3
4
0
0.1
0.2
0.3
0.4
0.5
0.6
0.7
0.8
0.9
1.0
$\cos^2 \psi$
$(m^*/m) \times 10^3$
5
10
15
20
0
20
40
60
80
ψ°

FIGURE 16

Calculated values of W as a function of (m^* / mH)

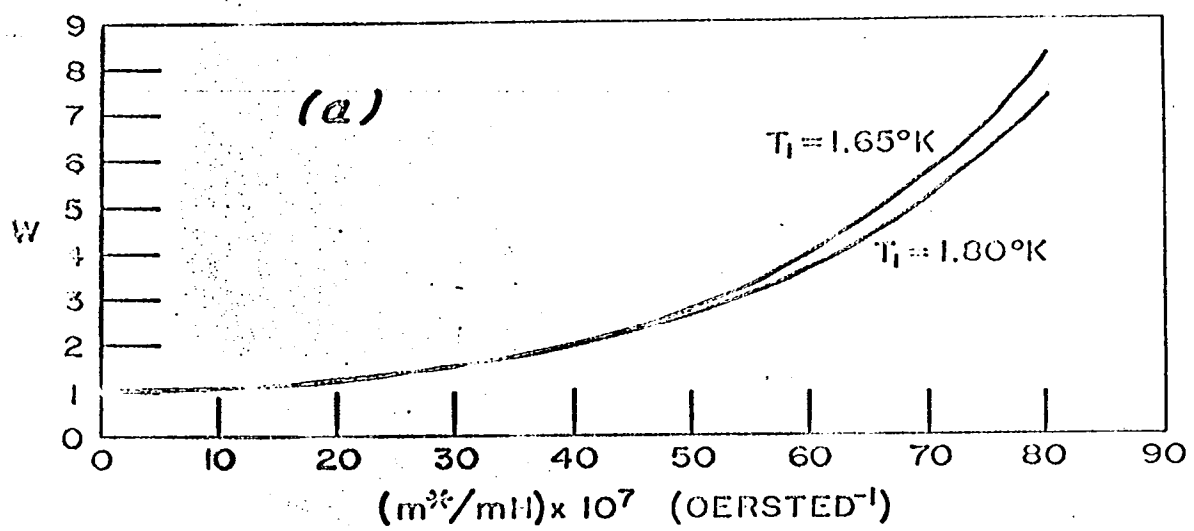
(a)
W
$T_1 = 1.65°K$
$T_1 = 1.80°K$
0
1
2
3
4
5
6
7
8
9
0
10
20
30
40
50
60
70
80
90
$(m^{3\%}/mH) \times 10^7$ (OERSTED^{-1})

orientation in the inset of FIGURE 15. As indicated in the figure, our value is slightly greater than that obtained by Dhillon and Shoenberg, (1955).[8] The value of the Fermi energy of pure zinc, measured from the bottom of the ellipsoid was calculated using equation 1.5 of CHAPTER I and found to be $3.8 \pm 0.2 \times 10^{-14}$ ergs.

Since the zinc alloy exhibits a low temperature resistance anomaly it was anticipated that the relaxation time would not be constant in the temperature range of the de Haas van Alphen effect measurements. This means that the effective mass of the electrons in the alloy cannot be determined by the above method. In order to carry out the analysis for the collision temperature for the alloy it was assumed that the effective mass of the electrons in the alloy was identical to that of the electrons in pure zinc. This is probably a reasonable assumption considering the extreme dilution (0.01 at. %) of the alloy.[6]

The collision temperature was determined from the slope of the line obtained by plotting as a function of H^{-1} (see equation 1.7 of CHAPTER I), as shown in FIGURE 17 for pure zinc and in FIGURE 18 for the zinc manganese alloy. As has been noted previously, the curves are linear only for low fields.[7] The collision temperature was deduced from the linear portion of the curves and is found to be independent of orientation and temperature for pure zinc and has a value of $1.3^{\circ}K$.[9] The collision parameter is apparently a function of both temperature and orientation for the zinc manganese alloy. This dependence will be discussed further in the next chapter. All the experimental results obtained from the de Haas van Alphen effect measurements are summarized in TABLE I.

6.) As is shown in CHAPTER V, this assumption is consistent with the experimental results.

7) Donnahoe and Nix (1954).

8) These values compare favourably with the values of m^*/m found by Joseph and Gordon (1962).

9) This value agrees with the values found by Joseph and Gordon (1962) for the range of orientations common to both sets of measurements.

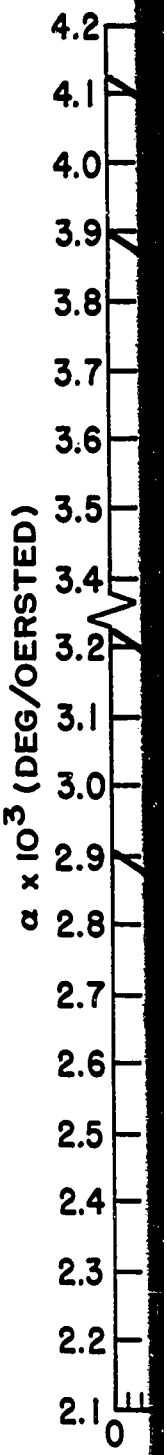

FIGURE 17

The field dependence of the amplitude of the oscillations for pure zinc.

● indicate data obtained at 4.2° K

▼ indicate data obtained at 1.7° K

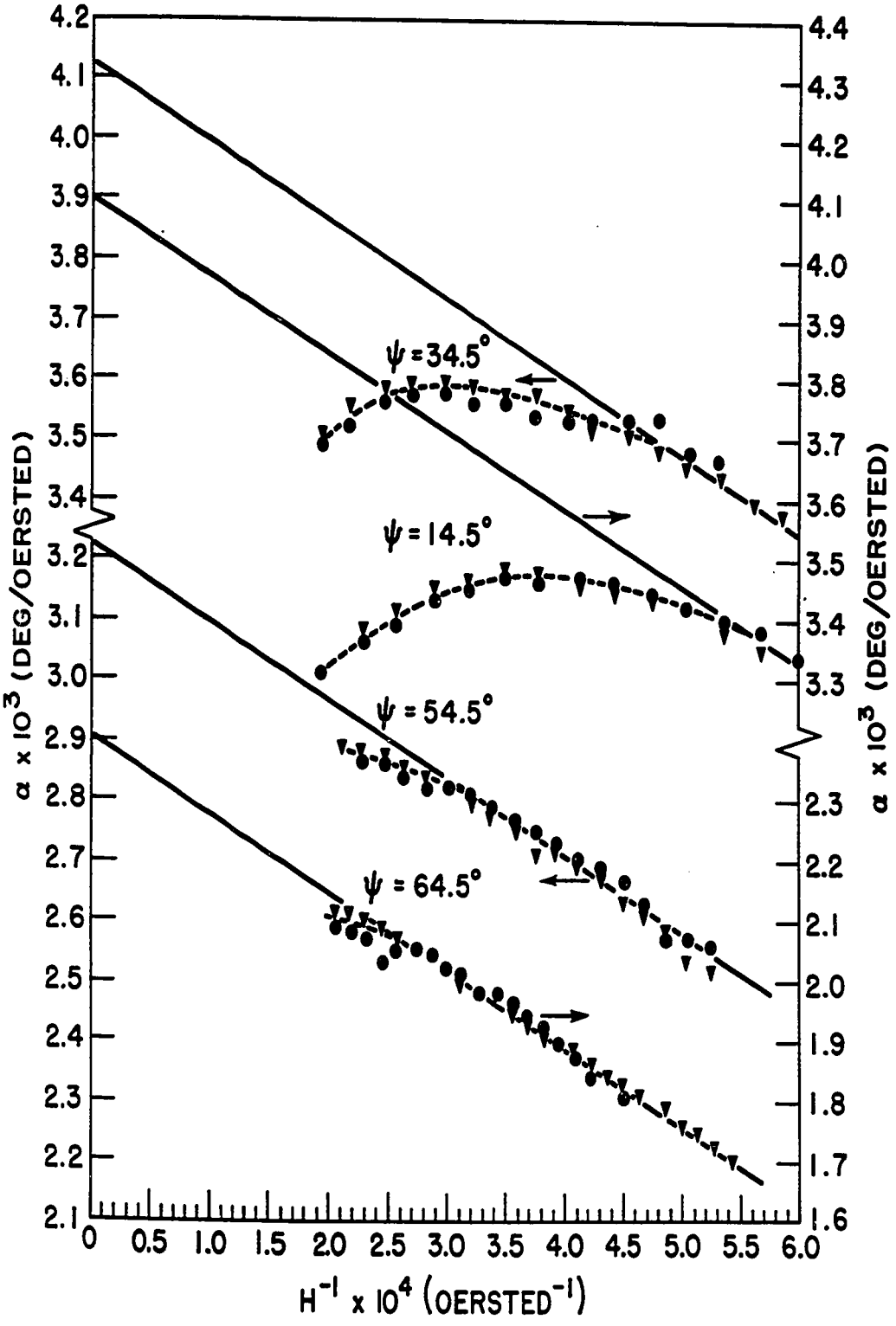
ψ = 34.5°
ψ = 14.5°
ψ = 54.5°
ψ = 64.5°
α x 10³ (DEG/OERSTED)
α x 10³ (DEG/OERSTED)
H⁻¹ x 10⁴ (OERSTED⁻¹)
4.2
4.1
4.0
3.9
3.8
3.7
3.6
3.5
3.4
3.2
3.1
3.0
2.9
2.8
2.7
2.6
2.5
2.4
2.3
2.2
2.1
4.4
4.3
4.2
4.1
4.0
3.9
3.8
3.7
3.6
3.5
3.4
3.3
2.3
2.2
2.1
2.0
1.9
1.8
1.7
1.6
0
0.5
1.0
1.5
2.0
2.5
3.0
3.5
4.0
4.5
5.0
5.5
6.0

FIGURE 18

Apparent field dependence of the amplitude of the oscillations for the 0.008 wt. % zinc manganese alloy.

● indicate data obtained at 4.2° K

■ indicate data obtained at 2.6° K

▼ indicate data obtained at 1.7° K

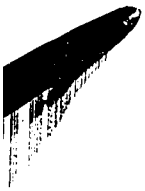

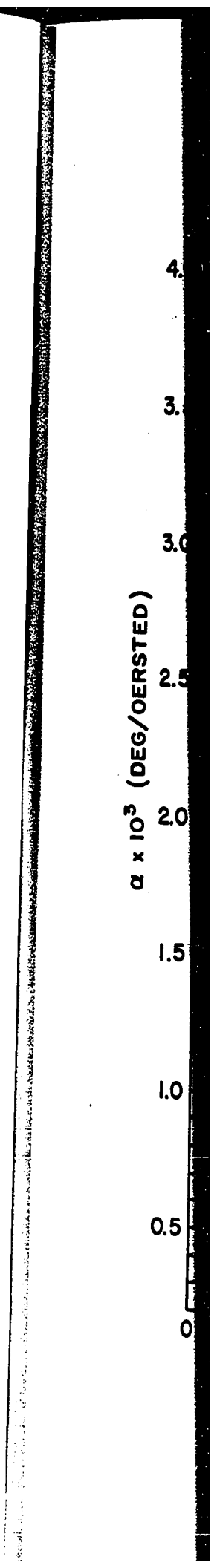

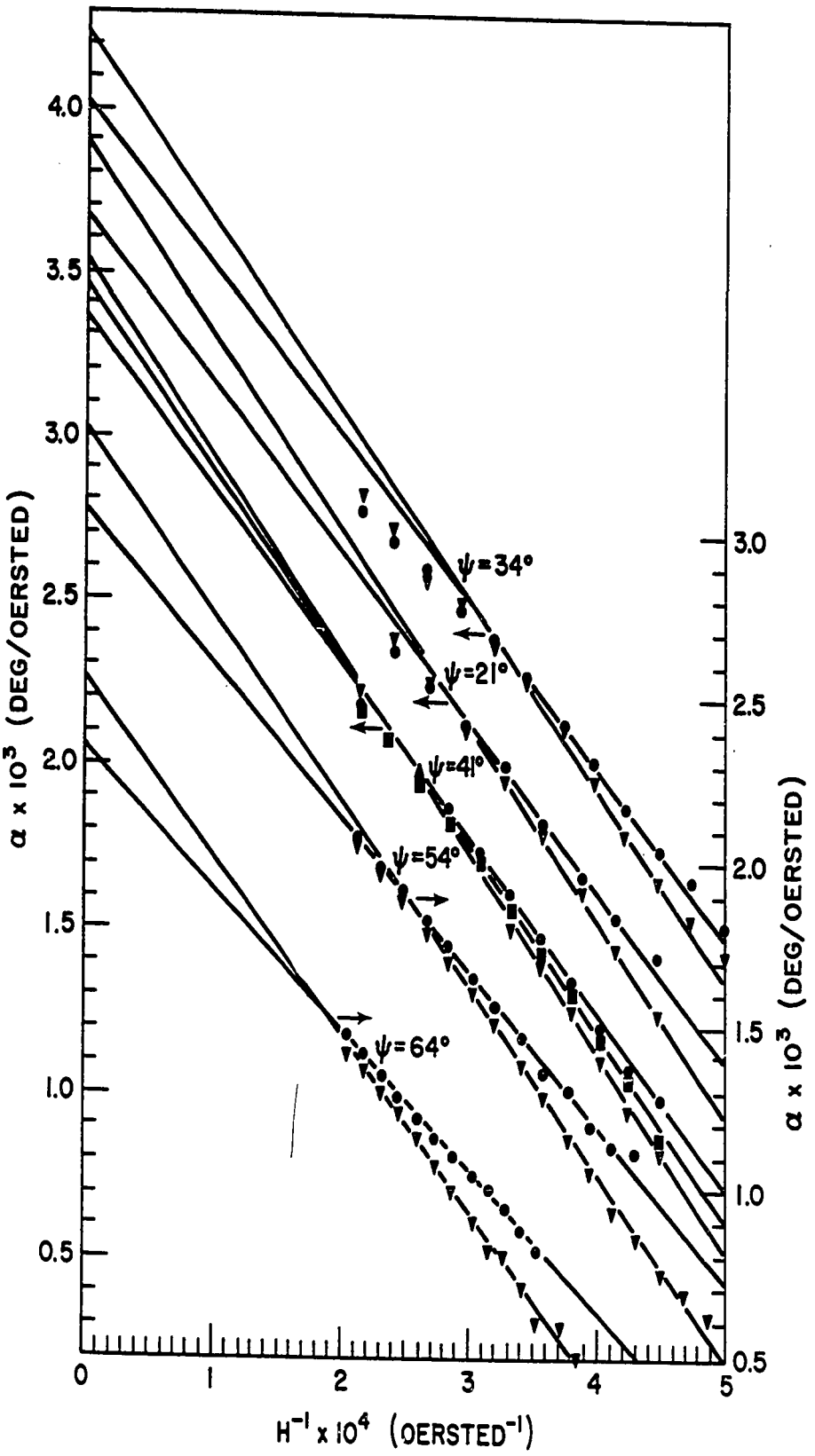
4.0
3.5
3.0
2.5
2.0
1.5
1.0
0.5
α x 10³ (DEG/OERSTED)
ψ=34°
ψ=21°
ψ=41°
ψ=54°
ψ=64°
0
1
2
3
4
5
H⁻¹ x 10⁴ (OERSTED⁻¹)
3.0
2.5
2.0
1.5
1.0
0.5
α x 10³ (DEG/OERSTED)

TABLE I

ψ^{o}	Period x 10^5 oersted^{-1}		Effective Mass, m^*/m x 10^3		Collision Temperature, x ^{o}K			
	Pure Zn	Zn-Mn	Pure Zn	Zn-Mn	Pure Zinc	Apparent Value Zn-Mn		
					4.2 + 1.7°K	4.2°K	2.6°K	1.7°K
14.5	6.10		7.9	Assumed to be the same as the values for pure zinc	1.3			
21		5.90				5.1		5.9
34		5.22				5.0		5.8
34.5	5.26		9.3		1.3			
41		4.80				5.2	5.7	6.1
54		3.68				4.7		5.6
54.5	3.72		12.8		1.3			
64		2.82				4.3		5.4
64.5	2.74		18.3		1.3			

$E_o = 3.8 \pm 0.2 \times 10^{-14}$ erg

CHAPTER V

DISCUSSION OF RESULTS

5.1 Field and Temperature Dependence of the Amplitude

Allowing for a temperature dependent relaxation time, which might be expected in an alloy exhibiting a resistance minimum, equation 1.7 of CHAPTER I shows that the slope of the lines in FIGURE 8 of CHAPTER IV may vary with temperature but their intercept at infinite field should be independent of temperature. The experimental results do not agree with theory and in fact a large variation of the intercept with temperature is observed. In order to determine whether or not this anomaly was another manifestation of an energy dependent relaxation time the free energy, and hence the amplitude of the de Haas van Alphen effect, was determined for the case of a simple energy dependent relaxation time.

The part of the free energy of the conduction electrons which varies periodically with inverse magnetic field has been shown by Dingle (1952) to be:

$$F_{periodic} = -\frac{2\pi(2m^*)^{3/2}kTV}{h^3}\left(\frac{\beta^* H}{2}\right)^{1/2}\sum_{\substack{r=-\infty \\ \neq 0}}^{\infty}(r)^{-1/2}(-1)^r Q \qquad 5.1$$

where $$Q = e^{-i\pi/4}\int_{-\infty}^{\infty} e^{-2\pi(a|r|-irE/\beta^* H)} \ln\left[1+e^{(E_0-E)/kT}\right] dE \qquad 5.2$$

and

$\beta^* = e\hbar/m^*c$ is an effective double Bohr magneton,

$a = \hbar/r\beta^* H$

and τ is the conduction electron relaxation time.

The simplest energy dependent relaxation time is that assumed by Korringa and Gerritsen (1953) in which $\tau = \tau_0$, a constant, except for $(E_0-\Delta) \lesssim E \lesssim (E_0+\Delta)$ when $\tau = 0$. Under this condition the integral Q , (equation 5.2) becomes:

$$Q = e^{-(2\pi a_0 |r| + i\pi/4)} \left[\int_{-\infty}^{\infty} e^{i2\pi r E/\beta^* H} \ln\{1+e^{(E_0-E)/kT}\} dE \right.$$

$$\left. - \int_{E_0-\Delta}^{E_0+\Delta} e^{i2\pi r E/\beta^* H} \ln\{1+e^{(E_0-E)/kT}\} dE \right], \qquad 5.3$$

$$= Q_1 + Q_2$$

since the integral Q is zero when $\tau = 0$. A value of $\tau/\tau_0 = 0,2$ is sufficiently small to make $Q \longrightarrow 0$. Combining Q_1 with equation 5.1 gives an expression for the free energy identical to that obtained by Dingle (1952) which is:

$$F_{\text{periodic}} = \frac{2\pi(2m^*)^{3/2} kT V(\beta^* H)^{3/2}}{h^3\sqrt{2}} \sum_{r=1}^{\infty} \frac{(-1)^r \cos(2\pi r E_0/\beta^* H - \pi/4)}{r^{3/2} \sinh(2\pi^2 r kT/\beta^* H)} \qquad 5.4$$

$$\times e^{-hr/\tau_0 \beta^* H}$$

It is thus seen that the effect of an energy dependent relaxation time is to add a term to the free energy which is determined by combining Q_2 with equation 5.1.

To evaluate Q_2 consider the two cases: i) $E_0 \gg \Delta$, ii) $E_0 \gtrsim \Delta$

Case i)

If $E_0 \gg \Delta$ then $e^{i2\pi r E/\beta^* H}$ can be put equal to $e^{i2\pi r E_0/\beta^* H}$ and putting $(E - E_0)/kT = x$ with

$\Delta = kT_\Delta$, Q_2 may be written:

$$Q_2 = -kT\, e^{-\left[2\pi a_0|r| - i(2\pi r E_0/\beta^* H - \pi/4)\right]} I(T_\Delta/T) \qquad 5.5$$

where

$$I(T_\Delta/T) = \int_{-T_\Delta/T}^{T_\Delta/T} \ln(1+e^{-x})\,dx \qquad 5.6$$

This integral has been evaluated by numerical methods and is shown in FIGURE I. Combining equation 5.5 with equation 5.1, the term t_r which must be added to the free energy to account for the energy dependent relaxation time, is calculated to be:

$$t = \frac{2\pi(2m^*)^{3/2} kTV(\beta^* H)^{3/2}}{h^3\sqrt{2}} \sum_{r=1}^{\infty} \left[r^{-1/2}(-1)^r (kT/\beta^* H) \cos(2\pi r E_0/\beta^* H - \pi/4)\, e^{-rh/\tau_0 \beta^* H} \right] \qquad 5.7$$

Adding equation 5.7 to equation 5.4, the periodic part of the free energy of the conduction electrons, in a metal having a resistance minimum due to the postulated energy dependent relaxation time, is given by:

$$F_{periodic} = \frac{2\pi(2m^*)^{3/2} kTV(\beta^* H)^{3/2}}{h^3\sqrt{2}} \sum_{r=1}^{\infty} \left[\frac{(-1)^r \cos(2\pi r E_0/\beta^* H - \pi/4)}{r^{3/2} \sinh(2\pi^2 r kT/\beta^* H)} e^{-rh/\tau_0 \beta^* H} \left\{ 1 + \frac{rkT \sinh 2\pi^2 r kT/\beta^* H}{\beta^* H} I(T_\Delta/T) \right\} \right] \qquad 5.8$$

FIGURE 1

$I(T_\Delta/T)$ as a function of T_Δ / T

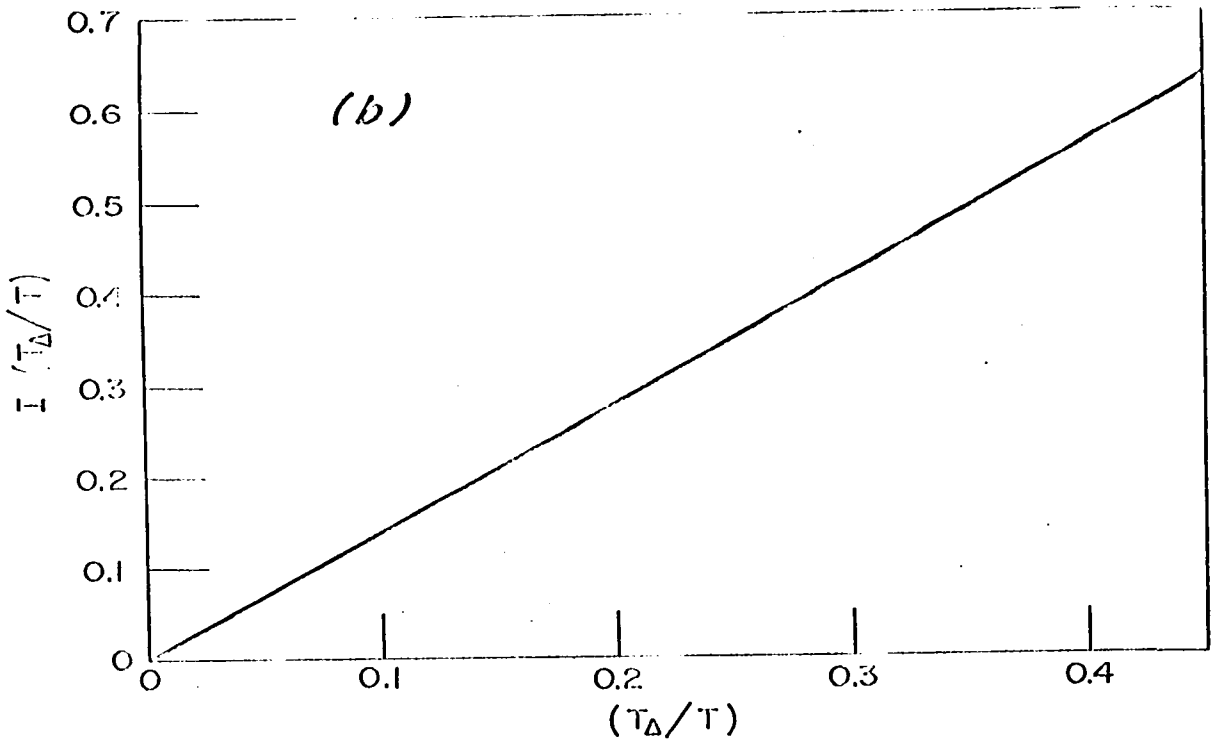
(b)
0.7
0.6
0.5
0.4
0.3
0.2
0.1
0
0
0.1
0.2
0.3
0.4
I (TΔ/T)
(TΔ/T)

In the present experiments the torque on a single crystal was measured. The torque, C, will be given by:

$$C = -\partial F/\partial \psi \qquad 5.9$$

where ψ is an angle denoting rotation in a plane normal to the axis of suspension of the crystal. In the differentiation of 5.8, to obtain the torque, the main contribution comes from the cosine term since $E_0 / \beta^* H \gg 1$. Thus the torque on the crystal is given by:

$$C = -\partial F/\partial \psi = \partial F/\partial(1/\beta^*) \cdot \partial(1/\beta^*)/\partial m^* \cdot \partial m^*/\partial \psi$$

$$= \left(\frac{e\hbar}{c}\right)^{1/2} \frac{E_0 kTV}{\pi \hbar^3} H^{1/2} \frac{\partial m^*}{\partial \psi} \sum_{r=1}^{\infty} \frac{(-1)^r \sin(2\pi r E_0/\beta^* H - \pi/4)}{r^{1/2} \sinh(2\pi^2 r kT/\beta^* H)} \cdots$$

$$\times e^{-r\hbar/\beta^* \tau_0 H} \left\{ 1 + \frac{rkT \sinh(2\pi^2 r kT/\beta^* H)}{\beta^* H} I(T_D/T) \right\}$$

5.10

Using the arguments following equation 1.2 in CHAPTER I, equation 5.10 reduces to:

$$C = BH^{1/2} T \frac{\sin(2\pi E_0/\beta^* H - \pi/4)}{\sinh(2\pi^2 kT/\beta^* H)} e^{-2\pi^2 k X_0/\beta^* H} \qquad 5.11$$

$$\left\{ 1 + \frac{kT \sinh(2\pi^2 kT/\beta^* H)}{\beta^* H} I(T_D/T) \right\}$$

for the case of a zinc manganese alloy, where $X_0 = \hbar/\pi k \tau_0$

Case ii

if $E_0 \gtrsim \Delta$, then $e^{i2\pi r E/\beta^* H}$ cannot be put equal to $e^{i2\pi r E_0/\beta^* H}$ in the expression for Q_2.

Instead, put $(E - E_0) / kT = x$ and the expression for Q_2 becomes:

$$Q_2 = -kT\, e^{-[2\pi a_0|r| - i(2\pi r E_0/\beta^* H - \pi/4)]} \int_{-\Delta/kT}^{+\Delta/kT} e^{-2\pi r x\, kT/\beta^* H} \ln(1+e^{-x})\, dx \qquad 5.12$$

Since it is desired mainly to know the qualitative effect of the energy dependent relaxation time on the period of the oscillations, equation 5.12 can be simplified at the cost of accuracy in the value of Q_2 by putting:

$$(1 + e^{-x}) = 2$$

whence:

$$Q_2 = -kT \ln 2\; e^{-[2\pi a_0|r| - i(2\pi r E_0/\beta^* H - \pi/4)]} \int_{-\Delta/kT}^{\Delta/kT} e^{i 2\pi r x\, kT/\beta^* H}\, dx$$

$$= \frac{\beta^* H \ln 2}{2\pi r}\, e^{-2\pi(a_0|r|)} \cdot i e^{i[2\pi r(E_0-\Delta)/\beta^* H - \pi/4]} - i e^{i[2\pi r(E_0+\Delta)/\beta^* H - \pi/4]} \qquad 5.13$$

Taking the real part of equation 5.13, Q_2 becomes:

$$Q_2 = \frac{\beta^* H \ln 2}{2\pi r}\, e^{-2\pi a_0|r|} \cos(2\pi r E_0/\beta^* H - \pi/4) \sin(2\pi r \Delta/\beta^* H) \qquad 5.14$$

Combining equation 5.14 with equation 5.1 and adding it to equation 5.4 the periodic part of the free energy of the conduction electrons in a metal exhibiting a resistance minimum due to the postulated energy dependent relaxation time is:

$$F_{\text{periodic}} = \frac{2\pi(2m^*)^{3/2} kTV(\beta^* H)^{3/2}}{h^3\sqrt{2}} \sum_{r=1}^{\infty} \left[\frac{(-1)^r \cos(2\pi r E_0/\beta^* H - \pi/4)}{r^{3/2} \sinh(2\pi^2 r kT/\beta^* H} \right. \qquad 5.15$$

$$\left. e^{-rh/\tau_0 \beta^* H} \left\{ 1 + \frac{2\sinh(2\pi^2 r kT/\beta^* H)}{\pi} \sin(2\pi r \Delta/\beta^* H) \right\} \right]$$

It is thus seen that the effect of Υ being equal to zero, in an energy range Δ about the Fermi energy, is to add a periodic term to the free energy whose amplitude is sinusoidally modulated. The period of the modulation, P_{mod}, is given by:

$$P_{mod} = \beta^*/\Gamma\Delta$$

The ratio of the period of the modulation to the period of the oscillations is:

$$P_{mod}/P = E_o/\Delta$$

For the zinc 0.008 wt. % zinc manganese alloy which has been measured, E_o is 3.8×10^{-14} ergs and Δ will be shown to be 1×10^{-16} ergs. Hence $P_{mod}/P \approx 400$ and the effect of the modulation will be negligible.

The field dependence of the amplitude of the oscillations will thus be analysed using equation 5.11. Excluding the periodic term equation 5.11 can be written:

$$\alpha - \lambda = \xi - x_o H^{-1}, \qquad 5.16$$

where

$$\lambda = \frac{\beta \ln\left\{1 + \frac{kT \sinh(2\pi^2 kT/\beta^* H)}{\beta^* H} I(T_\Delta/T)\right\}}{2\pi^2 k (m^*/m)}$$

and α and ξ have been defined in CHAPTER I. FIGURE 2 shows the results obtained by plotting $\alpha - \lambda$ as a function of H^{-1} for $T_\Delta = 0.75^\circ$ K. The value of 0.75° K for T was found by a process of trial and error to give the best fit of equation 5.16 to the experimental data. As would be expected, from equation 5.16, $\alpha - \lambda$ is seen

FIGURE 2

$\alpha - \lambda$ as a function of H^{-1} for the 0.008 wt. % zinc manganese alloy.

● indicates data obtained at 4.2° K

■ indicates data obtained at 2.6° K

▲ indicates data obtained at 1.7° K

The insert shows an estimate of the accuracy to which T may be determined. The difference between $\alpha - \lambda$ at 4.2° K and 1.7° K has been plotted as a function of T_Δ for $\psi = 64^\circ$ and $H^{-1} = 3.02 \times 10^{-4}$ oersteds^{-1}. The dashed lines indicate a difference in $\alpha - \lambda$ which is plainly discernable in the main figure.

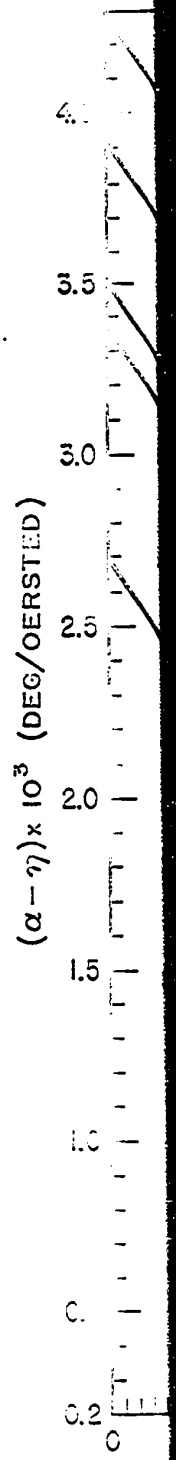

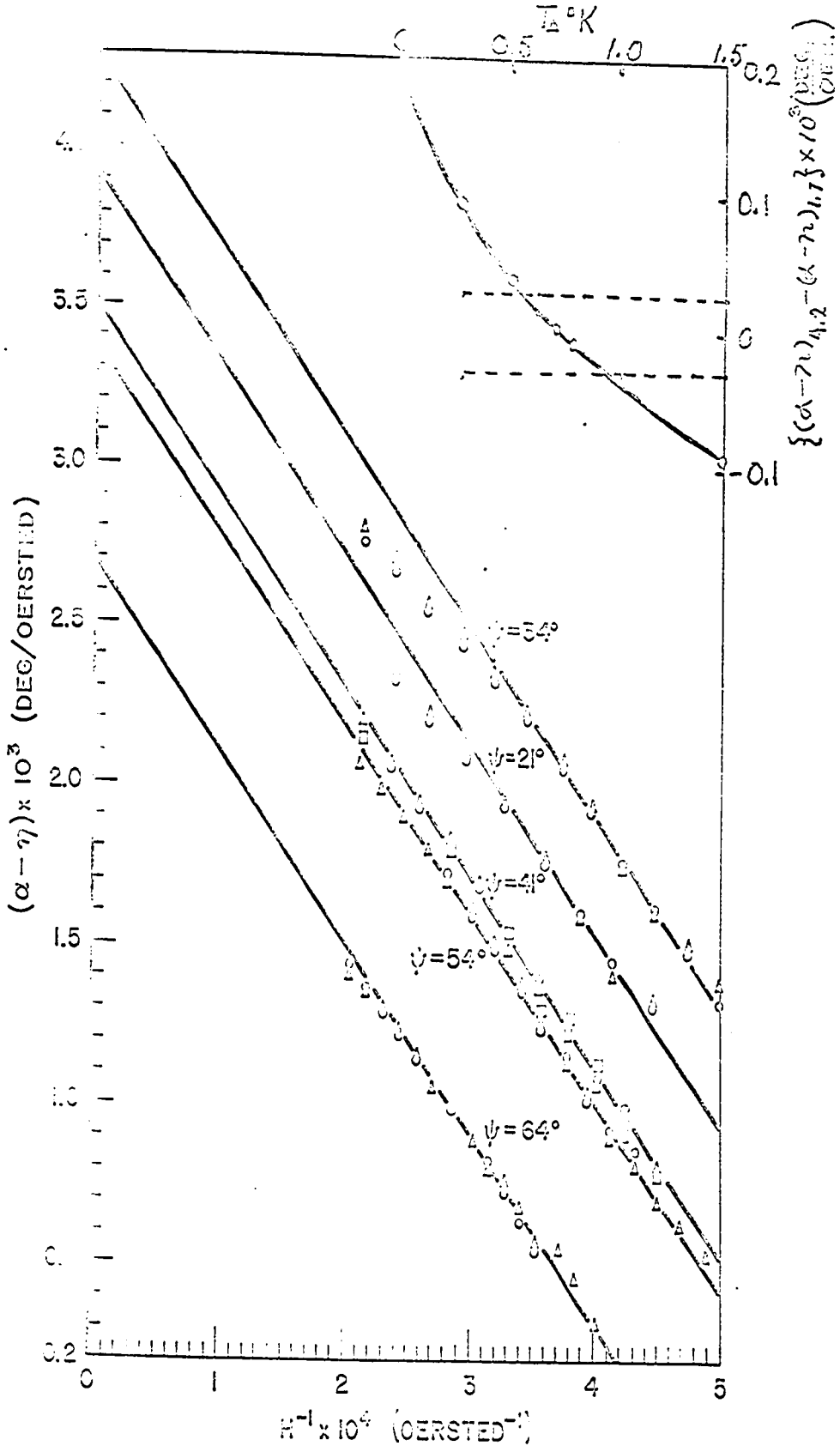
T_A °K
0
0.5
1.0
1.5
$(\alpha-\eta)\times 10^3$ (DEG/OERSTED)
3.5
3.0
2.5
2.0
1.5
1.0
0.5
0
1
2
3
4
5
$H^{-1}\times 10^4$ (OERSTED^{-1})
ψ=64°
ψ=54°
ψ=41°
ψ=21°
$\{(\alpha-\eta)_{4.2}-(\alpha-\eta)_{1.7}\}\times 10^3$ (DEG/OERSTED)
0.2
0.1
0
-0.1

to be a linear function of H^{-1} having a slope, $-x$, and an intercept, λ, at infinite field, both of which are independent of temperature. The collision temperature is now seen to be independent of orientation and has a value of 5.9° K. (cf. TABLE I, CHAPTER IV).

In the foregoing analysis it has been assumed that the effective mass of the electrons in the alloy was identical to that of the electrons in pure zinc. If this is the case, then from equation 5.16 and equations 1.7 and 1.4 of CHAPTER I, and the fact that the volume of the samples is the same in both cases, it is seen that $\alpha - \lambda$, for the alloy, and α , for pure zinc, should be equal when they are extrapolated to infinite field for any given orientation. As can be seen from FIGURE I, and FIGURE 17 of CHAPTER IV, the values of the intercepts agree to within about 10% thus confirming the correctness of the assumption.

In CHAPTER I it was mentioned that Domenicali (1960) has shown that an effective relaxation time which is sharply energy dependent near the Fermi surface can explain both the resistance minimum and the "giant" thermoelectric powers which are found in dilute alloys at low temperatures. Korringa and Gerritsen (1953) have shown that a simple energy dependent relaxation time, similar to the one just considered in connection with the de Haas van Alphen effect, will produce a resistance minimum. They showed, if the relaxation time was zero in an energy interval $\pm \Delta$ about the Fermi energy, E_0 , that the part of the resistivity, ρ_I , due to impurity scattering was given by:

$$\rho_I = \rho_0 (1 + \Delta / 2kT)$$

This term when combined with the thermal scattering term will produce a resistance minimum in the total resistivity. Experimentally it is

2a. It should be noted that the value of Δ, derived from the de Haas van Alphen effect measurements, refers to an extremely small portion of the Fermi surface. It is assumed, in making the resistance calculation, that the same value of Δ holds for the complete Fermi surface.

more convenie

ρ_I

or:

R_I

While it is kn
de Haas van Al
measured by el
ing a resistan
was assumed to
the contributio
using equation
de Haas van Alp
shown in FIGURE
mental and calc

The
state existing
uncertainty pri
probability betw
large and thus t
will be to induc
If a rigid band
atom ratio remai
alloy must incre

1. Equation 2.3
In either ca
of states ma
defined ener

2. In the prese
valence 2.

more convenient to measure the resistance ratio and hence:

$$\rho_I / \rho_{273} = (1 + \Delta/2kT)\, \rho_o / \rho_{273}$$

or:

$$R_I / R_{273} = (1 + \Delta/2kT)\, R_o / R_{273} \qquad 5.17$$

While it is known that the relaxation time which is measured using the de Haas van Alphen effect is quite different from that which is measured by electrical resistance it would seem that, for alloys exhibiting a resistance minimum, the energy range over which the relaxation time was assumed to be zero should be the same in both cases. On this basis the contribution of impurity scattering to the resistance was calculated using equation 5.17 and the value of $\Delta = 0.75\ k$ obtained from the de Haas van Alphen effect measurements.[2a] The results of doing this are shown in FIGURE 3 where R_o / R_{273} has been chosen so that the experimental and calculated values of R_T / R_{273} agree at 4.2° K.

The above theory suggests the following physical model. Any state existing in the energy interval in which $\tau = 0$ must, by the uncertainty principle, be very broad. As a consequence the transition probability between this state and any other unoccupied state will be large and thus the net effect of the energy dependent relaxation time will be to induce a gap in the effective density of states.[1] (FIGURE 4) If a rigid band model is assumed for the alloy and the electron to atom ratio remains unchanged on alloying[2] then the Fermi energy of the alloy must increase by an amount Δ in order to accommodate all the

---

1. Equation 2.3 in Dingle's (1952) paper also leads to this conclusion; see APPENDIX III In either case it should be pointed out that the concept of a density of states may not be plausible for states having such a poorly defined energy.

2. In the present case, zinc and manganese are both assumed to have valence 2.

FIGURE 3

The resistance of the zinc manganese crystal as a function of temperature. The solid line shows the value of the resistance calculated using the equation given by Korringa and Gerritsen (1953) and a value of $T_{\Delta} = 0.75^{\circ}$ K.

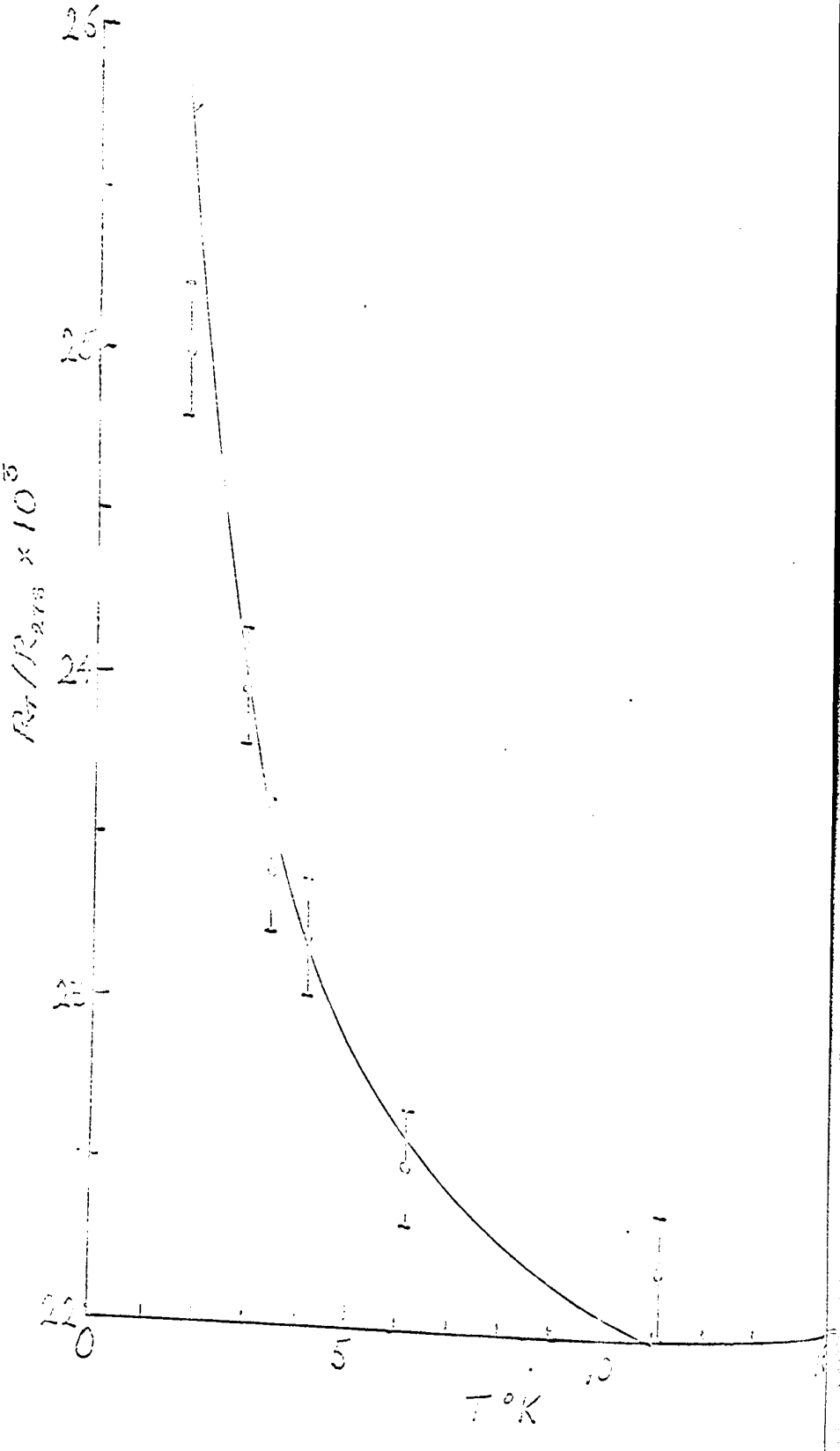

electrons. (C
leads to a de

where E_0 is th
$\Delta / E_0 \approx$
would be expe
of 1.5%.

The
van Alphen os
creases the ma
they depopulat
At energy (E
of oscillation
oscillations h
set of modulat
period of β^*/Δ
that another c
the transition
would normally
of the oscillat
temperature. A
behaviour.

One
been discussed
decrease upon a
pendent relaxat
the number of c

electrons. (Cf. FIGURES 4a and b). This increase in the Fermi energy leads to a decrease in the period which is given by:

$$P_{alloy} = (1-\Delta/E_o)\beta^*/E_o = (1-\Delta/E_o)\, P_{pure}$$

where E_0 is the Fermi energy of the solvent. In the present case $\Delta / E_0 \approx 1/400$ and hence a decrease in the period of 0.25% would be expected. This is well within the present experimental accuracy of 1.5%.

The effect of the gap in the density of states on the de Haas van Alphen oscillations can be seen from FIGURE 2c. As the field increases the magnetic levels move to the right. At energy $(E_0 - \Delta)$ they depopulate rapidly giving rise to oscillations of period $\beta^*/(E_0 - \Delta)$. At energy $(E_0 + \Delta)$ they repopulate and give rise to a second set of oscillations having period $\beta^*/(E_0 + \Delta)$. Since this pair of oscillations have nearly the same period they will beat and result in a set of modulated oscillations having period β^*/E_0 and a modulation period of β^*/Δ. (cf. equation 5.15). From FIGURE 2b it is seen that another consequence of the gap in the density of states is that the transition from populated to unpopulated states is more abrupt than would normally be expected. This results in an increase in the amplitude of the oscillations in a manner which is analogous to a reduction in temperature. As can be seen from equation 5.10 this is the expected behaviour.

One of the consequences of the physical model which has just been discussed is that the period of the oscillations was found to decrease upon alloying with an element which results in an energy dependent relaxation time. This decrease in period came about because the number of conduction electrons, N_A, was assumed to be constant, The

detailed analysis presented earlier was carried out under the assumption of a constant E_o rather than a constant number of conduction electrons, and consequently no change in period was predicted. In order to determine the change in E_o, and hence in the period, due to an energy dependent relaxation time the sum:

$$N = \sum_i 1/[1+e^{(\epsilon_i - \epsilon_o)/kT}]$$

must be evaluated using the expression for the density of states given by Dingle (1952). This must be done, both for the case of an energy dependent relaxation time, and for a constant relaxation time. The results can then be equated and the exact expression for the change in period, due to an energy dependent relaxation time, derived. This is a rather long and complex mathematical procedure. Also the change in period on alloying, with an element which induces an energy dependent relaxation time, depends not only on the relaxation time but also on the value of the electron to atom ratio in the alloy and the change, if any, in the density of states on alloying. Both of these quantities are uncertain and hence it was felt that no useful information could be obtained from attempting the above calculation.

5.2 Conclusions

The period of the de Haas van Alphen oscillations in pure zinc and in the 0.008 wt. % zinc manganese alloy were found to be the same within the 1.5% experimental error. However, the variation of the amplitude of the oscillations with field and temperature was found to be anomalous in the alloy. In order to explain this anomaly the effect of an energy dependent relaxation time on the de Haas van Alphen oscillations was investigated. A relaxation time that was assumed to be zero in an energy range $\Delta = kT_\Delta$ about the Fermi energy and constant elsewhere was found to fit the experimental results when $T_\Delta = 0.75^\circ$ K. The electrical resistance was calculated from the phenomenological theory of the resistance minimum given by Korringa and Gerritsen (1953) in which the

FIGURE 4

a) The density of populated states as a function of energy for the solvent.

b) The "effective" density of states as a function of energy for an alloy having the postulated energy dependent relaxation time.

c) A schematic representation of the magnetic energy levels which result in the de Haas van Alphen effect. Populated levels are indicated by heavy lines.

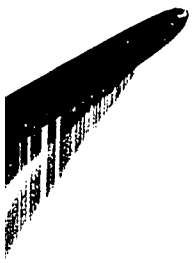

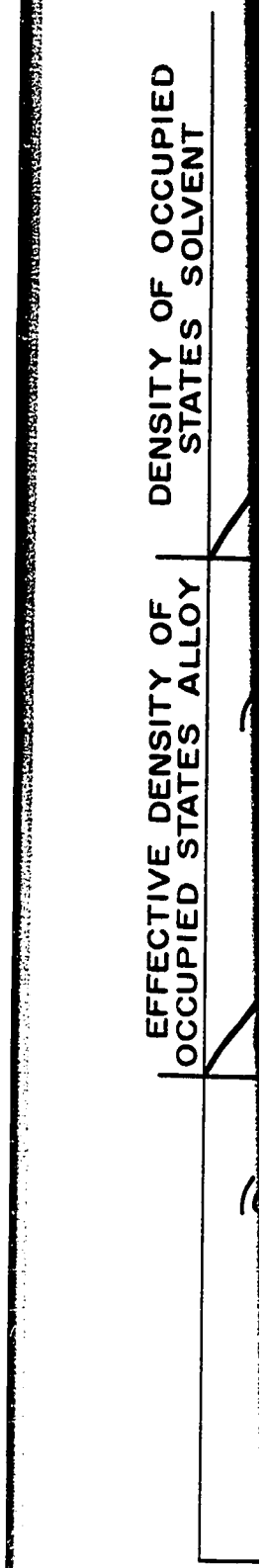

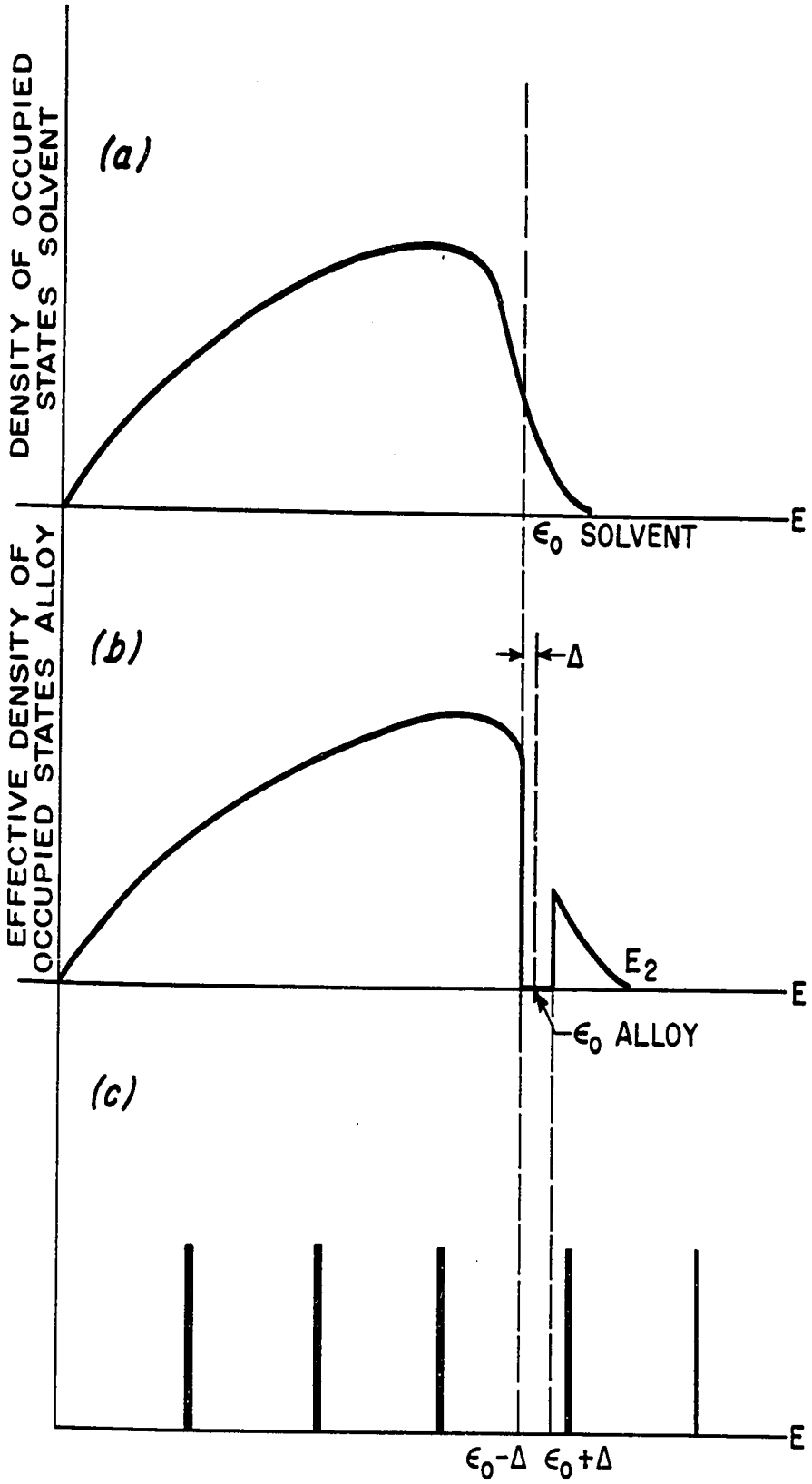
DENSITY OF OCCUPIED STATES SOLVENT
(a)
ϵ_0 SOLVENT
E
EFFECTIVE DENSITY OF OCCUPIED STATES ALLOY
(b)
Δ
E_2
ϵ_0 ALLOY
E
(c)
$\epsilon_0-\Delta$ $\epsilon_0+\Delta$
E

relaxation time was also assumed to have the above behaviour. With a value of $T_\Delta = 0.75^\circ$ K the calculated and measured resistance were found to agree within experimental error.

5.3 Suggestions for Further Research

Included in Appendix II is a discussion of the steady state magnetic anisotropy observed in a zinc manganese crystal. The effects briefly described are presumably a result of the anisotropic environment of the manganese ions in the crystal. This effect is presently under investigation.

It would also be interesting to extend the measurements to include:

1) a manganese alloy having no resistance anomaly, eg. Al Mn,
2) an alloy containing a non magnetic impurity, eg. Zn Cd,
3) other alloy systems exhibiting resistance anomalies.

APPENDIX I

Thermometer Calibration

FIGURE I shows the calibration for the carbon thermometers used in the resistance cryostat and in the thermo e.m.f. cryostat. The copper thermometers in these cryostats were calibrated using the Z function for copper tabulated by White (1959) as a function of temperature where:

$$Z = \frac{R_T - R_{4.2}}{R_{273} - R_{4.2}} = \frac{R_T/R_{273} - R_{4.2}/R_{273}}{1 - R_{4.2}/R_{273}}$$

FIGURE 2 shows the calibration for the gas thermometer used in the magnetic anisotropy measurements. It was calibrated using the method described by White (1959), and three fixed temperatures obtained by submerging the bulb in liquid oxygen, nitrogen, and helium. The temperature of the nitrogen and oxygen were measured using a tinsley platinum resistance thermometer and bridge which had been calibrated by the National Physical Laboratory.

APPENDIX I

Thermometer Calibration

FIGURE I shows the calibration for the carbon thermometers used in the resistance cryostat and in the thermo e.m.f. cryostat. The copper thermometers in these cryostats were calibrated using the Z function for copper tabulated by White (1959) as a function of temperature where:

$$Z = \frac{R_T - R_{4.2}}{R_{273} - R_{4.2}} = \frac{R_T/R_{273} - R_{4.2}/R_{273}}{1 - R_{4.2}/R_{273}}$$

FIGURE 2 shows the calibration for the gas thermometer used in the magnetic anisotropy measurements. It was calibrated using the method described by White (1959), and three fixed temperatures obtained by submerging the bulb in liquid oxygen, nitrogen, and helium. The temperature of the nitrogen and oxygen were measured using a tinsley platinum resistance thermometer and bridge which had been calibrated by the National Physical Laboratory.

FIGURE 1

Calibration curves for the carbon thermometers in the resistance and thermo e.m. f. cryostats.

eters

FIGURE 2

Calibration curve for the gas thermometer used in the magnetic anisotropy measurements. P_o and T_o are the pressure and temperature at which the thermometer was filled.

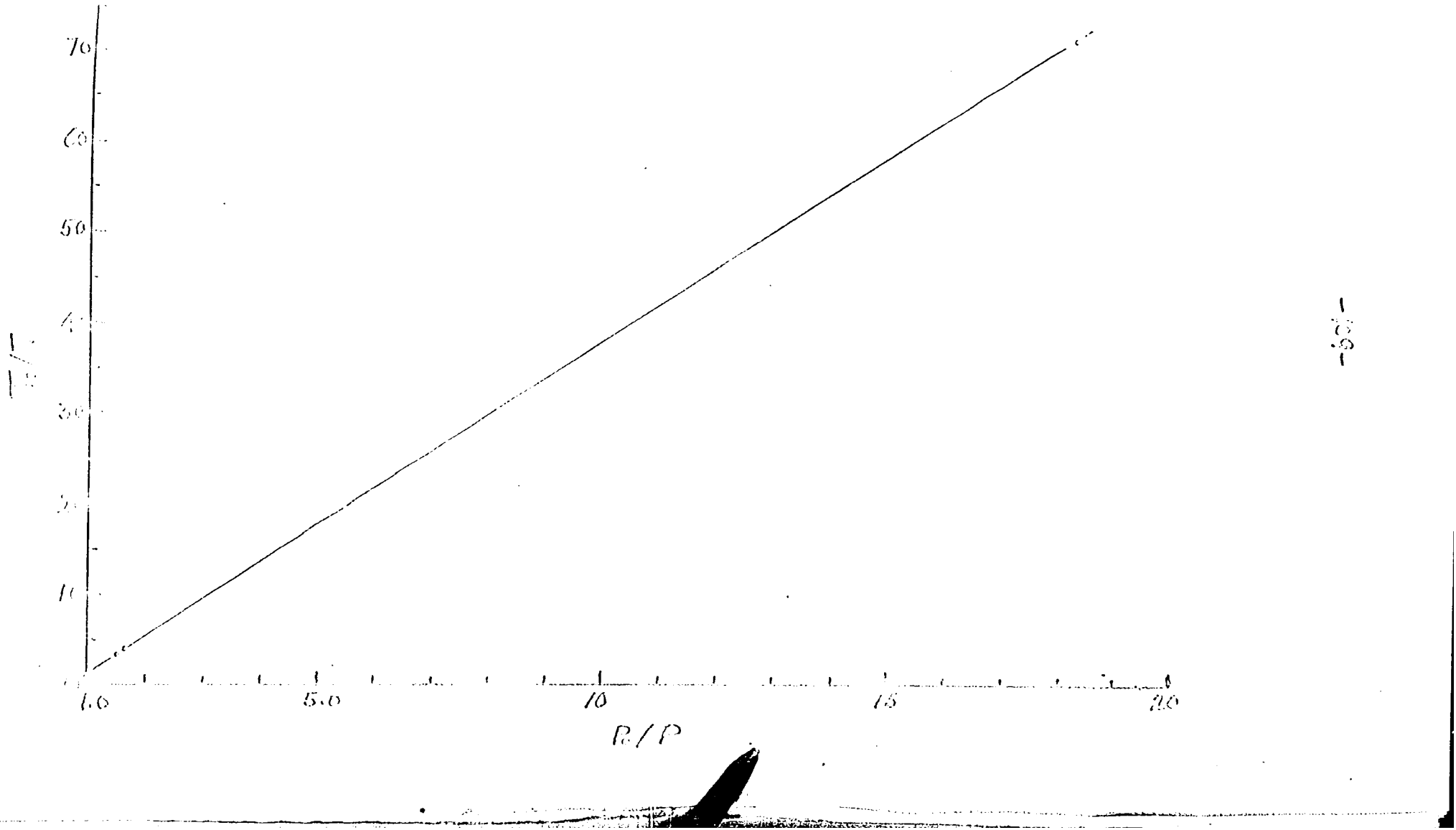
70
60
50
40
30
20
10
1.0
5.0
10
15
20
P/P

APPENDIX II

Magnetic Anisotropy

During an unsuccessful attempt to observe the de Haas van Alphen effect in a 0.025 wt. % zinc manganese crystal it was noticed that the crystal had a large magnetic anisotropy at 4.2° K. Also it was noted that the couple exerted on the crystal at 4.2° K was of the opposite sense to that of the couple observed at room temperature. In order to measure the couple as a function of temperature a helium boiloff cryostat similar to that described by Hedgcock and Muir (1960) was used. The Simon type gas thermometer which surrounds the crystal in this cryostat was calibrated using the method outlined by White (1959). The calibration is given in APPENDIX I.

Consider a magnetically anisotropic crystal of mass, m, having three mutually perpendicular magnetic axes. If the crystal is suspended in a magnetic field, H, so that it is constrained to rotate about one of its magnetic axes, the 2 axis say, then the torque, C, exerted on the crystal, due to the field, is given by:[1]

$$C/H^2 = \frac{1}{2}(\chi_3 - \chi_1) m \sin 2\psi \qquad 1$$

when the field lies in the plane defined by the 1 and 3 axes of the crystal. The quantities χ_1 and χ_3 are the magnetic susceptibilities of the crystal along the 1 and 3 directions respectively and ψ is the angle between the 3 axis and the field.

Torque measurements were made on the 0.025 wt. % zinc manganese crystal when it was suspended with its C axis parallel to, and perpendicular to,

1. See for instance L. F. Bates Modern Magnetism, Chapter IV, p. 161.

the suspension of the balance. With the C axis of the crystal parallel to the suspension no torque was observed for any position of the magnetic field either at room temperature or at 4.2° K. This indicates that the crystal is magnetically symmetrical in the basal plane. If the C axis of the crystal is denoted by 3, then in the notation of the previous paragraph:

$$\chi_1 = \chi_2 .$$

With the C or 3 axis of the crystal perpendicular to the suspension torque measurements were made as a function of temperature between room temperature and 1.7° K for known values of ψ . FIGURE I shows $(\chi_3 - \chi_1)$ for the 0.25 wt. % zinc manganese crystal as a function of temperature in units of $(\chi_3 - \chi_1)$ for pure zinc at room temperature. FIGURE 2 shows $(\chi_3 - \chi_1)$ as a function of H^{-1} for various values of temperature.[2] The increasing slope of the lines as the temperature is lowered might be interpreted as being due to the onset of ferromagnetic ordering in the alloy. Alternatively, this might be due to ferromagnetic impurities. On this assumption the values of $(\chi_3 - \chi_1)$, obtained by extrapolating to infinite field, were plotted as a function of temperature. The results are indicated by the dotted line in FIGURE 3. The peak in the susceptibility which is observed in this case could be interpreted as due to the onset of antiferromagnetism. Further investigation of this effect is planned.

---

2. This is essentially a Honda plot for the torque measurements.

FIGURE 1

The solid line shows the average value of $(X_3 - X_1)$ as a function of temperature. The dashed line shows the value of $(X_3 - X_1)$ obtained by extrapolating to infinite field as shown in FIGURE 18.

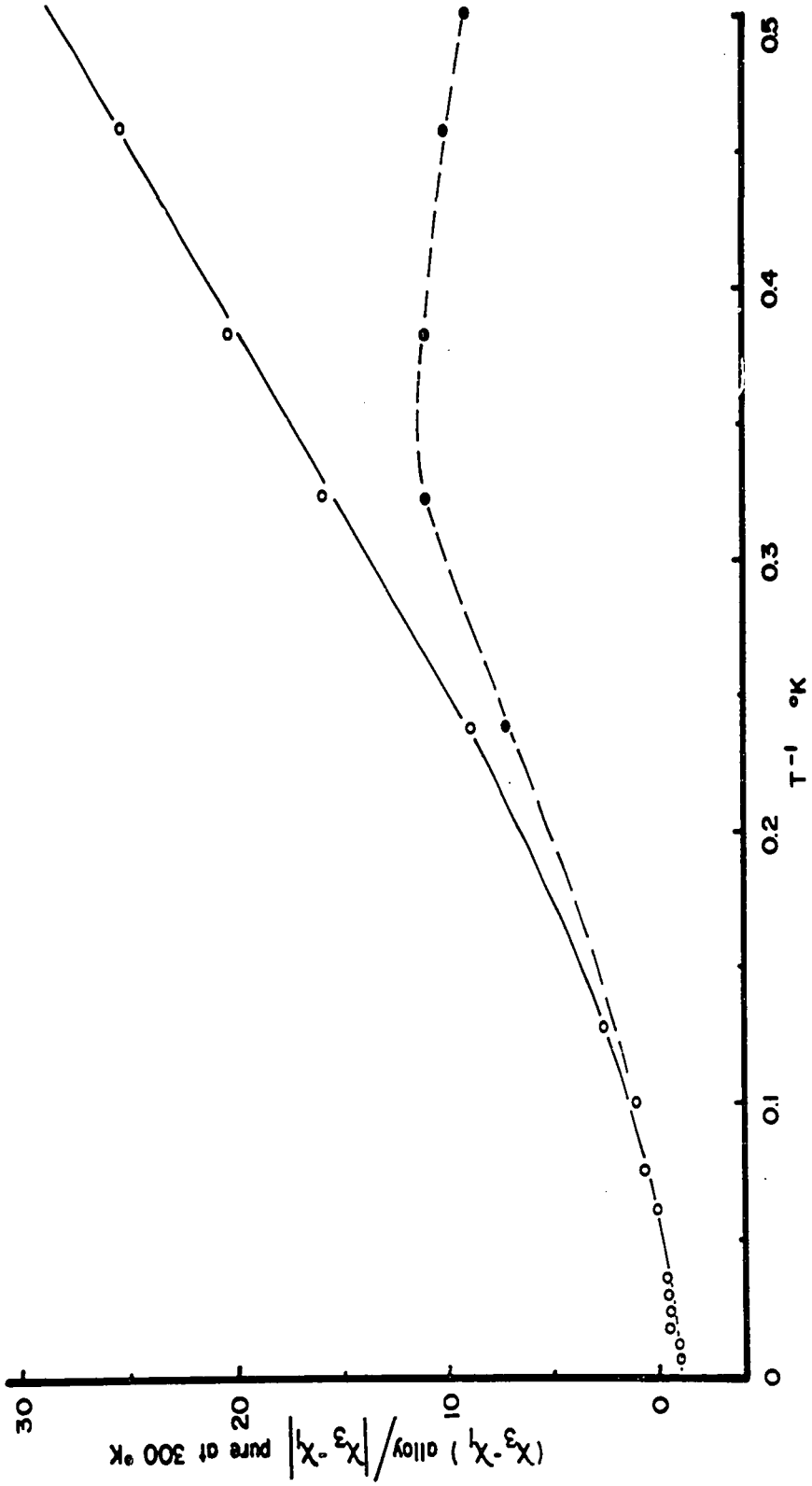
$(\chi_3-\chi_1)$ alloy / $|\chi_3-\chi_1|$ pure at 300 °K
30
20
10
0
0
0.1
0.2
0.3
0.4
0.5
T⁻¹ °K

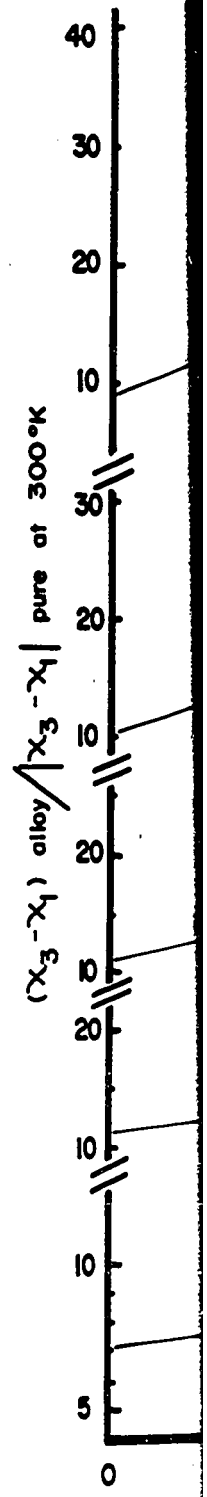

FIGURE 2.

$(X_3 - X_1)$ as a function of reciprocal magnetic field.

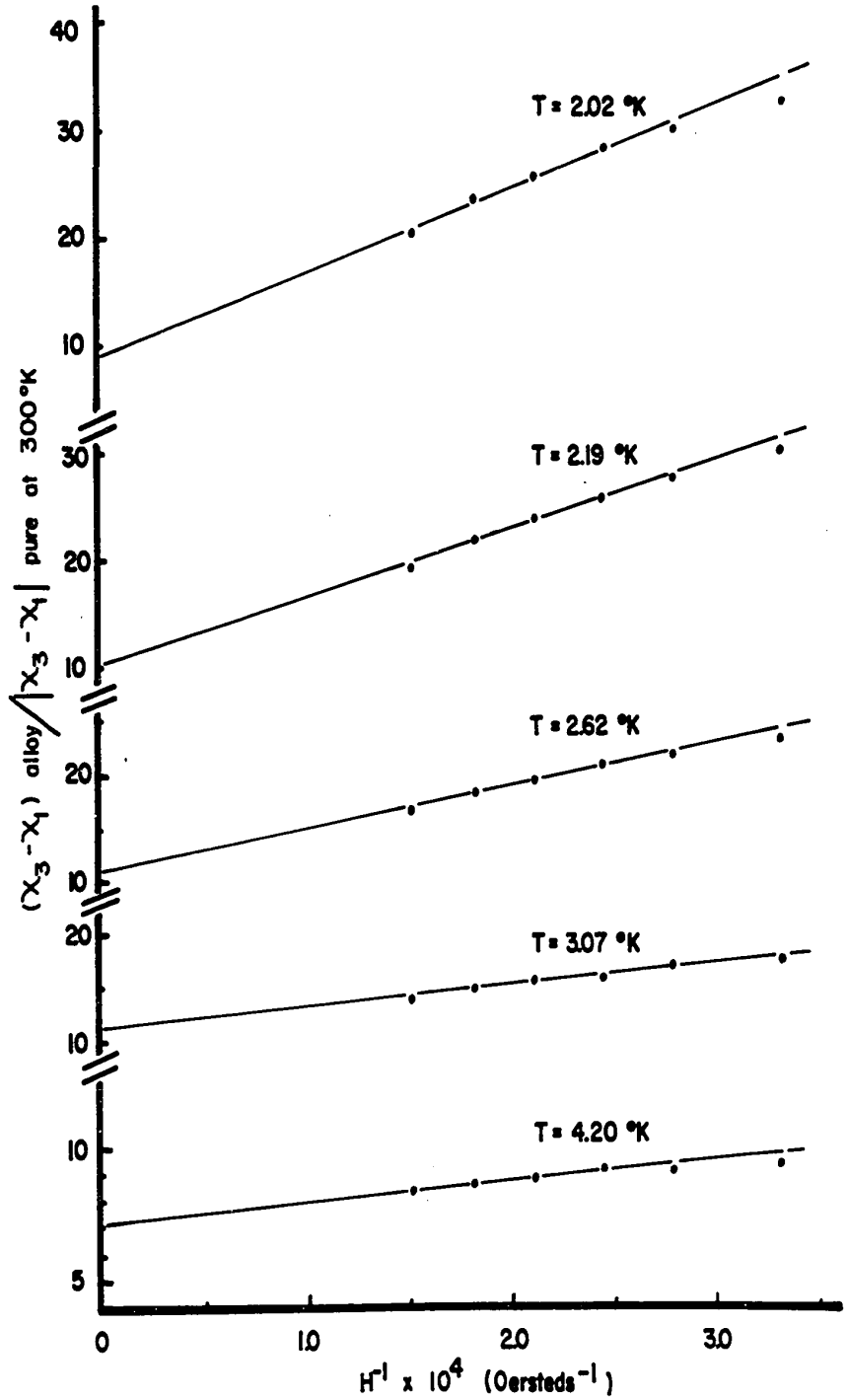
T = 2.02 °K
T = 2.19 °K
T = 2.62 °K
T = 3.07 °K
T = 4.20 °K
40
30
20
10
30
20
10
20
10
20
10
10
5
0
1.0
2.0
3.0
$H^{-1} \times 10^4$ (Oersteds^{-1})
$(\chi_3 - \chi_4)_{alloy} / |\chi_3 - \chi_4|_{pure\ at\ 300°K}$

APPENDIX III

Density of States

Dingle (1952) has shown that in a magnetic field, H, the density of states, $N(E)$, for conduction electrons having a relaxation time, τ, is given by:

$$N(E) = \frac{eHV}{\pi^2 hc}\left(\frac{2m^*}{E_{\parallel}}\right)^{1/2}\sum_{n=0}^{\infty} 1/\left\{\left[E_{\perp} - \frac{e\hbar H}{m^* c}(n+1/2)\right]^2\tau + \frac{\hbar^2}{\tau}\right\}.$$

$E_{\perp}$ is the roughly quantized energy of the electron orbits perpendicular to the magnetic field and $E_{\parallel}$ is the unquantized energy of the electrons along the direction of the magnetic field. By inspection it is seen that whenever the relaxation time is zero the density of states must also be zero.

REFERENCES

Anderson, E.A., (1948), Metals Handbook, 1948 edition, A.S.M.

Bailyn, M., (1961), Phys. Rev. (submitted for publication).

Bates, L.F., (1951), Modern Magnetism, Cambridge Univ. Press,

van den Berg, G. J., (1960), Proc. VII Int. Conf. Low Temp. Phys.

Clement, J.R., Logan, J.K., Gaffney, J. (1955), Phys. Rev. 100, 743.

Clement, J.R., Quinell, E.H., (1952), Rev. Sc. Inst., 23, 213.

Croft, G.I., Donnahoe, F.J., and Love, W.F., (1955), Rev. Sci. Inst., 26, 360.

Dhillon, J.S., and Shoenberg, D., (1955), Phil. Trans. Roy. Soc., A248, 1.

Dingle, R.B., (1952), Proc. Roy.Soc., A211, 517.

Donnahoe, F.J., and Nix, F.C., (1954), Phys. Rev. 95, 1395.

Domenicali, C.A., (1960), Phys. Rev., 117, 984.

Fawcett, E., (1961), Jour. Phys. Chem. Solids, 18, 320.

Gerritsen, A.N., (1959), Physica 25, 489.

de Haas, W.J. and van den Berg, G.J., (1934), Physica 1, 1115.

Harrison, W.A., (1960), Phys. Rev., 118, 1190.

Hedgcock, F.T., Muir, W.B., and Wallingford, E.E., (1960), Can. Jour. Phys., 38, 376.

Hedgcock, F.T., Muir, W.B., (1960), Rev. Sci. Inst., 31, 390.

Kasuya, T., (1959), Prog. Theo. Phys., 22, 227.

Korringa, J. and Gerritsen, A.N., (1953), Ph ysica 10, 457.

MacDonald, D.K.C., and Pearson, W.B., (1955), Acta. Met. 4, 392.

MacDonald, D.K.C., and Pearson, W.B., (1953), Proc. Roy. Soc., A219, 373.

MacDonald, D.K.C., (1947), Jour. Sci. Inst., 24, 232.

Meissner, W. and Voigt, B. (1930), Ann. Phys. 7, 761.

Muto, Y., Tawara, Y., Shibuya, Y., and Fukuroi, T., (1959) Jour. Phys. Soc. Japan, 14, 380.

Preston, J.S., (1946), Jour. Sci. Inst., 23, 173.

Rose-Innes, A.C., and Broom, R.F., (1956), Jour. Sci. Inst., 23, 173.

Schmitt, R.W., (1956), Phys. Rev., 103, 83.

Shoenberg, D. (1952), Phil. Trans. Roy. Soc., A245, 1.

Shoenberg, D., (1959), Progress in Low Temp. Phys. II, Interscience Pub.

Templeton, I.M., (1955), Jour. Sci. Inst., 32, 172.

Verkin, B.I. and Dmitrenko, I.M., (1958), I.S.V. Akad., Nauk, U.S.S.R., 19, 490.

Wallingford, E.E., (1961), M.Sc. Thesis, Ottawa.

White, G.K., (1959), Experimental Techniques in Low Temperatures Physics, Oxford.

Joseph, A.S., Gordon, W.L., (1962) Phys. Rev. 126, 489.

VITA

NAME:	Wilson Burnett Muir
BORN:	Montreal, Quebec, Canada, 1932
EDUCATED:	
Primary Secondary	St. George's School, 1937-47 Westhill High School, 1947-50
Universities	McGill, 1950-53 University of Western Ontario, 1953-55 University of Ottawa, 1958
Course	Physics
Degrees	B.Sc., 1953 M.Sc., 1955
APPOINTMENTS:	Scientific Officer, Department of Mines & Technical Surveys, 1955-57 Research Scientist, Franklin Institute, Philadelphia, Pennsylvania, 1961.
PUBLICATIONS:	The Absorption of Gamma Rays in Rocks, M.Sc., thesis.
	A Viscometer for Molten Metals, Department of Mines & Technical Surveys, Technical Report.
	Radioactive Tracer Investigations in a Floatation Circuit, G.G. Eichholz, W.B. Muir, M.J.S. Bennett, J.D. Wild, C. Lawton and S. Mostowy, Canadian Mining & Metallurgical Bulletin, March, 1957.
	Susceptibility Servo Balance for Measurements on Metals of Extremely Low Resistivity, F.T. Hedgcock and W.B. Muir, Review of Scientific Instruments, Vol. 31, 390, 1960.
	The Electrical Resistance of Dilute Magnesium Manganese and Aluminum Manganese Alloys, F.T. Hedgcock, W.B. Muir and E.E Wallingford, Canadian Journal of Physics, 38, 1134, 1960.
	The Resistance Minimum in a Dilute Cd Mn Alloy, W. B. Muir, J. Phys. Soc. Japan, 16, 2598, 1961.

PUBLICATIONS (cont'd)

Thermoelectric Effects in MgZn and Al containing Traces of Mn., F.T. Hedgcock and W.B. Muir, J.Phys. Soc. Japan, 16, 2599, 1961.

The Influence of Spin Ordering on the Low Temperature Properties of Zinc Manganese Alloys, E.W. Collings, F.T. Hedgcock, W.B. Muir, Proc. VIII, Int. Conf. Low Temp. Physics.